FUNCTION AND INHIBITION OF BRD9 IN ACUTE MYELOID LEUKEMIA CELLS

A Dissertation Presented to
The Watson School of Biological Sciences
at Cold Spring Harbor Laboratory

in Partial Fulfillment of the Requirements for
the Degree of Doctor of Philosophy

by

Anja Fides Hohmann

Cold Spring Harbor Laboratory
March 2016

Acknowledgements

I would like to express my appreciation for the great mentors, colleagues, friends, and family that have supported me throughout my Ph.D.

Special thanks go to my research mentor Chris Vakoc for his guidance and encouragement in the past years. Chris' enthusiasm, expertise, and high-speed approach to work of any kind are a true inspiration. Always available for scientific discussion, Chris' generous contribution of time and ideas has made for a productive and stimulating Ph.D. experience. I was honored to have John Inglis as my academic mentor and I thank him for being a wonderful friend and support over these last four and a half years. I further thank the other members of my Thesis Committee, Bruce Stillman, Dave Tuveson, and Chris Hammell for their valuable feedback in various meetings. Thanks also to former and present Watson School staff including Leemor, Alex, Carrie, Alyson, Keisha, Dawn, Kim C., and Kim G. for putting this program together and for running the school in their humorous and friendly manner.

I would like to extend special thanks to all past and present members of the Vakoc Lab for the friendly and enjoyable lab life. I thank Joe, Anand, Jae, Junwei, and Chen for teaching me various lab techniques over the last years. Many thanks to Jess for her contributions to my project, especially the many long hours she spent pipetting in the virus room. I am also very grateful to Jae, who contributed various ChIP-Seq data sets to my project. I would further like to thank Leemor for allowing me to explore protein crystallography in her lab, and I thank Jon for his amazing teaching skills and numerous entertaining hours in the lab. Special mention goes to Manfred and Laetitia at Boehringer Ingelheim, who provided me with the small molecule BRD9 inhibitor, which added such an exciting component to my project. I also thank Oliver and Yuan in Molly Hammell's lab for willingly answering many questions about computational analyses. Additionally, I would like to thank Bob, Amy, Kelly, and Vinnie, who do a great job running the Hillside shared resources, as well as Pam for making sure the flow cytometers are operating smoothly. While assembling this thesis Carrie Cowan, Victoria Küttner, and Simone Mayer willingly proof-read various sections and I am very grateful for their helpful comments.

My Boehringer Ingelheim Fonds Ph.D. fellowship was not just financial support, but a fantastic enrichment of my studies through various seminars and meetings and I cannot thank Claudia, Anja, and Sandra enough for the awesome job they do running this foundation.

I would further like to thank the many people who made the past years fun, enjoyable, and memorable on a daily basis - the many wonderful members of the Tuveson, M. Hammell, and Egeblad labs who share the Quick building, tissue culture and virus rooms with us; all members of the CSHL Development Office, in particular the amazing Karen Orzel, for involving me in their fundraising efforts, and for allowing me to attend so many great functions; Teri Willey and the CSHL Tech Transfer office for providing me with the opportunity to explore CSHL's Tech Transfer pipeline and to learn about the biotech commercialization process; and all the wonderful friends I have made here over the years. In particular I want to mention Joe(y) and Anand - they are the best and the worst, and they bestowed an entirely new way of thinking upon me. Everyday at 12 pm, we met for lunch at Hillside and our lunch circle would not have been the same without Bobby, Tomoki, Jess, Yali, and most recently Tim. Special thanks also to my amazing housemates and everyone else whom I have enjoyed so many good times with, in particular Santiago, Ewa, Jan, Sarah, and Olivia.

Special mention further goes to all my friends in far away cities and countries, especially Lio, Sophie, Simone, and Matthias, who stay in touch no matter how far the distance. And then there are my wonderful Mum, Dad, and my brother Johannes, as well as my aunts, uncle and cousins, who are only ever a phone call away, and without whose understanding, cheerfulness, support, and continuous supply of German chocolates this thesis would not have happened.

Summary

Recent studies have revealed vital roles of SWI/SNF complexes in leukemia and a variety of other cancers, making this chromatin remodeler a candidate drug target in human malignancy. Chemical modulation of SWI/SNF activity, however, remains to be achieved. Given the success of pharmacological bromodomain inhibition, we evaluated the role of bromodomain-carrying SWI/SNF subunits and identified Bromodomain-containing protein 9 (BRD9) as critical for the growth of Acute Myeloid Leukemia (AML). In AML cells, BRD9 binds the enhancer of the *MYC* proto-oncogene and sustains *MYC* transcription, rapid cell proliferation, as well as a block in differentiation. We found the bromodomain pocket to be essential for BRD9 function in AML. Based on these observations, we derived a small-molecule inhibitor targeting the BRD9 bromodomain (BI-7273), which partially displaces BRD9 from *MYC* enhancer elements and selectively suppresses the proliferation of mouse and human AML cell lines.

Given the known role of other bromodomains, namely those of BRD4, in leukemia growth, ruling out potential off-target activity of BI-7273 was critical. Traditionally, bromodomain inhibitor selectivity is tested using *in vitro* binding assays that examine a subset of other bromodomains. We sought to sample the entire space of potential off-target proteins in order to determine whether BRD9 constitutes the phenotypically relevant target of BI-7273. To this end we engineered a bromodomain-swap allele of *BRD9*, by replacing its bromodomain with the first bromodomain of BRD4. Unexpectedly, this 'BRD9-BET' mutant retains functionality similar to wild-type BRD9 in AML cells. However, cells expressing BRD9-BET are resistant to BI-7273 at all tested concentrations. The reduction in proliferative capacity provoked by BI-7273 is thus based exclusively on its interference with BRD9 activity in these leukemia cells, which was independently supported by the highly similar gene expression changes following chemical vs. genetic BRD9 targeting. Additionally, we used an analogous domain-swap strategy to generate an inhibitor-resistant allele of EZH2.

Our study provides the first evidence for a role of BRD9 in cancer and further highlights a simple genetic strategy for constructing resistance alleles to demonstrate on-target activity of chemical probes in cells.

Contents

Abbreviations

ALL	Acute lymphoid leukemia
AML	Acute myeloid leukemia
ADP	Adenosine diphosphate
ARID1	AT rich interactive domain
ATP	Adenosine triphosphate
BAF	BRG1-associated factors
BET	Bromodomain and extraterminal
B-NHL	B cell non-Hodgkin lymphoma
BRD	Bromodomain-containing protein
BRG1	Brahma-related gene 1
BRM	Brahma
cDNA	complementary DNA
ChIP	Chromatin immunoprecipitation
ChIP-Seq	ChIP-Sequencing
CLL	Chronic lymphocytic leukemia
CML	Chronic myeloid leukemia
CMML	Chronic myelomonocytic leukemia
DLBCL	Diffuse large B cell lymphoma
DNA	Deoxyribonucleic acid
DNMT(i)	DNA methyltransferase (inhibitor)
EZH	Enhancer of zeste
FDA	Food and drug administration
FL	Follicular lymphoma
GI50	Half maximal growth inhibitory concentration
H3K4me3	Histone 3 lysine 4 trimethyl
H3K9me3	Histone 3 lysine 9 trimethyl
H3K27ac	Histone 3 lysine 27 acetyl
H3K27me3	Histone 3 lysine 27 trimethyl

H3K79	Histone 3 lysine 79
HAT	Histone acetyltransferase
HDAC(i)	Histone deacetylase (inhibitor)
HNSCC	Head and neck squamous cell carcinoma
HSC	Hematopoietic stem cell
IC50	Half maximal inhibitory concentration
iMEF	Immortalized mouse embryonic fibroblast
MBP	Methyl binding protein
MBT domain	Malignant brain tumor domain
MDS	Myelodysplastic syndrome
MLL1	Mixed lineage leukemia 1
MPD	Myeloproliferative disease
MPP	Multipotent progenitor
(m)RNA	(messenger) Ribonucleic acid
MRT	Malignant rhabdoid tumor
NHL	Non-Hodgkin lymphoma
NMC	NUT midline carcinoma
NSCLC	Non-small cell lung cancer
OCC	Ovarian clear cell carcinoma
PBAF	Polybromo, BRG1-associated factors
PBRM1	Polybromo 1
PCR	Polymerase chain reaction
PHD	Plant homeodomain
PRC2	Polycomb repressive complex 2
qRT-PCR	Quantitative reverse transcription PCR
RNA-Seq	RNA-Sequencing
SAGA	Spt-Ada-Gcn5-Acetyl transferase
SCLC	Small cell lung cancer
SEM	Standard error of the mean

sgRNA	Single guide RNA
shRNA	Short hairpin RNA
SIRT1	Sirtuin 1
SUMO	Small ubiquitin-like modifier
SUV39H1	Suppressor of variegation 3-9 homolog 1
SWI/SNF	Switch/Sucrose non-fermentable
TCC	Transitional cell carcinoma
TET	Ten-eleven translocation
T-PLL	T cell prolymphocytic leukemia

Formatting of gene and protein names in this thesis

Murine gene names	Capitalized first letter, italisized (*Brd9*)
Murine protein names	Capitalized first letter (Brd9)
Human gene names	Capitalized, italisized (*BRD9*)
Human protein names	Capitalized (BRD9)

List of Figures

List of Tables

List of Appendices

List of Publications

Some of the text appearing in this thesis has been published in the following article:

Hohmann, A. F. and Vakoc, C. R. (2014). A rationale to target the SWI/SNF complex for cancer therapy. *Trends in Genetics* 30(8): 356-363.

Additionally, the data and corresponding text presented in this thesis is part of a manuscript that is accepted for publication at *Nature Chemical Biology*:

Hohmann, A. F., Martin, L. J., Minder, J., Roe, J-S., Shi, J., Steurer, S., Bader, G., McConnell, D., Pearson, M., Gerstberger, T., Gottschamel, T., Thompson, D., Suzuki, Y., Koegl, M. and Vakoc, C. R. Sensitivity and engineered resistance of myeloid leukemia cells to BRD9 inhibition.

Some data presented in this thesis were generated by people other than myself. I am very grateful for my collaborators' additions to this study and to the best of my knowledge, I have disclosed all their contributions in the corresponding figure legends.

1 Introduction

1.1 Epigenetic determinants of gene expression

The human body consists of approximately 10^{13} cells, leaving the human microbiome aside [Bianconi et al., 2013]. All 10^{13} cells contain essentially the same DNA, yet cellular identities vary greatly. This diversity is due to differential gene expression, which is not determined by alterations in the underlying DNA sequence, but is instead controlled by 'epigenetic' mechanisms that control the accessibility of DNA in the nucleus [Gibney and Nolan, 2010].[1]

Gene expression requires the interaction of nuclear factors with DNA to achieve orderly positioning of RNA polymerase at the transcription start site - a task that appears particularly challenging considering the crowded nuclear environment [Orphanides and Reinberg, 2002, Li and Gilmour, 2011]. According to the Human Genome Project, DNA contained within the nucleus of a haploid human cell is made up of close to 3,200 million bases [Brown, 2002]. Assuming the average length of a base to be 0.34 nm, a connection of all 46 chromosomes from a diploid human cell end-to-end in a straight line would yield a DNA molecule of roughly 2.2 m in length[2]. Fitting such a long molecule into a cell nucleus with a diameter of only 10 µm requires significant compaction [Dundr and Misteli, 2001]. Orderly compaction is achieved through the formation of chromatin in which DNA is wrapped around histone octamers to form nucleosomes [Kouzarides, 2007]. Two copies of each of the conserved histone proteins H2A, H2B, H3 and H4 make up the histone octamer, while a fifth histone, H1, can bind the exterior of the nucleosome thereby locking the DNA in place (Fig. 1a) [Dundr and Misteli, 2001, Kouzarides, 2007]. Each nucleosome holds 147 base pairs of wrapped DNA, with the contained nucleotide sequence being relatively inaccessible to nuclear proteins (Fig. 1a) [Kouzarides, 2007, Gibney and Nolan, 2010]. The linker DNA between adjacent nucleosomes is 20 to 50 bp in length and more available to DNA-binding proteins (Fig. 1a) [Dawson et al., 2012]. Each of the core

[1] The term 'epigenetics' was first introduced by C. H. Waddington in 1956 to describe heritable changes in phenotype that were not determined by alterations in DNA sequence and were maintained even in the absence of the signal that originally established them [Waddington, 1956]. In keeping with the contemporary use of this term, I will consider all chromatin modifications as epigenetic despite their varying potential to be stably propagated through cell divisions [Gibney and Nolan, 2010, Dawson et al., 2012].

[2] Length of base $\times$ Number of base pairs in haploid genome $\times$ 2 = 0.34×10^{-9} m $\times 3,200 \times 10^{6} \times 2 = 2.176$ m

histones comprises a C-terminal globular domain as well as an N-terminal unstructured tail, which protrudes out from the core of the nucleosome and may form interactions with other histones, DNA or chromatin-binding proteins (Fig. 1b) [Kornberg and Lorch, 1999, Kouzarides, 2007]. Such interactions allow for further packaging of nucleosomes into higher-order structures, to which the linker histone H1 also contributes [Kornberg and Lorch, 1999]. Generally, chromatin can exist in either of two states: heterochromatin, a condensed structure, which is not permissive to gene expression; and euchromatin, a relaxed structure, which contains actively transcribed genes [Bannister and Kouzarides, 2011, Dawson et al., 2012]. A variety of mechanisms influence the dynamic accessibility of DNA within the chromatin context.

1.1.1 Histone modifications

It has long been accepted that the role of chromatin in gene regulation is not a passive one, but that active mechanisms to package and unpackage chromatin are integral components of eukaryotic gene regulation [Strahl and Allis, 2000]. Important mediators of the transition between "closed" and "open" chromatin are post-translational modifications on histone tails [Kouzarides, 2007]. Such modifications include acetylation, phosphorylation, methylation, ubiquitylation, SUMOylation, ADP ribosylation, deimination, and proline isomerization (Fig. 1b) [Gibney and Nolan, 2010, Bannister and Kouzarides, 2011]. Special enzymes catalyze these reactions (e.g. histone acetyltransferases (HATs) and histone deacetylases (HDACs)) and are frequently found in transcriptional co-activator and -repressor complexes. Addition of chemical groups to histone tails is believed to affect chromatin structure by altering the contacts formed between histones and other molecules [Strahl and Allis, 2000]. Acetylation, for example, is traditionally considered to play an activating role in transcription [Berger, 2007]. This can be attributed to the neutralization of the positively charged lysine residues, which leads to diminished electrostatic interactions, e.g. with the negatively charged phosphates in the DNA backbone, thereby loosening the tight association of DNA and histones [Kuo and Allis, 1998, Gibney and Nolan, 2010]. Accordingly, histone 3 lysine 27 acetylation (H3K27ac) marks active promoters and enhancers [Kimura, 2013]. Phosphorylation of serine or threonine residues and methylation of arginines play additional roles in transcriptional activation [Berger, 2007].

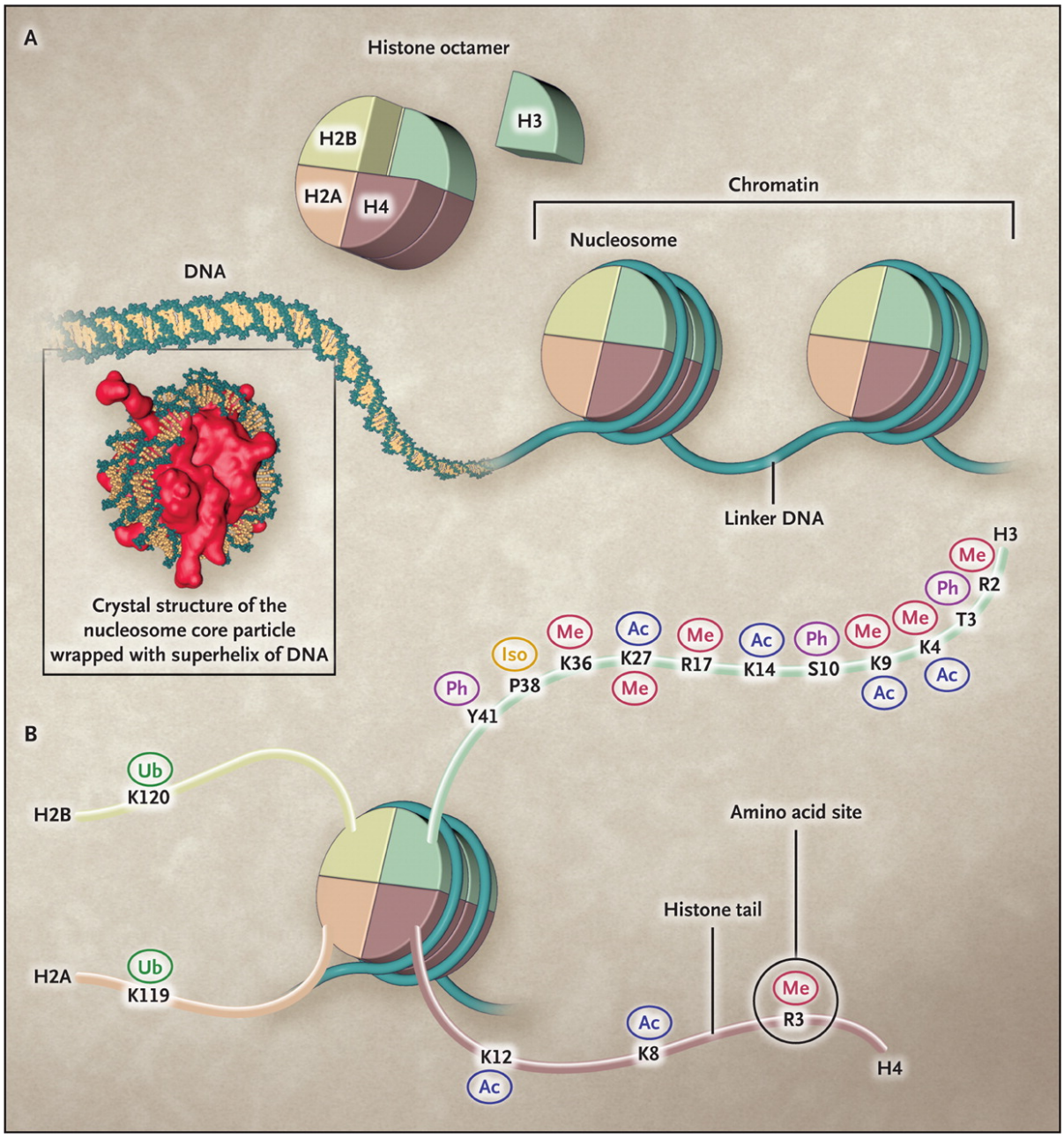

Figure 1. The nucleosome and post-translational histone modifications.
(a) Two H2A:H2B dimers and one H3:H4 tetramer assemble into a histone octamer around which DNA is wrapped to form a nucleosome - the basic unit of chromatin. Nucleosomes are separated by linker DNA. The linker histone H1 is not shown. The inset depicts the crystal structure of a nucleosome.
(b) The N-terminal tails of the four core histones are flexible and project out from the nucleosome. Specific residues in these tails are subject to post-translational modifications. The most well characterized modifications are depicted. Individual amino acids can be subject to different modifications. Me, methylation; Ac, acetylation; Ph, phosphorylation; Ub, ubiquitylation; Iso, proline isomerization.
Figure and legend (adapted) from [Dawson et al., 2012].

In contrast, methylation and ubiquitylation of lysines seem to provoke activation or repression depending on the specific lysine residues to which these chemical groups are added [Berger, 2007]. For example, histone 3 lysine 4 trimethylation (H3K4me3) is consistently found at promoters of active genes, but trimethylation of histone 3 lysine 9 (H3K9me3) is associated with promoters and gene bodies of silent genes [Gibney and Nolan, 2010]. These examples highlight that in addition to the type of chemical group added, its location within histone tails and, in the case of methylation, the number of groups added per amino acid (up to three methyl groups on lysines and up to two on arginines) further increase the complexity of these modifications [Gibney and Nolan, 2010, Dawson et al., 2012].

In addition to controlling electrostatic interactions and chromatin condensation, histone modifications furthermore provide a scaffold for the assembly of chromatin binding proteins. Also known as epigenetic 'readers', such proteins possess at least one of a variety of different chromatin binding domains [Yun et al., 2011]. While conserved amino acids in such domains confer binding preferences for specific post-translational modifications (e.g. acetylation vs. methylation), residues at the outer surface of the binding pocket can interact with flanking amino acids and thus confer specificity for modified residues at specific positions in histone tails [Dawson et al., 2012]. An overview of the primary epigenetic reader domains described to date and their associated histone modification preferences is shown in Fig. 2.

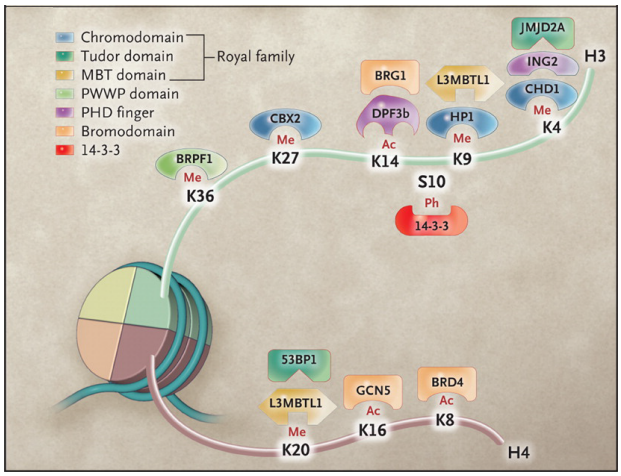

Figure 2. Epigenetic reader domains and their preferred binding substrates. Epigenetic reader domains are separated into families based on domain structure and binding preference for specific histone modifications. Within a family, preferred binding substrates might further vary depending on slight alterations in domain structure and amino acid composition. Examples of proteins that contain epigenetic reader domains with specific binding preferences are shown. Figure and legend (adapted) from [Dawson et al., 2012].

Bromodomains - epigenetic readers of acetylated lysines

In the context of this study, particular attention will be paid to bromodomains. Bromodomains represent chromatin reader modules that engage in acetyl-lysine recognition and are found in a diverse array of transcriptional coactivators and chromatin regulators [Brand et al., 2014]. Bromodomains are composed of a left-handed four α-helix bundle, which forms a hydrophobic cavity that accommodates acetylated lysine residues [Dhalluin et al., 1999]. Interaction with the acetyl group is mediated by hydrogen bonding from the bottom of the cavity as well as by additional water-mediated intermolecular hydrogen bonds [Yun et al., 2011]. The human bromodomain family encompasses 61 domains found in 46 proteins [Filippakopoulos and Knapp, 2014]. Large-scale biochemical assays have revealed that individual bromodomains have distinct binding preferences for acetyl-lysine containing peptides, which implies functional specialization among these proteins in the cell [Filippakopoulos et al., 2012]. However, these assays have also revealed that bromodomains do not exert unique sequence specificity, which can be partly attributed to less pronounced interactions with flanking amino acids [Yun et al., 2011]. Overall, the interaction between acetyl-lysines and bromodomains is relatively weak, and some proteins contain more than one bromodomain to engage in chromatin binding (e.g. BRD4: two bromodomains; PBRM1: six bromodomains) [Yun et al., 2011]. Additionally, several protein complexes contain more than one bromodomain-containing subunit (e.g. SAGA complex: two bromodomain-containing proteins; SWI/SNF complex: two to three bromodomain-containing proteins depending on composition (see below)) [Yun et al., 2011].

1.1.2 DNA Methylation

The addition of chemical groups is not limited to histone proteins in chromatin. The surface of DNA itself can be altered by the reversible addition of a methyl group to the 5'-position of cytosine (C) nucleotides, which is associated with gene repression [Berger, 2007]. Methylated cytosines are generally located 5' to a guanine (G) residue and CpG dinucleotides can cluster together in so-called CpG islands [Berger, 2007, Gibney and Nolan, 2010]. While CpG dinucleotides outside of CpG islands are methylated in 80 % of cases, 85-90 % of cytosines inside CpG islands remain free of methylation [Jaenisch and Bird, 2003, Gibney and Nolan,

2010, Tsai and Baylin, 2011]. These unmethylated CpG islands are frequently found in the vicinity of promoter regions, though they have now also been described in intra- and intergenic locations [Jaenisch and Bird, 2003, Gibney and Nolan, 2010].

The transfer of a methyl group from a S-adenosyl-methionine donor to a cytosine residue is catalyzed by DNA methyltransferases (DNMTs) [Tsai and Baylin, 2011]. In mammals, three DNMTs account for this activity. DNMT1 is considered the 'maintenance DNMT' as it copies the methylation pattern from parent to daughter strand during DNA replication [Jaenisch and Bird, 2003, Gibney and Nolan, 2010]. DNMT3A and DNMT3B carry out *de novo* methylation and can further repair errors made by DNMT1 [Gibney and Nolan, 2010].

Mechanisms of DNA demethylation are less well understood. While passive demethylation can occur due to the failure or deactivation of DNMT activity during DNA replication, active demethylation has been attributed to TET enzymes [Gibney and Nolan, 2010, Álvarez-Errico et al., 2015]. These catalyze the sequential oxidation of 5-methylcytosines to 5-hydroxymethylcytosine, 5-formylcytosine, and 5-carboxycytosine [Álvarez-Errico et al., 2015]. Such 5-methylcytosine derivatives are then recognized by base excision repair machinery, excised and replaced with unmethylated cytosine nucleotides [Álvarez-Errico et al., 2015].

When added to the 5' position of a cytosine's pyrimidine ring, the methyl group extends into the major groove of the DNA double helix and is thus accessible to DNA binding proteins [Gibney and Nolan, 2010]. As such, it can interfere with DNA binding of some proteins and simultaneously attract others. Several methyl-binding proteins (MBPs) act as transcriptional repressors by recruiting co-repressors and histone deacetylases or by acting as a physical barrier to the transcriptional apparatus [Jaenisch and Bird, 2003, Gibney and Nolan, 2010].

Correspondingly, DNA methylation generally opposes gene expression and has been found to contribute to gene silencing during imprinting, X chromosome inactivation, and the inhibition of transposable elements [Jaenisch and Bird, 2003, Tsai and Baylin, 2011, Álvarez-Errico et al., 2015].

1.1.3 ATP-dependent chromatin remodelers

In addition to chemical modifications of histones and DNA, specific enzymatic remodelers further regulate chromatin structure and gene accessibility. These chromatin remodeling complexes utilize energy derived from ATP hydrolysis to disrupt histone-DNA contacts and change the composition or location of nucleosomes along DNA, thereby controlling which DNA sequences are exposed to nuclear machinery [Becker and Hörz, 2002]. Four classes of chromatin remodeling complexes have been defined: SWI/SNF, ISWI, CHD, and INO80. These share a conserved ATPase domain but function in a largely non-redundant manner to influence discrete aspects of transcriptional regulation as well as DNA replication and repair in the chromatin environment [Clapier and Cairns, 2009, Hargreaves and Crabtree, 2011].

The mammalian SWI/SNF complex

The multi-subunit SWI/SNF complex is one of the most thoroughly studied chromatin remodelers. Early studies in the budding yeast *S. cerevisiae* implicated the complex in a variety of transcriptional responses that were accompanied by changes in DNA accessibility at the associated promoter regions [Neigeborn and Carlson, 1984, Stern et al., 1984, Hirschhorn et al., 1992, Peterson and Herskowitz, 1992]. The requirement for SWI/SNF at these genes could be alleviated by reducing the expression of core histones, which first suggested that SWI/SNF acts to overcome the nucleosome barrier to allow transcription [Hirschhorn et al., 1992]. However, the influence of SWI/SNF activity on gene expression is highly contextual, in that it can facilitate activation of some genes while it yields repression at other promoters [Martens and Winston, 2002]. Biochemical purifications led to the description of yeast SWI/SNF as a 12 subunit complex that can disrupt histone-DNA contacts in an ATP-dependent manner on purified nucleosome templates, thereby allowing transcription factors to access their cognate DNA elements [Cairns et al., 1994, Côté et al., 1994, Peterson et al., 1994]. *In vitro* and *in vivo*, chromatin remodeling by yeast SWI/SNF can lead to a variety of different outcomes, including nucleosome sliding, nucleosome eviction, and selective removal of H2A:H2B dimers [Narlikar et al., 2013].

The mammalian SWI/SNF complex (also known as BAF complex for 'BRG1-associated fac-

tors') exhibits a similar nucleosome remodeling activity *in vitro* as its yeast counterpart [Khavari et al., 1993, Imbalzano et al., 1994, Kwon et al., 1994, Wang et al., 1996a]. This activity can be reconstituted with a set of four core subunits (BRG1, SNF5, BAF155, and BAF170), which have orthologs in the yeast complex [Phelan et al., 1999]. However, mammalian SWI/SNF contains several subunits not found in yeast that can provide interaction surfaces for chromatin (e.g. bromodomains) or transcription factors and thus contribute to the genomic targeting of the complex (Fig. 3a) [Wang et al., 1996a, Wang et al., 1996b, Nie et al., 2000].

A key attribute of mammalian SWI/SNF (hereafter referred to simply as SWI/SNF) is the heterogeneity of subunit compositions that can exist in different tissues, cell types and even within a single cell (Fig. 3b-f) [Wang et al., 1996a, Wang et al., 1996b, Wu et al., 2009]. Based on the incorporation of select subunits, SWI/SNF complexes are broadly partitioned into SWI/SNF-A (BAF) and SWI/SNF-B (PBAF) (Fig. 3b, c). Further complexity arises as several individual SWI/SNF subunits are encoded by gene families whose protein products are mutually exclusive in the complex [Wu et al., 2009]. Thus, only one paralog is incorporated in a given SWI/SNF assembly. Combinatorial association of SWI/SNF subunits could in principle give rise to hundreds of distinct complexes, although the exact number has yet to be determined [Wu et al., 2009, Ho and Crabtree, 2010]. Additionally, the composition of SWI/SNF can be dynamically reconfigured during cell fate transitions through cell type-specific expression patterns of certain subunits (Fig. 3d-f). For example, BAF53A is repressed and replaced by BAF53B during neuronal differentiation, a switch that is essential for proper neuronal functions *in vivo* (Fig. 3d, e) [32-35] [Lessard et al., 2007, Wu et al., 2007, Yoo et al., 2009].

Genetic evidence suggests that distinct subunit configurations of SWI/SNF are equipped to perform specialized functions. As an example, SWI/SNF contains one of two ATPase subunits, BRG1 or BRM, which share 75% amino acid sequence identity [Khavari et al., 1993]. In certain cell types BRG1 and BRM can functionally compensate for loss of the other subunit. In other contexts, however, these two ATPases perform divergent functions [Reyes et al., 1998, Strobeck et al., 2002]. In osteoblasts, BRG1 and BRM can even functionally oppose one another to regulate differentiation [Flowers et al., 2009]. The functional specificity of BRG1 and BRM has been linked to sequence variations near their N-terminus, which have different interaction

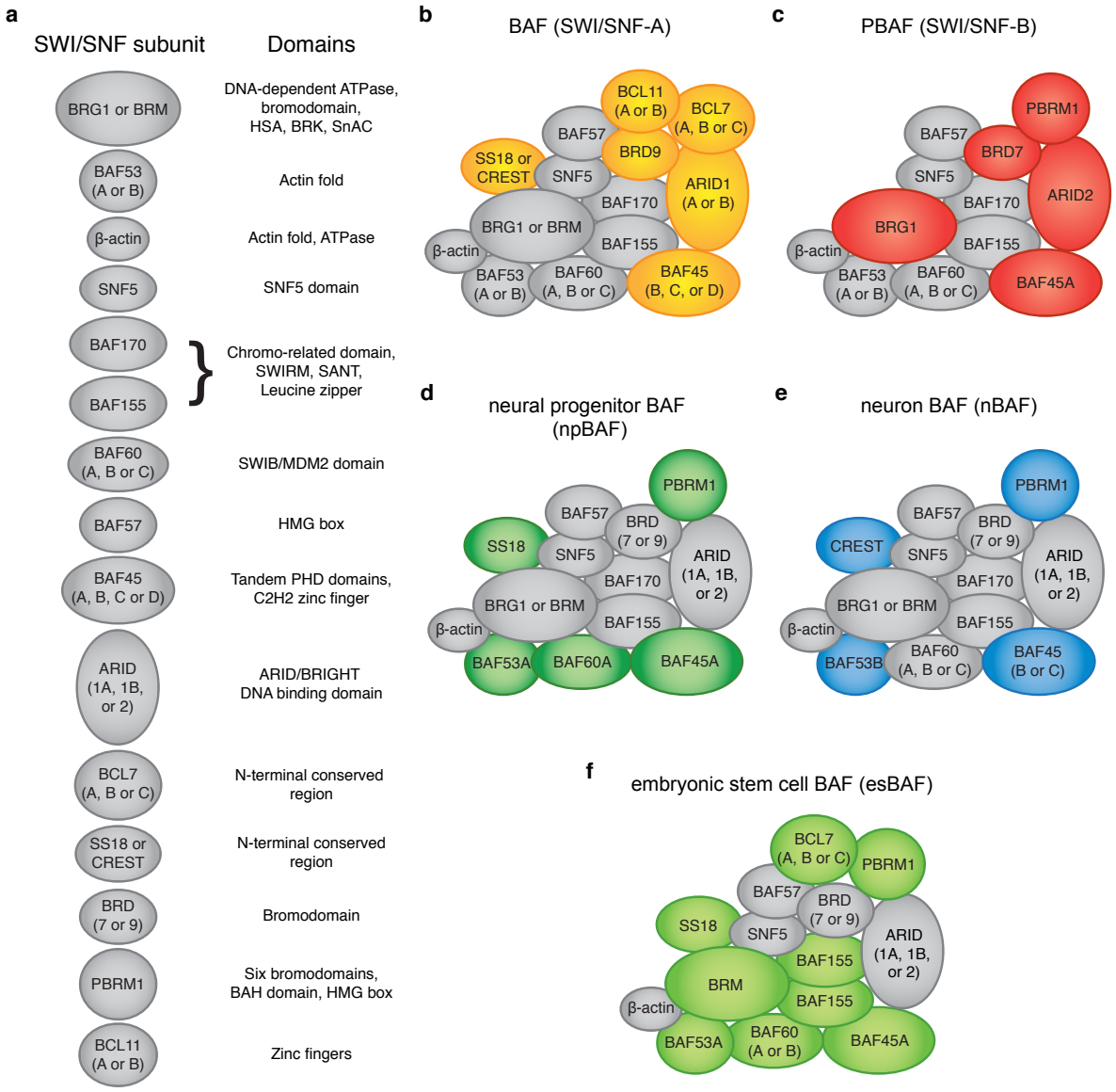

Figure 3. Overview of mammalian SWI/SNF complexes.
(a) Subunits that comprise the mammalian SWI/SNF complex. Protein domains present in each subunit are listed on the right. Subunit nomenclature was chosen based on prevailing usage in the literature.
(b - f) Examples of known SWI/SNF subunit configurations. BAF and PBAF represent two alternative subunit arrangements for SWI/SNF that can exist in the same cell type (b, c). Examples of cell type-specific SWI/SNF subunit configurations are shown in panels (d - f). The different coloring is used to highlight the most well established subunits that distinguish these different assemblies. The position of individual subunits within the diagram is not intended to imply direct interactions within the complex.

specificities for transcription factors [Kadam and Emerson, 2003]. Another example of paralogous subunits that form mutually exclusive SWI/SNF-A (BAF) complexes are ARID1A and ARID1B [Wang et al., 2004]. *ARID1A* and *ARID1B* open reading frames are 60% identical, yet their protein products can perform opposing functions in regulating the cell cycle by recruiting repressors or activators to key target genes, respectively [Nagl et al., 2007]. These studies stress that SWI/SNF represents a collection of multi-subunit complexes whose integrated functions control diverse cellular processes.

1.2 Epigenetics in cancer

Epigenetic mechanisms influence not only transcription but also DNA replication and repair as well as chromosome condensation and segregation. As such, it is not surprising that epigenetic abnormalities have been implicated in the pathogenesis of cancer. Although differences in DNA methylation between cancers and normal tissues were reported as early as 1983, cancer epigenetics was long overshadowed by a focus on genetic mutations as drivers of oncogenesis [Feinberg and Tycko, 2004]. Advances in genome-wide technologies over the past twenty years revealed that cancer cells harbor substantial epigenetic alterations, including global changes in histone modification patterns, DNA hypomethylation at repetitive DNA sequences as well as DNA hypermethylation at CpG islands in promoter regions associated with gene silencing [Baylin and Jones, 2011]. The discovery of recurrent mutations in chromatin modifiers further linked genetic and epigenetic processes in oncogenesis [Baylin and Jones, 2011].

A list of all epigenetic readers, erasers, and writers commonly mutated in cancer patients reveals their disproportionate occurrence in hematopoietic malignancies, which is particularly noteworthy given the comparatively low mutation rate in these cancers (Table 1) [Dawson and Kouzarides, 2012, Kandoth et al., 2013]. As a consequence of the preponderance of epigenetic mutations in hematopoietic neoplasms, our understanding of epigenetic contributions to tumorigenesis is most advanced in this cancer class and in Acute Myeloid Leukemia (AML) in particular [Cai et al., 2015]. The characteristics of normal hematopoiesis provide insights into the special significance of epigenetic control in the blood lineage.

Class	Epigenetic regulator	Mutation type	Tumor
DNA methyltranserases	DNMT3A	M, F, N, S	AML, MDS, MPD
DNA demethylases	TET1	T	AML
	TET2	M, N, F	AML, MPD, MDS, CMML
Histone acetyltransferases	KAT3A (CBP)	T, N, F, M	AML, ALL, DLBCL, B-NHL, TCC
	KAT3B (p300)	T, N, F, M	AML, ALL, DLBCL, TCC, Colorectal, Breast, Pancreatic
	KAT6A (MOZ)	T	AML, MDS
	KAT6B (MORf)	T	AML, Uterine leiomyoma
Histone acetyl readers	BRD1	T	ALL
	BRD3	T	Midline carcinoma
	BRD4	T	Midline carcinoma
	TRIM33	T	Papillary thyroid
	PBRM1	N, F, M, S	Renal, Breast
Histone methyltransferases	KMT2A (MLL1)	T, PTD	AML, ALL, TCC
	KMT2B (MLL2)	N, F, M	Medulloblastoma, Renal, DLBCL, FL
	KMT2C (MLL3)	N	Medulloblastoma, TCC, breast
	KMT3A (SETD2)	N, F, S, M	Renal, breast
	KMT3B (NSD1)	T	AML
	NSD2	T	Multiple myeloma
	NSD3	T	AML
	KMT6 (EZH2)	M	DLBCL, MPD, MDS
Histone demethylases	KDM5A (JARID1A)	T	AML
	KDM5C (JARID1C)	N, F, S	Renal
	KDM6A (UTX)	D, N, F, S	AML, TCC, Renal, Oesophageal, Multiple myeloma
Histone methyl readers	TRIM33	T	Papillary thyroid
	ING1	M, D	Melanoma, Breast
	ING4	D	HNSCC
	MSH6	M, N, F, S	Colorectal
Histone kinases	ATM	D, M, N, F, S	T-PLL, AML, ALL, Medulloblastoma, Glioma
	JAK2	T, M	AML, ALL, MPD, CML
	PIM1	T	NHL
Histone phosphate readers	BRCA1	D, M, N, F, S	Ovarian, Breast, Prostate

Table 1. Cancer-associated mutations in epigenetic writers, readers, and erasers.
Mutation types - D, Deletion; F, Frameshift; M, Missense; N, Nonsense; PTD, Partial tandem duplication; S, Splice site mutation; T, Translocation.
Tumors - AML, Acute myeloid leukemia; ALL, Acute lymphoid leukemia; B-NHL, B cell non-Hodgkin lymphoma; CML, Chronic myeloid leukemia; CMML, Chronic myelomonocytic leukemia; DLBCL, Diffuse large B cell lymphoma; FL, Follicular lymphoma; HNSCC, Head and neck squamous cell carcinoma; MDS, Myelodysplastic syndrome; MPD, Myeloproliferative disease; NHL, Non-Hodgkin lymphoma; NMC, NUT midline carcinoma; SCLC, Small cell lung cancer; TCC, Transitional cell carcinoma; T-PLL, T cell prolymphocytic leukemia.
Table adapted from[Dawson and Kouzarides, 2012]

1.2.1 Epigenetic control in the hematopoietic system

The blood is an organ that relies heavily on the tight yet dynamic control of transcription. Many mature blood cells are short-lived and thus require constant replenishing, with more than 10^{11} - 10^{12} of these cells being formed in the adult human every day [Boulais and Frenette, 2015, Doulatov et al., 2012]. The pluripotent hematopoietic stem cell (HSC) at the apex of the hematopoietic system can give rise to any type of mature blood cell while simultaneously possessing self-renewal capacities (Fig. 4) [Cedar and Bergman, 2011]. Located in a HSC niche in the bone marrow, these rare cells are kept quiescent and divide infrequently [Boulais and Frenette, 2015]. In contrast, multipotent progenitors (MPPs), which derive from HSCs, can proliferate rapidly but possess only transient self-renewal capacities [Cedar and Bergman, 2011]. Growth factors and cytokines control the delicate balance between proliferation and maturation. MPP daughter cells bifurcate into the myeloid and lymphoid lineage precursors and become progressively more committed through a series of progenitor intermediates until they form mature blood cells (Fig. 4) [Bonifer, 2005, Cedar and Bergman, 2011, Doulatov et al., 2012]. Terminally differentiated blood cells have lost their capacity to proliferate, and, as the effectors of the hematopoietic system, they are responsible for oxygen transport (erythrocytes), wound healing (platelets), as well as innate and adaptive immunity (e.g. innate: neutrophils and macrophages; and adaptive: B and T cells, which can be re-activated to proliferate and differentiate further by specific antigens) (Fig. 4) [Bonifer, 2005, Boulais and Frenette, 2015].

Preventing the exhaustion of HSCs while simultaneously ensuring the constant supply of mature blood cells of different lineages capable of performing specialized functions requires exquisite control and plasticity of gene expression. Reversible epigenetic mechanisms are ideally suited to provide such flexibility. The profiling of DNA methylation and histone modification patterns in purified hematopoietic cell populations at various stages of lineage commitment has revealed numerous specification-associated epigenetic changes [Cedar and Bergman, 2011].

A special feature of HSCs is the co-occurrence of activating H3K4 and repressing H3K27 methylation marks at several genes encoding lineage-specific transcription factors, including Pax5, Ebf1, C/EBPα [Cui et al., 2009, Weishaupt et al., 2010]. Such bivalently marked chromatin

was originally described in embryonic stem cells (ESCs) as a means to silence developmental genes while keeping them poised for activation during later differentiation [Bernstein et al., 2006]. Accordingly, the number of bivalent loci decreases with hematopoietic differentiation [Cedar and Bergman, 2011].

Linage-specific promoters furthermore experience selective DNA demethylation [Bonifer, 2005]. In contrast, genes associated with progenitor cells and other lineages can become silenced by *de*

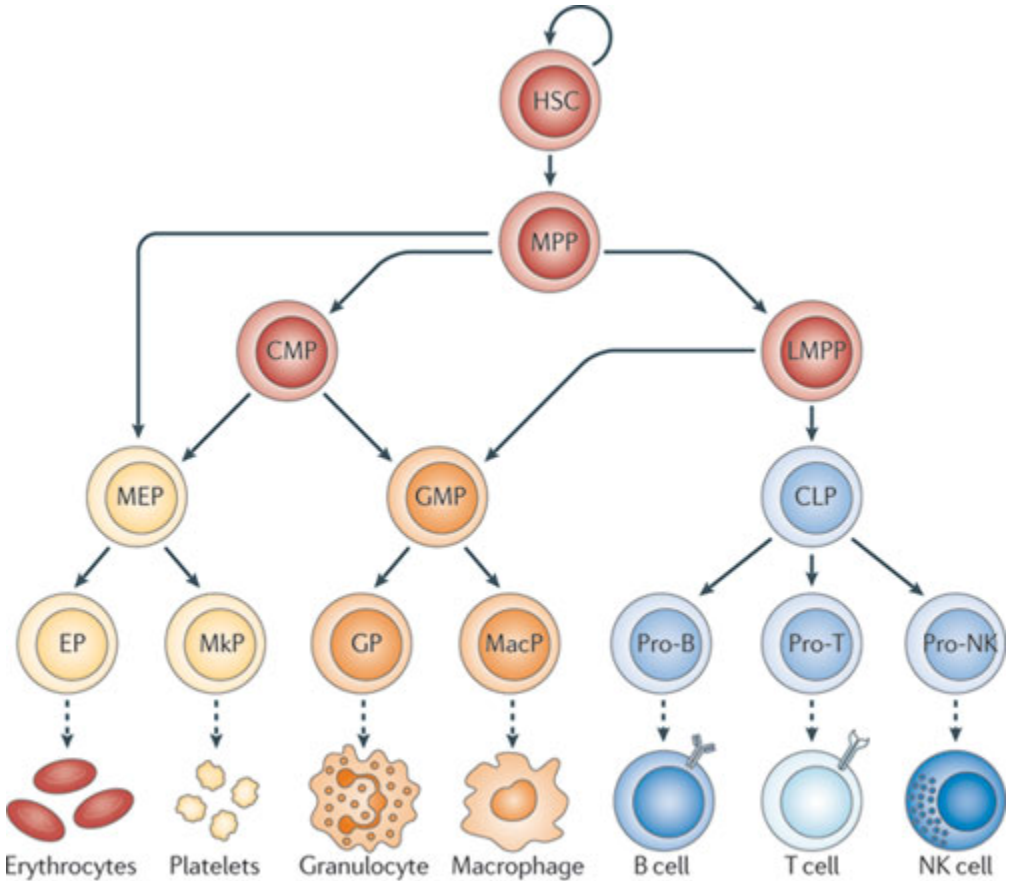

Figure 4. Hierarchy of differentiation in the hematopoietic system.
Mature blood cells are derived from the hematopoietic stem cell through step-wise differentiation of progressively more committed progenitor cells. Fully committed progenitors can give rise to one lineage only. The maturation of these committed progenitors (e.g. Pro-B cells) into functional effector cells is a multistage process, represented by dashed arrows.
CLP, common lymphoid progenitor; CMP, common myeloid progenitor; EP, erythrocyte progenitor; GMP, granulocyte/macrophage progenitor; GP, granulocyte progenitor; LMPP, lymphoid primed multipotent progenitor; MacP, macrophage progenitor; MEP, megakaryocyte-erythrocyte progenitor; MkP, megakaryocyte progenitor; MPP, multipotent progenitor; NK, natural killer. Figure and legend (adapted) from [Cedar and Bergman, 2011].

novo methylation [Cedar and Bergman, 2011]. This often occurs at target sites of the Polycomb repressor complex 2 (PRC2). The PRC2 component EZH2 deposits repressive H3K27 trimethyl marks (H3K27me3) and has also been reported to interact directly with DNMTs, highlighting the interplay of epigenetic mechanisms in this process [Viré et al., 2006]. The importance of (de)methylation is further highlighted by findings implicating mutations of (de)methylating enzymes in abnormal hematopoietic proliferation and differentiation. Expression of a DNMT1 hypomorph in HSCs prevents self-renewal and skews these cells toward myeloid differentiation due to an inability to repress myeloid regulators (e.g. GATA1 and C/EBPα) [Cedar and Bergman, 2011, Álvarez-Errico et al., 2015]. In contrast, deletion or inhibition of methylcytosine dioxygenase TET2 causes increased self-renewal of HSCs [Álvarez-Errico et al., 2015]. Similarly, DNMT3A and DNMT3B double mutant HSCs also show enhanced self-renewal capacities [Álvarez-Errico et al., 2015]. It is therefore conceivable, how malfunction of epigenetic regulators can interfere with differentiation and corrupt blood cells into unlimited proliferation and cancer. Accordingly, mutations in DNMT3A and TET2, as well as metabolic inhibition of TET2 caused by gain-of-function mutations in isocitrate dehydrogenases (IDHs), have been identified as drivers in myeloid neoplasms [Chan and Majeti, 2013].

1.2.2 Acute myeloid leukemia

Given the dependence of the hematopoietic system on stable epigenetic states and lineage-specific transcription factors, it is perhaps not surprising that these protein classes constitute the major targets for mutations in hematopoietic malignancies [Network et al., 2013]. Acute myeloid leukemia (AML) is a particularly aggressive hematopoietic malignancy. Caused by heterogeneous chromosomal rearrangements and mutations in hematopoietic stem/progenitor cells, the five-year survival rate is only 5 - 20 % in the adverse risk patient group [Zeisig et al., 2012]. The acquired genetic alterations block myeloid differentiation such that clonal expansion of transformed cells leads to the accumulation of undifferentiated, immature myeloid cells (blasts) in the bone marrow [Kumar et al., 2014]. This interferes with normal hematopoiesis and frequently causes shortage of functional effector cells (e.g. granulocytopenia, thrombocytopenia and anemia) [Lowenberg et al., 1999]. Therapeutic intervention aims to clear the bone

marrow of transformed cells to allow resumption of normal hematopoiesis [Kumar et al., 2014]. The current standard-of-care treatment consists of cytotoxic chemotherapy (daunorubicin and cytarabine), often in combination with hematopoietic stem cell transplantation [Zeisig et al., 2012]. A better understanding of cancer-specific vulnerabilities might allow for more directed therapies and some promising advances in this direction have recently been made.

1.2.3 Epigenetic cancer therapies

In contrast to genetic mutations, epigenetic alterations are reversible, thereby opening new routes for pharmacological intervention. Two DNA methyltransferase inhibitors (DNMTis) and four histone deacetylase inhibitors (HDACis) have received FDA approval for treatment of hematopoietic malignancies 2 [Cai et al., 2015]. Importantly, the molecular determinants of clinical responses to DNMTis and HDACis remain to be established [Dawson et al., 2012]. DNMTis were reported to trigger stress and damage signaling pathways, and HDACi-treated human cancer cell lines demonstrated hyperacetylation of 1750 non-histone proteins, such that it is not clear whether either drug exerts its effects by affecting chromatin states [Rius and Lyko, 2012, Helin and Dhanak, 2013]. The lack of a detailed mechanism of action for these drugs has limited their broader use in cancer treatment [Dawson et al., 2012, Helin and Dhanak, 2013]. However, efforts to expand the range of epigenetically treatable cancers by means of combination epigenetic therapy have recently had encouraging outcomes in non-small cell lung cancer (NSCLC), AML, and CML [Fiskus et al., 2009, Zhang et al., 2010, Juergens et al., 2011, Fiskus et al., 2014]. Epigenetic modulation was further proposed to improve responses to subsequent chemotherapy or targeted cancer therapy, thereby raising efficacy limits of existing therapeutics [Essers et al., 2009, Juergens et al., 2011].

Several additional efforts to utilize altered chromatin states for the improvement of cancer care are underway. DNA methylation and histone modification patterns are investigated for their potential as biomarkers [Seligson et al., 2005, Brock et al., 2008]. The discovery of cancer cell subpopulations that demonstrate chromatin-mediated reversible drug tolerance or distinct slow-cycling behavior link cancer epigenetics to therapeutic resistance [Sharma et al., 2010, Roesch et al., 2010]. Of particular interest are a growing number of cancer-specific

epigenetic dependencies that have lead to the development of new pharmacologic agents for clinical evaluation with potentially fewer side effects [Helin and Dhanak, 2013, Cai et al., 2015]. Table 2 provides an overview of epigenetic therapies currently in (pre)clinical development. Three of these examples are discussed in more detail below.

Class	Epigenetic Regulator	Function	Relevant Diseases	Stage of Drug Development
DNA methyltransferases	DNMT1	Maintenance DNA methylation	MDS, CMML	FDA-approved (decitabine, azacitidine)
	DNMT3A	*de novo* DNA methylation	AML, MDS	Preclinical development
Histone methyltransferases	DOT1L	H3K79 methylation	AML, ALL	Phase I trial
	EZH2	H3K27 methylation	B cell lymphomas, Solid tumors	Phase I trial
Histone demethylases	LSD1	H3K4 demethylation	AML, SCLC	Phase I trial
Histone acetyltransferases	p300/CBP	H3K27 acetylation	AML, Prostate cancer	Preclinical development
Histone deacetylases	HDAC1, 2, etc.	Histone deacetylation	Multiple myeloma, Cutaneous T cell lymphomas, Peripheral T cell lymphomas	FDA-approved (panobinostat, vorinostat, romidepsin, belinostat)
Histone acetyl readers	BET	Binding acetylated lysines	AML, MDS, Lymphoma, Multiple myeloma, Glioblastoma multiforme, Solid tumors, NMC advanced	Phase I trial

Table 2. Epigenetic therapeutic targets in (pre)clinical development
AML, Acute myeloid leukemia; ALL, Acute lymphoid leukemia; CMML, Chronic myelomonocytic leukemia; MDS, Myelodysplastic syndrome; NMC, NUT midline carcinoma; SCLC, Small cell lung cancer. Table adapted from [Cai et al., 2015]

1.2.4 Targeting cancer-specific epigenetic dependencies

DOT1L

A prominent example of cancers driven by the mutation of an epigenetic regulator are acute leukemias harboring translocations of the *Mixed lineage leukemia 1* (*MLL1*) gene [Popovic and

Licht, 2012]. Wild-type (wt) MLL1 is a H3K4 methyltransferase. However, the chimeric fusion proteins generated by *MLL1* translocation do not contain the methyltransferase SET domain [Helin and Dhanak, 2013]. Instead, the catalytically inactive N terminus of MLL1 is fused to one of over 70 different partners, the most common being AF4, AF9, AF10, ENL, and ELL [Cai et al., 2015]. Several of these fusion partners interact with the histone methyltransferase DOT1L, which deposits activating H3K79 marks at MLL1-fusion genes and interferes with chromatin localization of repressive complexes (composed of SIRT1 and H3K9 methyltransferase SUV39H1) at these loci [Bernt et al., 2011, Chen et al., 2015a]. Activation of MLL1 target genes HOXA9 and MEIS1A is sufficient for leukemia transformation. Small-molecule-mediated inhibition of DOTL1 results in selective killing of leukemic cells expressing MLL1 fusions, with minimal effects on non-MLL1-translocated cells [Bernt et al., 2011].

EZH2

The histone methyltransferase EZH2 is part of Polycomb repressor complex 2 (PRC2) and catalyzes the repressive trimethylation of H3K27 (H3K27me3), which is associated with gene silencing and heterochromatin formation [Helin and Dhanak, 2013]. It was discovered that the activity of the PRC2 complex is antagonized by SWI/SNF chromatin remodelers [Wilson et al., 2010]. Malignant rhabdoid tumors (MRTs) harboring inactivating mutations in the core SWI/SNF component SNF5 exhibit robust PRC2-mediated repression, which modulates stem cell-associated gene expression programs to drive tumor growth [Wilson et al., 2010]. In fact, the absence of SNF5 expression confers a dependence on EZH2, and pharmacological inhibition of the methyltransferase activity of EZH2 selectively inhibits growth of MRT cell lines with SNF5 mutations but not those with wild type SNF5 [Knutson et al., 2013]. Mutations in SWI/SNF subunits are a frequent occurrence in various cancers (see below), and it was shown that EZH2 constitutes a requirement in ARID1A and PBRM1-mutant cancer lines as well [Kim et al., 2015]. Additionally, EZH2 amplification and overexpression has been found in a multitude of solid cancers, and EZH2 knockdown inhibits growth, invasion and migration in multiple tumor types [McCabe and Creasy, 2014]. Cancer-associated gain-of-function mutations that stimulate the H3K27 trimethylation activity of EZH2 have been identified in B cell lymphomas, and these cancers are also sensitive to small molecule inhibitors of EZH2 [McCabe and Creasy,

2014].

An alternative to small molecule-mediated inhibition of EZH2 was recently discovered in the form of a cell-permeable stabilized peptide, SAH-EZH2 [Kim et al., 2013]. This hydrocarbon stapled peptide mimics an α-helical domain of EZH2, disrupts PRC2 complexes and was shown to inhibit the growth of MLL-AF9 rearranged leukemia cells [Kim et al., 2013]. Disruption of PRC2 complexes in this manner might be a particularly attractive strategy in the aforementioned SWI/SNF mutant cancers, as it was discovered that these rely predominantly on the PRC2 stabilizing function of EZH2 and to a lesser extent on its catalytic activity [Kim et al., 2013].

Importantly, EZH2 seems to play a dual role in cancer as inactivating mutations in hematopoietic neoplasms have also been found [Cai et al., 2015]. It will thus be critical to evaluate potential on-target toxicities of EZH2-targeting compounds.

BRD4

Blocking enzymatic activities has predominated the field of targeted cancer therapy. The discovery of potent and effective inhibitors of Bromodomain-containing protein 4 (BRD4) has brought attention to epigenetic reader domains as potential drug targets. BRD4 is a member of the Bromodomain and extraterminal (BET) family and regulates transcription through interaction with several co-factors including P-TEFb and the Mediator complex [Cai et al., 2015]. The acetyl-lysine-binding bromodomain pocket can be targeted with small-molecules [Brand et al., 2014]. Inhibitors of the BET family of bromodomains, such as JQ1 and I-BET, bind their target bromodomains in an acetyl-lysine competitive manner leading to the displacement of BET proteins from chromatin [Filippakopoulos et al., 2010, Nicodeme et al., 2010].

Efficacy of BRD4 inhibitors was first described in NUT midline carcinomas. These cancers predominantly carry translocations between the *NUT* gene and *BRD4* [Cai et al., 2015]. Exposure to JQ1 displaced BRD4-NUT from chromatin, induced differentiation and arrested proliferation [Filippakopoulos et al., 2010]. Additionally, an unbiased RNAi screen to investigate the requirement of chromatin modulators for MLL-fusion AML identified BRD4 as critical for disease maintenance *in vivo*, while it was dispensable for growth of untransformed hematopoietic

lineages [Zuber et al., 2011b]. Screening of primary patient samples revealed that BRD4 is essential for the growth of the majority of AML subtypes, independent of the underlying genetic lesions [Zuber et al., 2011b]. A similar cancer-specific requirement for BRD4 was found in multiple myeloma and lymphoma [Delmore et al., 2011, Mertz et al., 2011]. Down-regulation of the *MYC* proto-oncogene was identified as a predominant effect of BRD4 inhibitors, and sensitive cells share a MYC addiction [Cai et al., 2015].

1.3 Roles of the SWI/SNF complex in cancer

The link between chromatin and cancer is not limited to epigenetic writers, erasers and readers. In fact, the most frequently mutated chromatin regulator in cancer is the SWI/SNF nucleosome remodeler [Kadoch et al., 2013].

1.3.1 Tumor suppressor functions of SWI/SNF

Two recently published meta-analyses of cancer genome sequencing data estimate that nearly 20 % of human cancers harbor mutations in one or more of the genes encoding the SWI/SNF complex [Kadoch et al., 2013, Shain and Pollack, 2013]. Such mutations are predominantly loss-of-function, implicating SWI/SNF as a major tumor suppressor in diverse cancers. Specific SWI/SNF subunit mutations are generally linked to a defined subset of cancer lineages: SNF5 is mutated in malignant rhabdoid tumors (MRT) [Versteege et al., 1998, Biegel et al., 1999], PBRM1 is frequently inactivated in renal carcinoma [Varela et al., 2011], and BRG1 is mutated in NSCLC among several others [Wong et al., 2000, Medina et al., 2008, Imielinski et al., 2012] (Table 3). The association of mutations in specific SWI/SNF subunits with unique tumor spectra implies that SWI/SNF performs multiple distinct tumor suppressor functions across these different malignancies rather than a single common protective activity.

The role of SNF5 in the pathogenesis of MRT has been most extensively characterized to date, owing to its early discovery as a tumor suppressor in 1998 [Versteege et al., 1998, Biegel et al., 1999]. Despite being a core subunit of SWI/SNF, loss of SNF5 does not disrupt the integrity of the complex but instead leads to gene-specific alterations of transcription in concert

Gene	Tumor
ARID1A	Bladder, Breast, CLL, Colorectal, DLBCL, Endometrioid, Gastric, HNSCC, Hepatocellular, Lung, Medulloblastoma, Melanoma, OCC, Pancreatic, Renal, SCC, TCC
ARID1B	Breast, Colorectal, DLBCL, Gastric, HNSCC, Hepatocellular, Lung, Melanoma, OCC
ARID2	Colorectal, Hepatocellular, Lung, Melanoma
BAF60A	Breast
BAF155	Colorectal
BCL7A	B-NHL, Multiple myeloma
BCL11A	Colorectal, Glioma, Lung, Melanoma, OCC
BCL11B	Colorectal, Hematopoietic, Melanoma
BRD7	CLL
BRG1	Breast, Colorectal, HNSCC, Hepatocellular, Lung, OCC, Pancreatic, Medulloblastoma, Melanoma, Rhabdoid, Prostate
BRM	Colorectal, HNSCC, Lung
DPF2	DLBCL
PBRM1	Breast, DLBCL, HNSCC, Lung, Pancreatic, Renal, SCC
SNF5	Chondrosarcoma, Chordoma, Epethelioid sarcoma, Familial schwannomatosis, Meningioma, Rhabdoid, Small-cell hepatoblastoma, Undifferentiated sarcoma

Table 3. Subunits of the SWI/SNF complex mutated in cancer.
Tumors - B-NHL, B cell non-Hodgkin lymphoma; CLL, Chronic lymphocytic leukemia; DLBCL, Diffuse large B cell lymphoma; HNSCC, Head and neck squamous cell carcinoma; OCC, Ovarian clear cell carcinoma; SCC, Squamous cell carcinoma; TCC, transitional cell carcinoma
Compiled from [Wilson and Roberts, 2011, Dawson and Kouzarides, 2012, Kadoch et al., 2013, Shain and Pollack, 2013]. Conditions for inclusion: >3% mutation frequency [Kadoch et al., 2013]; >1 mutation per gene per tumor type [Shain and Pollack, 2013].

with the aforementioned unopposed silencing activity of PRC2 complexes in SNF5-mutant cancers [Doan et al., 2004]. The resulting gene expression changes deregulate several oncogenic signaling pathways, including HEDGEHOG, WNT, and MYC [Jagani et al., 2010, Wang et al., 2011a, Mora-Blanco et al., 2014] .

The mechanisms underlying tumorigenesis provoked by mutations in SWI/SNF subunits other than SNF5 are less well understood but are likely to differ between individual subunits. ARID1A and BRG1 have been implicated in preventing DNA entanglements during mitosis, hence their mutational inactivation could lead to genomic instability in addition to altered gene expression [Dykhuizen et al., 2013]. In several cellular contexts, loss of SWI/SNF function leads to impaired cell differentiation or even de-differentiation, which is a hallmark of many cancers [Romero et al., 2012, Eroglu et al., 2014]. SWI/SNF mutations can be mutually exclusive with other tumor suppressor mutations (e.g. PTEN and p53) in certain tumor types, suggesting that SWI/SNF could perform tumor protective functions that overlap with known pathways [Kadoch et al., 2013, Shain and Pollack, 2013].

1.3.2 Synthetic lethality-based SWI/SNF dependencies

Targeting the aberrant molecular pathways of cancer cells is the central paradigm of modern cancer therapy. Restoring the lost functions of an inactivated tumor suppressor is, however, far more difficult than inhibiting the function of a hyperactive oncoprotein. An alternative to reviving inactivated tumor suppressors is to target dependencies created by their absence, thereby exploiting synthetic-lethal genetic interactions [Kaelin, 2005]. Synthetic lethality describes a scenario in which mutations in either of two (or more) individual genes are compatible with cell viability, while simultaneous mutation of both genes results in cell death. As an example, the antagonism between SNF5 and EZH2, described above, renders SNF5-mutant tumors dependent on EZH2 for disease maintenance and illustrates how SWI/SNF mutations can create cancer-specific chromatin regulator dependencies [Wilson et al., 2010, Knutson et al., 2013].

When a mutated tumor suppressor is part of a multi-subunit protein complex, such as SWI/SNF, the question arises whether it is the lost function of the mutated subunit, the disassembly of the entire complex, or the deregulated activities of an aberrant residual complex that drive tumor growth and could be targeted. In the case of SNF5-mutant cancers it was found that the inactivation of this subunit is not equivalent to a complete loss of SWI/SNF function, as biochemical studies showed that SNF5 is dispensable for the integrity of SWI/SNF complexes and for specific cellular transcriptional functions of BRG1 [Doan et al., 2004]. RNAi-based knockdown of the residual SWI/SNF complexes in human MRT cell lines revealed that SNF5-deficient cells were dependent on BRG1 for their proliferation, whereas BRG1 was dispensable in various SNF5-proficient cancer lines [Wang et al., 2009]. This result was further verified in a genetically-engineered mouse model of SNF5-mutant lymphoma, which was also found to be dependent on BRG1 for disease progression *in vivo* [Wang et al., 2009]. This study suggested that loss of a single SWI/SNF subunit might drive tumorigenesis by unmasking an oncogenic function of residual BRG1-containing SWI/SNF complexes [Wang et al., 2009]. However, the observed dependence could also be explained by the residual SWI/SNF complex performing a lineage-specific function in allowing cell survival, as BRG1 is also essential for normal lymphoid development [Chi et al., 2003]. While elucidation of the underlying mechanism will require

further investigation, these observations suggest that targeting residual SWI/SNF complexes could be a therapeutic strategy in SWI/SNF-mutant cancers.

Importantly, an analogous dependence on residual SWI/SNF activity has been also been found in other SWI/SNF-mutant tumors. The SWI/SNF ATPase subunit BRG1 is mutationally inactivated or epigenetically silenced in diverse cancers, including NSCLC, medulloblastoma, and Burkitt's lymphoma [Imielinski et al., 2012, Robinson et al., 2012, Love et al., 2012]. A study investigating the importance of the BRG1 homolog BRM across a panel of human cancer cell lines revealed that knockdown of BRM led to growth inhibition in all BRG1-deficient NSCLC lines but not in wild type BRG1 proficient cancer or untransformed cells [Oike et al., 2013]. Re-introduction of wild type BRG1 cDNA in BRG1-deficient cell lines could alleviate the BRM requirement, thus verifying the causal relationship between the genetic status of BRG1 and the level of addiction to BRM [Oike et al., 2013]. Importantly, BRG1-deficiency can often co-occur with epigenetic silencing of the BRM gene in primary NSCLC tumors, such that this synthetic lethal interaction is likely to be relevant only in a subset of BRG1-mutant tumors [Reisman et al., 2003, Oike et al., 2013]. The synthetic lethal interaction between BRG1 and BRM has been independently corroborated by two other studies that used unbiased negative-selection shRNA screens [Hoffman et al., 2014, Wilson et al., 2014]. Both screening strategies evaluated dependencies across a large panel of human cancer cell lines with known genetic backgrounds and revealed BRM as a top cancer dependency in cell lines with BRG1 mutations [Hoffman et al., 2014, Wilson et al., 2014]. These studies highlighted that, not only NSCLC, but also ovarian, liver, endometrial and skin cancer cell lines with complete loss of BRG1 were sensitive to BRM knockdown [Hoffman et al., 2014, Wilson et al., 2014].

A similar synthetic lethal interaction has also been uncovered between ARID1A and ARID1B [Helming et al., 2014]. ARID1A is one of the most commonly mutated subunits of SWI/SNF with mutations occurring in a broad spectrum of cancers [Kadoch et al., 2013]. ARID1B is also inactivated in certain cancers, albeit at a lower frequency [Kadoch et al., 2013]. Through large-scale negative selection shRNA screens, ARID1B was identified as the top differential dependency among ∼10,000 candidate genes that was selectively required for growth of ARID1A-mutant as compared to ARID1A wild type lines [Helming et al., 2014]. Interestingly, ARID1B

and ARID1A are often co-mutated in human cancer, but these tumors always retain one copy of a wild type ARID1B allele, which presumably is sufficient to preserve residual SWI/SNF complexes necessary for tumor viability [Helming et al., 2014]. This study raises the possibility that synthetic lethal interactions might exist more broadly between mutated SWI/SNF subunits and their wild type paralogs.

1.3.3 A tumor-maintenance function for BRG1-SWI/SNF in acute leukemias

As SWI/SNF is an integral component of numerous transcriptional programs, cancers that are driven by aberrant transcriptional regulators and chromatin modifiers could conceivably become reliant on SWI/SNF to sustain a transformed cellular state, even in the absence of genetic alterations in the complex. As highlighted above, AML is an example of a malignancy that is driven in large part by mutations in transcription factors, chromatin modifiers, and DNA methylation machinery [Network et al., 2013]. However, SWI/SNF mutations are rarely found in this particular cancer, suggesting that the complex does not perform a significant tumor suppressor function in this context [Network et al., 2013].

In contrast, our lab has found that AML mouse models and human cell lines are particularly dependent on BRG1 for disease progression [Shi et al., 2013]. By means of an shRNA screen performed in cells derived from a mouse model of MLL-rearranged AML, our group identified BRG1 as a top chromatin regulator dependency in this cancer [Zuber et al., 2011b]. A ∼4-fold reduction of BRG1 levels triggered leukemia cell apoptosis and terminal differentiation, while a similar degree of knockdown in non-hematopoietic cell lines (e.g. fibroblasts and various carcinomas) had no effect on cell proliferation or viability [Shi et al., 2013]. Using a conditional knockout allele, it was independently shown that BRG1 is essential for AML initiated by overexpression of the Hoxa9/Meis1 transcription factor oncoproteins, with BRG1-deficient leukemia cells undergoing cell cycle-arrest and apoptosis [Buscarlet et al., 2014].

Mechanistically, it was found that BRG1 is critical for maintaining expression of specific genes within the transcriptional program induced by the MLL-AF9 oncoprotein, including *Myc* and

Hoxa9 [Shi et al., 2013]. The role of BRG1 in maintaining *MYC* transcription appears to be unique to normal and malignant hematopoietic cells, as BRG1 knockdown in other cell lineages was found to have negligible effects on MYC expression [Chi et al., 2003, Shi et al., 2013]. To account for this observation, it was shown that BRG1 occupies a cluster of 3' enhancer elements at the *MYC* locus that are only activated in hematopoietic cells [Shi et al., 2013]. At these distal enhancers, BRG1 is critical to sustain occupancy of several hematopoietic transcription factors and for long-range enhancer-promoter looping interactions [Shi et al., 2013]. Furthermore, the ATPase activity of BRG1 is critical for its leukemia maintenance function, consistent with nucleosome remodeling of enhancer elements being essential for transcription factor occupancy [Shi et al., 2013]. These results suggest that leukemia cells promote *MYC* transcription through a unique enhancer-based mechanism, which is particularly sensitive to SWI/SNF perturbation.

1.4 Targeting the SWI/SNF complex for cancer therapy

The aforementioned genetic evidence provides ample rationale to pursue pharmacological SWI/SNF inhibition. A BRG1/BRM bromodomain inhibitor has been developed but did not affect the growth of either BRG1-deficient lung cancer or AML cells [Vangamudi et al., 2015]. This finding is not surprising, however, given that cDNA rescue experiments linked the BRG1 ATPase to cancer maintenance but did not implicate the bromodomain in this function [Shi et al., 2013]. Small-molecule ATPase inhibitors of BRG1/BRM would be essential to study the response of cancer cells to acute inactivation of the SWI/SNF remodeling function. However, strategies to inhibit this function pharmacologically have yet to be achieved. Importantly, BRG1 knockout mice show severe developmental abnormalities, and potential toxicities of BRG1 inhibition in a fully-developed animal remain to be examined [Bultman et al., 2000]. In light of the critical roles of BRG1 in normal development and tumor suppression, tolerability of BRG1 ATPase inhibitors might pose a key challenge.

While it appears that SWI/SNF-mutant cancers are often exquisitely sensitive to perturbations of the mutated subunit's paralog, AML cells display a BRG1 dependence in the absence of SWI/SNF mutations and might thus depend on the complex as a whole. We hypothesized that

an alternative approach to exploit the SWI/SNF-dependence of AML cells could be to target subunits other than BRG1. The significance of these proteins to cancer-relevant SWI/SNF functions would first need to be established, but they might provide opportunities for more selective perturbations of the complex with potentially greater tolerability in other tissues. Importantly, several other SWI/SNF subunits contain bromodomains: PBRM1, BRD7, and BRD9. The pharmacological tractability of BET bromodomains has prompted efforts to develop compounds targeting other bromodomain-containing proteins to explore biological activities and therapeutic potential. As a result, bromodomains outside of the BET family, such as those of CBP, BAZ2B, and TRIM24, have now also been successfully targeted [Hay et al., 2014, Bennett et al., 2015, Chen et al., 2015b]. PBRM1, BRD7 and BRD9 are thus theoretically targetable with small-molecule inhibitors. BRD7 and BRD9 are homologous proteins and were only recently identified as SWI/SNF associated factors [Middeljans et al., 2012]. BRD7, like PBRM1, is a subunit of SWI/SNF-B (PBAF) and was found to be mutually exclusive with BRD9, which was purified as part of SWI/SNF-A (BAF) complexes [Middeljans et al., 2012]. Data from The Cancer Genome Atlas shows that PBRM1 and BRD7 are mutated in different cancers [Wilson and Roberts, 2011, Dawson and Kouzarides, 2012], and BRD7 was validated to have tumor suppressor functions in human fibroblasts, breast tumors and nasopharyngeal carcinoma cells [Peng et al., 2007, Harte et al., 2010, Drost et al., 2010]. In contrast, BRD9 is predominantly amplified across a variety of different cancer samples available through The cBioPortal for Cancer Genomics (unpublished observation), and preliminary data from our own group suggested a possible role in the maintenance of AML proliferation [Gao et al., 2013, Cerami et al., 2012].

The overall aim of this study was to assess the potential of interfering with SWI/SNF function in leukemia through subunits other than BRG1. To this end, we evaluated the role of bromodomain-carrying SWI/SNF subunits and identified BRD9 as a critical requirement for the proliferation of mouse and human AML cells (Chapter 2). We found that BRD9 requires its bromodomain to maintain Myc expression and prevent differentiation of AML blasts (Chapter 2). Based on our genetic evidence for the importance of the BRD9 bromodomain in leukemia maintenance, our collaborators at Boehringer Ingelheim generated small-molecule inhibitors

that I found reduce SWI/SNF-chromatin binding and selectively limit the growth of AML cells (Chapter 3).

1.5 A need for better tools to establish the cellular target of chromatin-modulating compounds

Due to the structural similarities of bromodomains and the conservation of acetyl-lysine binding residues, generating bromodomain inhibitors that selectively interfere with a single bromodomain has proven to be challenging [Filippakopoulos and Knapp, 2014]. JQ1 and I-BET, for example, inhibit all members of the BET bromodomain subfamily (BRD2, BRD3, BRD4 and BRDT) [Filippakopoulos et al., 2010, Nicodeme et al., 2010]. Similarly, our own BRD9 inhibitors bind to BRD9, BRD7 and CECR2 bromodomains (Chapter 3). This complicates the assignment of phenotypic effects to a specific bromodomain target. Importantly, this complication is not limited to bromodomain inhibitors. Achieving selectivity, both within a family of conserved protein domains and across the diverse proteome of the cell is a general challenge in developing tool compounds [Arrowsmith et al., 2015]. While biochemical methods exist to identify the binding partners of a small-molecule, such approaches offer little insight into the physiological relevance of the identified interactions [Schenone et al., 2013]. As was recently highlighted by the Chemical Probes Portal initiative, adequate characterization of tool compounds is paramount to facilitate conclusive, reproducible results [Arrowsmith et al., 2015]. However, establishing on-target activity of chemical probes in cells is a major challenge.

Strong support for a physiologically important drug-target interaction is lent by naturally arising or engineered mutations in a target protein that confer resistance to a compound of interest [Arrowsmith et al., 2015]. Such mutants generally need to preserve protein function in the cell, but abrogate binding of the chemical inhibitor. While such mutants have been successfully used in the study of kinase inhibitors (e.g. gatekeeper mutations), a genetic strategy has yet to be devised to establish the relevant targets of the expanding class of chromatin-modulating small molecules [Balzano et al., 2011]. In this study, we present a *BRD9* bromodomain-swap allele, which retains functionality, but is insensitive to inhibitor binding (Chapter 4). We employ this allele to validate BRD9 as the cellular target underlying the phenotypic consequences of

AML cell exposure to our BRD9 inhibitors (Chapter 4). We further present a complementary approach, which couples RNA-Seq and Gene Set Enrichment Analysis (GSEA), and provides independent support for BRD9 being the key target of our inhibitors (Chapter 4). Lastly, we extend the domain-swap approach to validate the relevant target of a second chromatin-modifying compound, thereby demonstrating that this assay might have broader utility as a tool to discriminate on-target from off-target effects in cells (Chapter 5).

2 Genetic perturbation of BRD9 function in AML cells

2.1 A role of SWI/SNF subunit BRD9 in AML maintenance

2.1.1 BRD9 is a SWI/SNF subunit in AML cells

Prior work in our lab had identified the BRG1 ATPase of the SWI/SNF chromatin remodeling complex as essential for AML growth [Shi et al., 2013]. However, direct chemical inhibition of BRG1 in cancer cells has yet to be achieved, and might be associated with on-target toxicities in other tissues. Therefore, we pursued a strategy of indirect BRG1 modulation by targeting subunits of its associated SWI/SNF complex. As SWI/SNF composition is known to vary depending on cell type, we initially sought to define BRG1-associated SWI/SNF subunits in AML cells [Wu et al., 2009]. To this end, we immunoprecipitated endogenous BRG1 from human MLL-AF9/KRAS^{G13D} AML cell nuclear lysates (NOMO-1 cell line) and analyzed the co-precipitated proteins by iTRAQ mass spectrometry. Unlike the control antibody (IgG), the BRG1 antibody precipitated several well-established SWI/SNF subunits alongside BRG1 itself. Additionally, we detected peptides derived from BRD9, but not the other bromodomain-containing subunits BRD7 or PBRM1 in two independent replicates (Fig. 5a). BRD9 is a largely unstudied SWI/SNF subunit, and its role in the complex remains to be evaluated [Middeljans et al., 2012, Kadoch et al., 2013]. The recovery of BRD9 as a BRG1-associated protein in AML cells was unexpected, since a prior report had found that Brd9 was absent from SWI/SNF complexes isolated from murine leukemia cells, which instead contained the homologous protein Brd7 [Buscarlet et al., 2014]. We thus sought to assess the BRG1-BRD9 linkage in an independent assay. Following the rationale that proteins which are part of the same complex co-occur across the genome, we compared the chromatin occupancy of both proteins by Chromatin Immunoprecipitation-Sequencing (ChIP-Seq) in murine MLL-AF9/Nras^{G12D} AML cells (RN2 cell line) [Zuber et al., 2011a]. Following MACS peak calling of the mapped sequencing reads obtained from Brg1 ChIP-Seq, we considered high confidence Brg1 binding sites as those with a false discovery rate (FDR) < 0.05 % and a fold enrichment over input of greater than 5 (Fig. 5b). These sites ('peaks') were partitioned into promoters and enhancers based on their

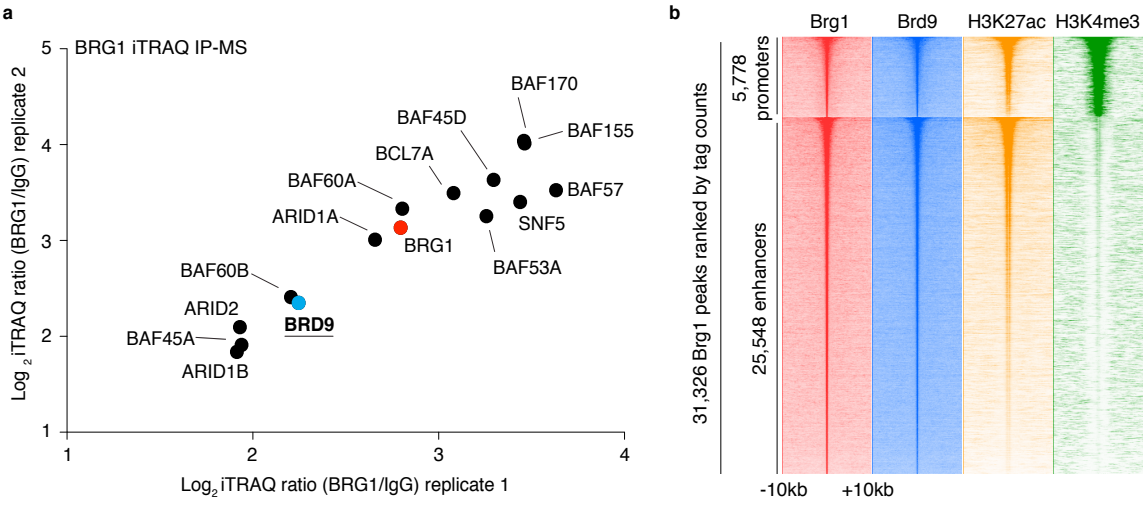

Figure 5. BRD9 associates with SWI/SNF complexes in AML cells.
(a) iTRAQ IP-MS using BRG1 and IgG antibodies and NOMO-1 cell nuclear extracts to identify BRG1-associated factors. Log-transformed iTRAQ ratios of two independent replicates are plotted for all precipitated proteins previously reported to be part of the SWI/SNF complex [Kadoch et al., 2013, Middeljans et al., 2012]. Data collected by Junwei Shi.
(b) Density plot of different ChIP-Seq datasets in RN2 cells centered on Brg1 peaks. Brg1 peaks were identified by MACS peak calling and all peaks with a false discovery rate (FDR) <0.05 % and a fold enrichment over input of greater than 5 were included. The plot depicts tag counts in 50 bp bins in the +/-10 kb region surrounding the Brg1 peak center. Each row represents a single peak. Data collected by Jae-Seok Roe.

overlap with annotated transcription start sites (TSS) - if the Brg1 binding site showed at least 1 bp overlap with a +/- 200 bp window surrounding RefSeq gene TSSs, it was considered a promoter, otherwise it was classified as an enhancer. ChIP-Seq datasets of the active chromatin mark H3K27ac and the promoter mark H3K4me3 in RN2 cells were used to assess the accuracy of this partitioning (Fig. 5b). Plotting the Brd9 ChIP-Seq read counts at the Brg1 peak regions revealed a striking co-occurrence of Brd9 at Brg1 chromatin binding sites across the genome at both, acetylated promoters and enhancers, which is consistent with both proteins existing in one complex in these cells (Fig. 5b, 6a). Like Brg1, Brd9 was significantly enriched at the promoter as well as the distal cluster of enhancers (or super-enhancer) of the *Myc* proto-oncogene in RN2 cells, which are elements through which Brg1 regulates Myc expression in this cell type as explained above (Fig. 6a) [Shi et al., 2013]. Binding of BRD9 to the *MYC* promoter and enhancer region was also observed in ChIP-Seq datasets obtained from NOMO-1 cells using two independent BRD9 antibodies (Fig. 6b, c).

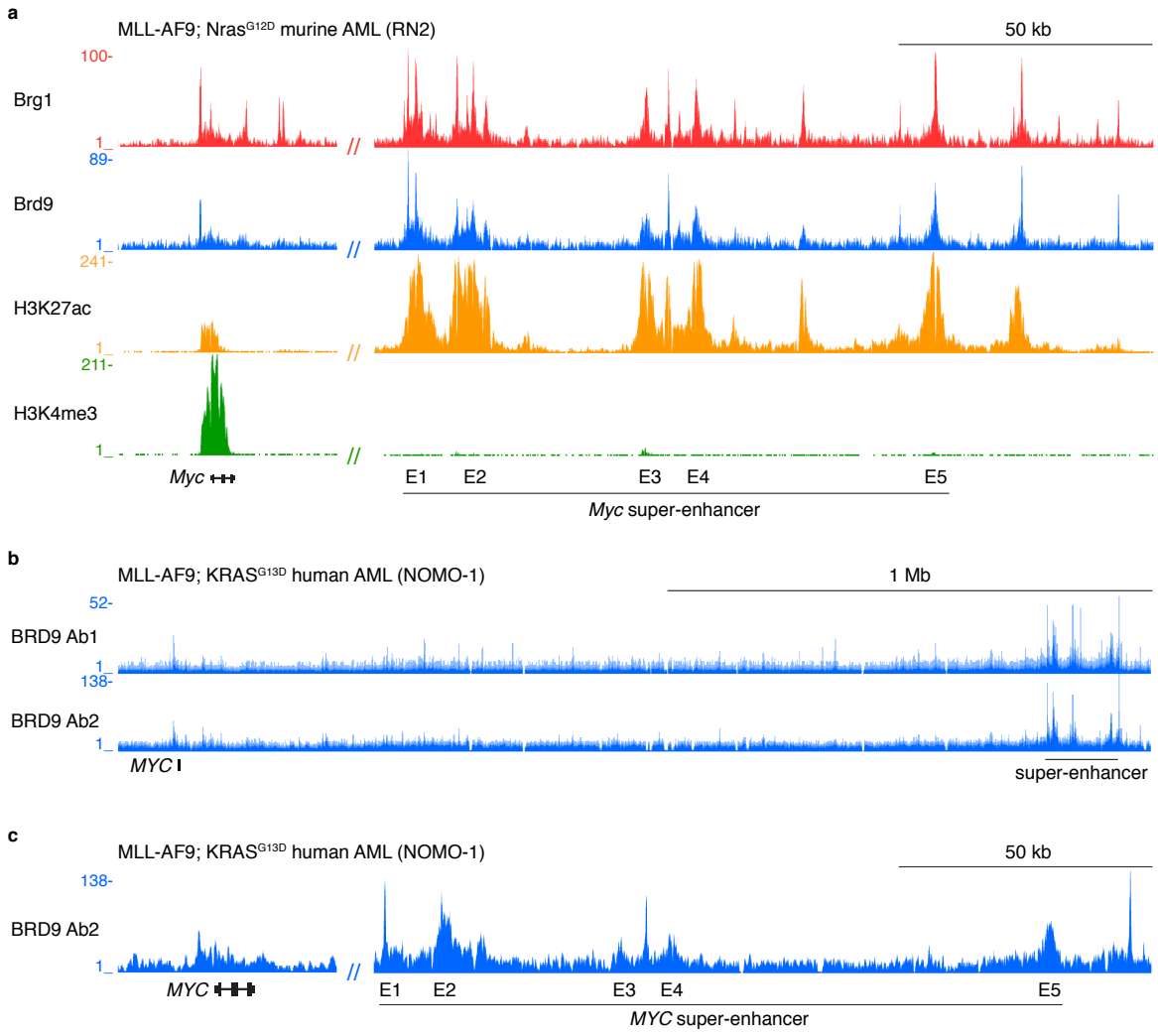

Figure 6. BRD9 binds the *MYC* enhancer in AML cells.
(a) ChIP-Seq occupancy profiles for Brg1, Brd9, H3K27Ac and H3K4me3 at the *Myc* locus and enhancer in RN2 cells. The y-axis reflects the number of cumulative tag counts within a 50-100 bp bin surrounding each region.
(b) ChIP-Seq occupancy profiles for BRD9 at the *MYC* locus in NOMO-1 cells derived using two different antibodies for BRD9. The y-axis reflects the number of cumulative ChIP-Seq tag counts within a 50-100 bp bin surrounding each region. Ab1: Bethyl #A303-781A; Ab2: Abcam #ab66443.
(c) Magnified ChIP-Seq occupancy profile of BRD9 at the *MYC* promoter and super-enhancer region in NOMO-1 cells.
Data collected by Jae-Seok Roe.

When ranking BRD9-occupied sites from lowest to highest ChIP-Seq read counts, it became apparent that the *Myc* enhancer elements were among the most highly occupied BRD9-binding sites in both RN2 and NOMO-1 cells (Fig. 7). Collectively, these findings suggest that BRD9 constitutes a SWI/SNF subunit in AML.

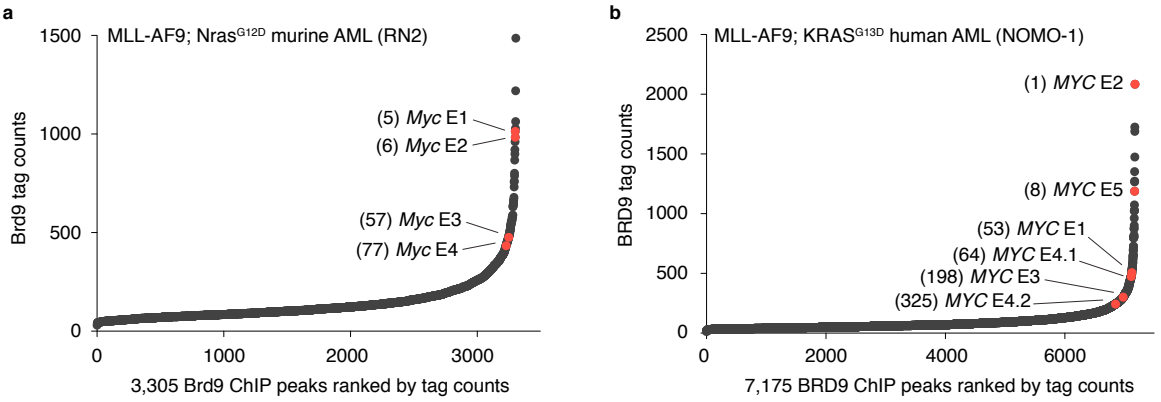

Figure 7. The *MYC* enhancer is among the most highly occupied BRD9 binding sites.
(a) Ranking of Brd9-occupied sites based on tag counts obtained from ChIP-Seq analysis in RN2 cells.
(b) Ranking of BRD9-occupied sites based on tag counts obtained from ChIP-Seq analysis in NOMO-1 cells.
Data collected by Jae-Seok Roe.

2.1.2 BRD9 supports AML cell proliferation

Having identified BRD9 as a BRG1-associated factor in AML cells, we next performed functional experiments to evaluate whether Brd9 acts in a similar manner to Brg1 in supporting leukemia maintenance. Using a competition-based proliferation assay, we evaluated the effect of shRNA-mediated Brd9 knockdown on AML cell growth. RN2 cells were transduced with Brd9 shRNAs and hairpin-expressing cells were identified by the co-expression of GFP (linked to our shRNAs through an IRES) two days post infection. The percent of GFP positive cells in culture was then tracked over at least 12 days. In this assay, shRNAs that target genes which do not impact the proliferative capacity of the investigated cells (such as our control hairpin targeting *Renilla* luciferase, shRen) generally show stable GFP percentages over time. In contrast, shRNAs

targeting genes that support or limit cell proliferation, generally show decreases and increases in GFP percentages, respectively. Similar to shBrg1-transduced cells, shBrd9-expressing cells were rapidly outcompeted by untransduced cells during culturing indicating a leukemia maintenance function of Brd9 (Fig. 8a). A shortcoming when working with shRNAs is the potential off-target

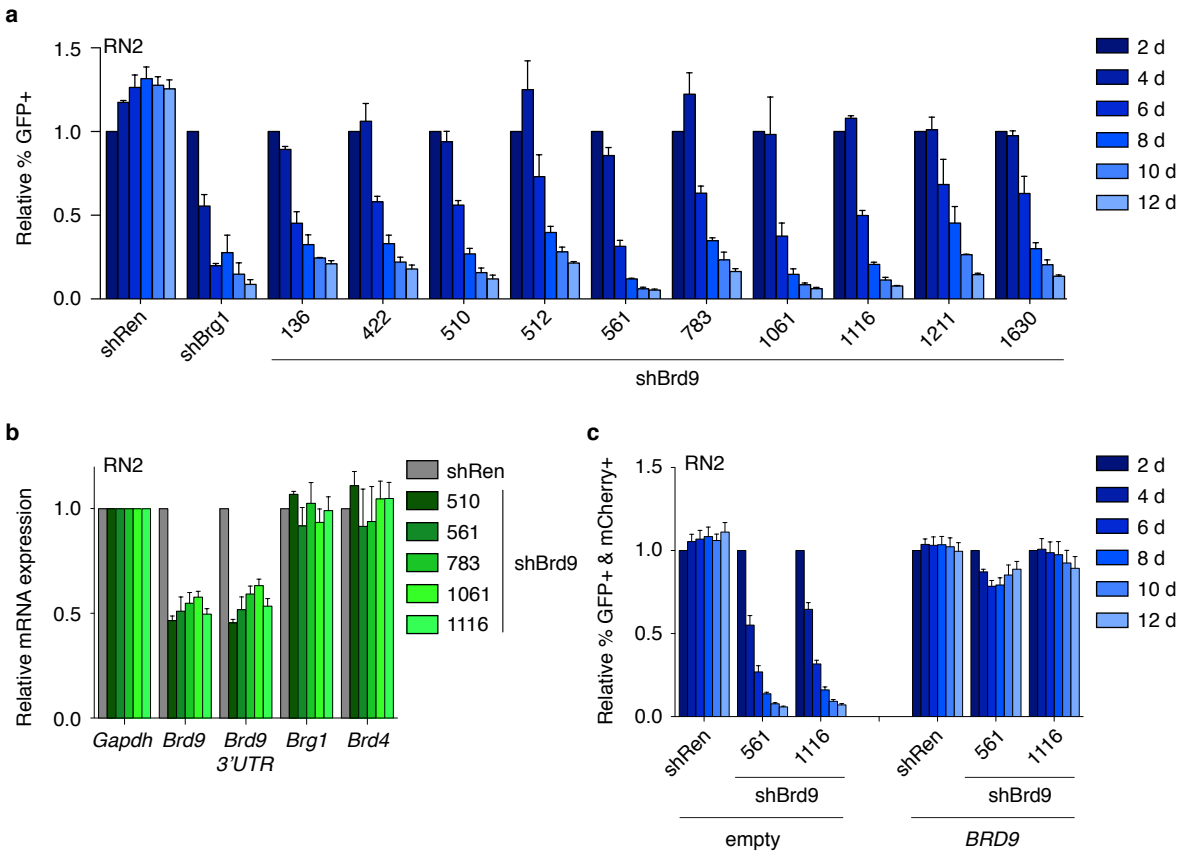

Figure 8. Brd9 is required for the proliferation of AML cells.
(a) Competition-based assay to measure the effect of shRNAs on the growth of RN2 cells. Transduced (shRNA-expressing) cells were identified by the co-expression of GFP (LMN vector). The percentage of GFP+ cells was tracked over 12 days and normalized to the GFP percentage on day 2. n = 2-3
(b) qRT-PCR analysis to test knockdown the efficiency of Brd9 shRNAs in RN2 cells. mRNA levels were examined after 48 hours of shRNA expression (TRMPV-Neo vector). Values were normalized to Gapdh within each sample and to shRen values across samples. n = 2-7
(c) cDNA complementation assay to demonstrate on-target effects of shRNAs. BRD9 (linked to GFP, MSCV-based vector) was expressed in RN2 cells prior to expression of shRNAs (linked to mCherry, LMN vector). The percentage of double positive cells was tracked and normalized to day 2 values. n = 4-6
shRen targets Renilla luciferase and serves as a negative control. All error bars in this figure represent SEM.

activity of individual hairpins. The reproducibility of the phenotype with ten independent shRNAs targeting different regions along the *Brd9* gene was therefore important. Additionally, we confirmed that our Brd9 hairpins had no off-target effect on the mRNA levels of the known leukemia dependencies Brg1 or Brd4 in RN2 cells by qRT-PCR (Fig. 8b). As further evidence for the depletion effects occurring as a consequence of Brd9 knockdown, expression of a human *BRD9* cDNA, which is not recognized by the shRNAs targeting murine Brd9, rescued the growth-arrest phenotype (Fig. 8c).

To rule out the possibility that Brd9 constitutes a general requirement for the proliferation of all cells, which would limit the potential therapeutic window of Brd9 targeting, we repeated the competition-based proliferation assay in immortalized mouse embryonic fibroblasts (iMEFs). In contrast to the effects observed in AML cells, Brd9 knockdown did not influence the growth of iMEFs, although shRNAs were functional and reduced Brd9 mRNA levels in these cells (Fig. 9). This is a similar context-dependence as observed previously with Brg1 knockdown [Shi

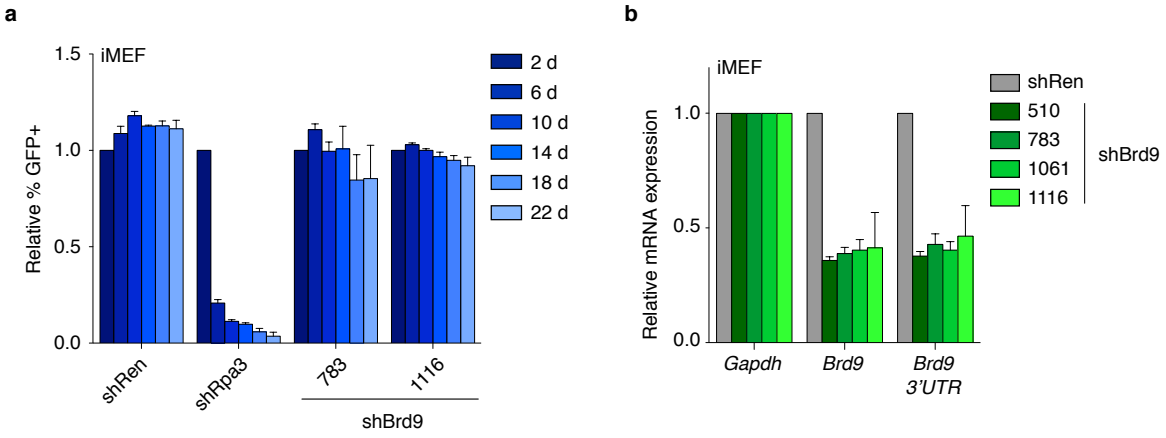

Figure 9. Brd9 is dispensable for the proliferation of iMEF cells.
(a) Competition-based assay to measure the effect of Brd9 shRNAs on the growth of iMEF cells. Transduced (shRNA-expressing) cells were identified by the co-expression of GFP (LMN vector). The percentage of GFP+ cells was normalized to the GFP percentage on day 2. shRpa3 targets Replication Protein A3 and serves as a positive control. n = 2-3. Data collected by Joseph Milazzo.
(b) qRT-PCR analysis to test knockdown the efficiency of Brd9 shRNAs in iMEF cells. mRNA levels were examined after 48 hours of shRNA expression (TRMPV-Neo vector). Values were normalized to Gapdh within each sample and to shRen values across samples. n = 2
shRen targets Renilla luciferase and serves as a negative control. All error bars in this figure represent SEM.

et al., 2013].

The closest homolog of Brd9 is Brd7. To evaluate whether the leukemia maintenance function was unique to Brd9 or potentially shared with Brd7, we identified six Brd7 shRNAs that effectively reduced Brd7 mRNA levels in RN2 cells (Fig. 10b). Interestingly, knockdown of Brd7 did not impair RN2 cell expansion (Fig. 10a). Instead it appeared that four out of six Brd7 hairpins were positively selected during culturing, which suggests that Brd7 might instead restrict proliferation in these cells. This finding led to the idea that Brd7 and Brd9 might perform opposing functions in leukemia cells by directly antagonizing each other as alternative subunits of the SWI/SNF complex. To investigate whether the Brd7-Brd9 balance might determine the proliferative capacity of AML cells, we carried out double knockdown experiments. Simultaneous knockdown of Brd7 and Brd9, however, did not equal the state in which neither of the two proteins was targeted. In fact, there was no difference in the depletion of cells in which Brd7 and Brd9 were knocked down and cells in which only Brd9 had been targeted (Fig. 10c). It thus appears that these proteins do not balance each others effects, but rather that the requirement of Brd9 for AML growth outweighs the capacity of Brd7 to limit proliferation.

To evaluate the BRD9 requirement in human cells, we validated shRNAs that decrease human BRD9 protein levels (as assayed by Western Blot) and assessed their effect on the growth of a panel of 15 human cancer cell lines using the competition-based proliferation assay (Fig. 11). This cell line panel included several different liquid and solid cancer types to allow evaluation of context-specific BRD9 dependencies. Our analysis revealed that the majority of myeloid leukemia cell lines spanning diverse genetic backgrounds were dependent on BRD9 for cell expansion. In contrast, the growth of several epithelial cancer lines was found to be insensitive to BRD9 knockdown (Fig. 11c, d). Among the profiled cells were two lung cancer lines (A549 and H1299), which carry mutations in the *SMARCA4* gene, are deficient in BRG1 expression and require the alternative SWI/SNF ATPase BRM for their growth, which raised the possibility that these cells might rely on the entire residual SWI/SNF complex. While the SWI/SNF incorporation of Brd9 in these cells remains to be investigated, Brd9 did not constitute a dependency in these cells. A quick analysis of cancer cell DNA sequencing and copy number

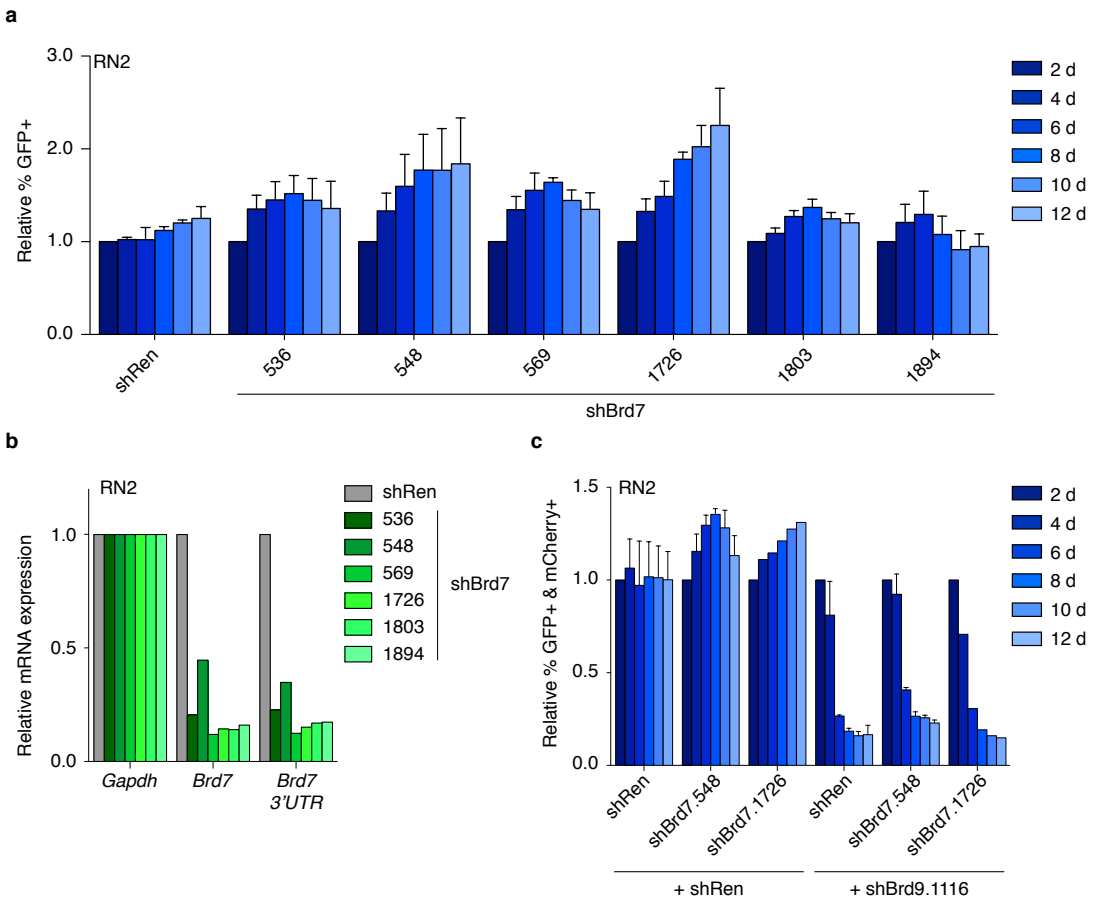

Figure 10. Brd7 is not required for the proliferation of AML cells.
(a) Competition-based assay to measure the effect of Brd7 shRNAs on the growth of RN2 cells. Transduced (shRNA-expressing) cells were identified by co-expression of GFP (LMN vector). The percentage of GFP+ cells was normalized to the GFP percentage on day 2. n = 2-3
(b) qRT-PCR analysis to test Brd7 shRNA knockdown efficiency in RN2 cells. mRNA levels were examined after 48 hours of shRNA expression (LMN vector). Values were normalized to Gapdh expression within each sample and to shRen values across samples. n = 1
(c) Competition-based assay to measure the effect of Brd7 and Brd9 double knockdown on the growth of RN2 cells. Doubly-transduced (double shRNA-expressing) cells were identified by the co-expression of GFP and mCherry (LMN vector). The percentage of GFP+ and mCherry+ cells was normalized to the double positive percentage on day 2. n = 1-2
shRen targets Renilla luciferase and serves as a negative control. All error bars in this figure represent SEM.

alteration data available through the cBioPortal, an online tool for the analysis and visualization of cancer genomics, had revealed that the *BRD9* gene is predominantly amplified and only rarely mutated or deleted across a variety of solid tumors [Gao et al., 2013, Cerami et al., 2012]. The functional significance of *BRD9* amplifications in cancer, however, is unknown. Our cell line

panel contained one breast cancer cell line (HCC1954) with a focal amplification involving the *BRD9* gene. We observed elevated levels of BRD9 mRNAs in these cells by qRT-PCR, but

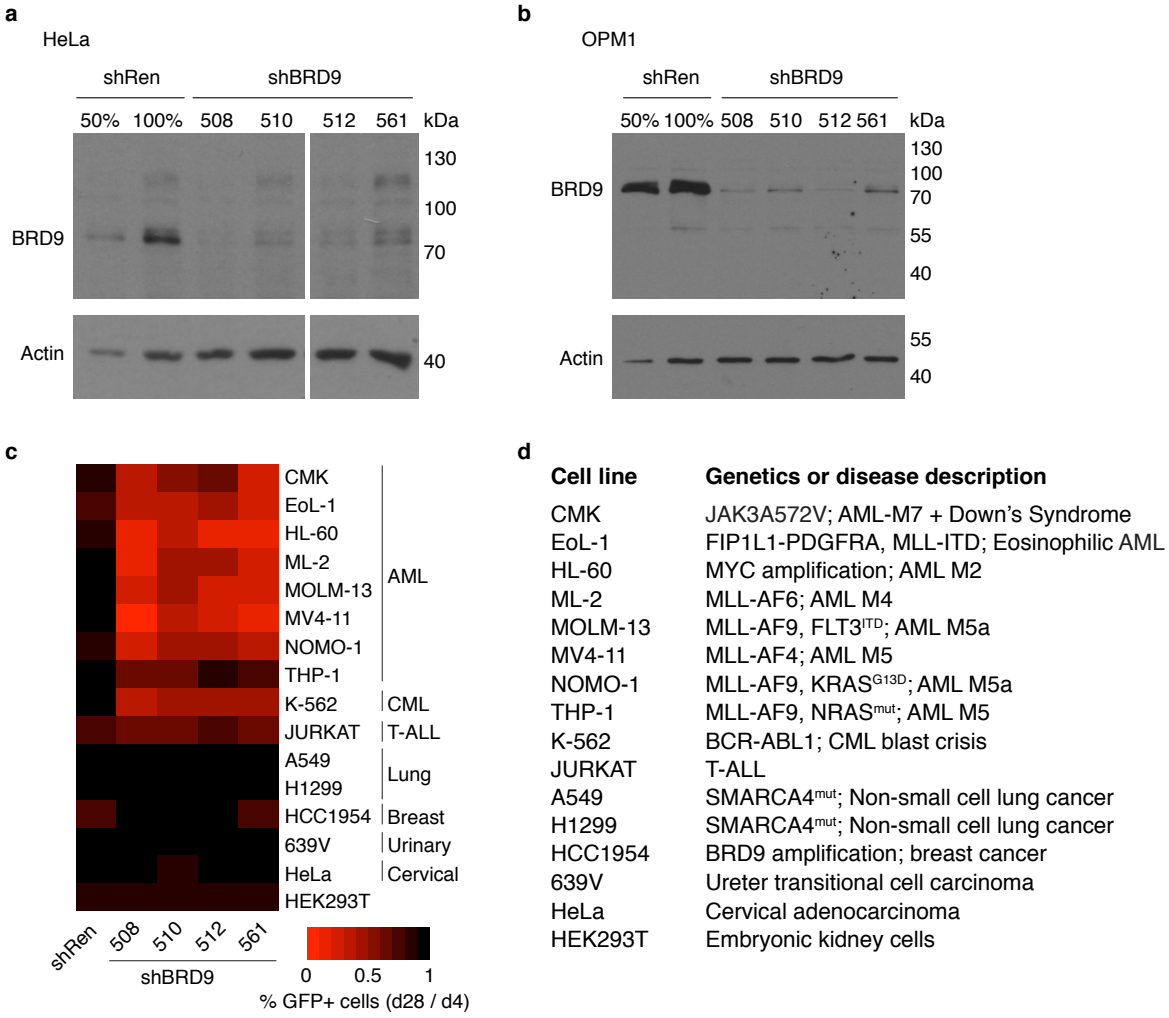

d

Cell line	Genetics or disease description
CMK	JAK3A572V; AML-M7 + Down's Syndrome
EoL-1	FIP1L1-PDGFRA, MLL-ITD; Eosinophilic AML
HL-60	MYC amplification; AML M2
ML-2	MLL-AF6; AML M4
MOLM-13	MLL-AF9, $FLT3^{ITD}$; AML M5a
MV4-11	MLL-AF4; AML M5
NOMO-1	MLL-AF9, $KRAS^{G13D}$; AML M5a
THP-1	MLL-AF9, $NRAS^{mut}$; AML M5
K-562	BCR-ABL1; CML blast crisis
JURKAT	T-ALL
A549	$SMARCA4^{mut}$; Non-small cell lung cancer
H1299	$SMARCA4^{mut}$; Non-small cell lung cancer
HCC1954	BRD9 amplification; breast cancer
639V	Ureter transitional cell carcinoma
HeLa	Cervical adenocarcinoma
HEK293T	Embryonic kidney cells

Figure 11. BRD9 constitutes a leukemia-specific dependency among human cancer cell lines.
(a, b) Western blot to test knockdown efficiency of human BRD9 shRNAs in HeLa (a) and OPM-1 (b) cells. shRen samples were loaded twice: 1. at half the volume (50 %) and 2. at the same volume (100 %) as shBRD9 samples. Actin blot serves to control for gel loading.
(c) Heatmap summarizing competition-based assay to measure the effect of shRNAs on the growth of a panel of human cancer cell lines. Transduced (shRNA-expressing) cells were identified by the co-expression of GFP (MLS-E vector). The percentage of GFP+ cells was tracked over 28 days and normalized to the GFP percentage on day 4. Plotted is the percentage of GFP+ cells on day 28 normalized to that on day 4. n = 3
(d) Genetic background and/or disease descriptions of human cell lines profiled for sensitivity to BRD9 knockdown.
shRen targets Renilla luciferase and serves as a negative control.
Data collected with help from Jessica Minder.

HCC1954 cells did not rely on BRD9 for their proliferation. Collectively, these findings suggest a context-dependent BRD9 requirement for the proliferation of AML cells.

2.2 The molecular and cellular mechanism underlying Brd9-mediated AML growth

2.2.1 Brd9 maintains Myc expression in AML cells

To better understand the leukemia-supporting role of Brd9, we next evaluated the transcriptional program maintained by Brd9 in AML cells. For this purpose, we isolated RNA and performed a deep sequencing analysis of mRNA abundance (RNA-seq) in RN2 cells following 48 hours of shRNA expression. mRNA levels obtained using three independent Brd9 shRNAs were averaged and compared to mRNA levels in cells expressing our negative control shRNA targeting *Renilla* luciferase. In agreement with our prior analyses supporting the on-target activity of the Brd9 hairpins, Brd9 was the 20th most down-regulated gene in the data set (Fig. 12a). Addtionally, as expected based on the Brd9 ChIP-seq analysis, Myc was among the most down-regulated mRNAs (#21) following Brd9 knockdown (Fig. 12a). We also observed altered expression of several genes related to myeloid differentiation (*Mmp9*, *Itgam*, *Mpo*, and *Ccr2*) (Fig. 12a). These changes correspond to gene expression changes observed previously after Brg1 knockdown in RN2 cells [Shi et al., 2013]. However, the pro-apoptotic genes Btg1 and Bid, which are highly up-regulated by Brg1 shRNAs, were not affected by Brd9 knockdown, suggesting that Brd9 does not influence all genes regulated by Brg1, and that Brg1 has some Brd9-independent activities in these cells. We confirmed the down-regulation of Myc after shBrd9 expression by qRT-PCR (Fig. 12b). No such effect on Myc expression was observed after Brd7 knockdown, which is in agreement with the unimpaired proliferative capacity of these cells (Fig. 12c).

To systematically characterize Brd9-dependent gene expression in RN2 cells, we applied Gene Set Enrichment Analysis (GSEA) to the RNA-seq dataset [Subramanian et al., 2005]. GSEA is a computational method to evaluate the enrichment of a previously defined group of genes (a 'gene set') at either end of a ranked list of genes (a 'data set', such as the one in Fig. 12a).

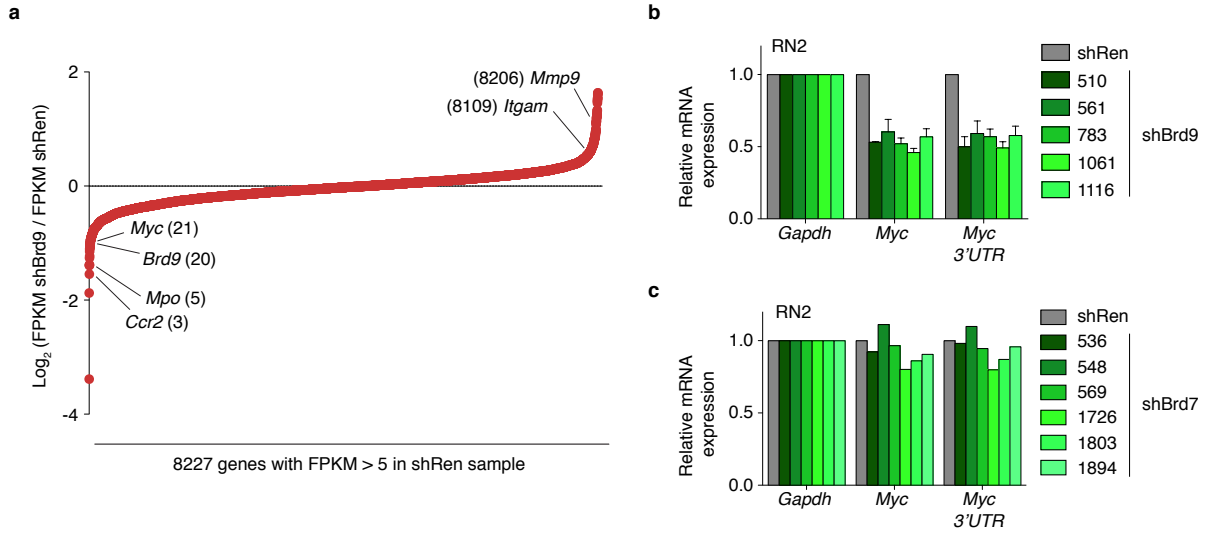

Figure 12. Brd9 sustains Myc expression in AML cells.
(a) RNA-Seq analysis of gene expression changes in RN2 cells expressing Brd9 shRNAs for 2 days (TRMPV-Neo vector). Averaged FPKM values for three independent Brd9 shRNAs were normalized to mRNA levels in control cells expressing shRen. Genes with a FPKM value < 5 in the shRen sample were excluded. Genes are plotted from the most down-regulated genes on the left to the most up-regulated genes on the right.
(b) qRT-PCR analysis to test the effect Brd9 knockdown on Myc expression in RN2 cells. mRNA levels were examined after 48 hours of shRNA expression (TRMPV-Neo vector). Values were normalized to Gapdh expression within each sample and to shRen values across samples. n = 2-7
(c) qRT-PCR analysis to test effect of Brd7 knockdown on Myc expression in RN2 cells. Performed as in (b), except that the LMN vector was used for shRNA expression. n = 1
shRen targets Renilla luciferase and serves as a negative control. All error bars in this figure represent SEM.

Enrichment is quantified as a Normalized Enrichment Score (NES) with higher absolut values indicating greater enrichment. When RNA-Seq data is used to generate a list of genes ranked from lowest to highest fold change in expression between two biological conditions, such as shRen vs. shBrd9 expressing cells, GSEA allows to assess whether the expression of the previously defined gene set is significantly different between these two biological conditions. More than 10,000 annotated gene sets have been collected in the Molecular Signatures Database (MSigDB) online and can be used for the purpose of GSEA. To identify enriched gene sets in an unbiased fashion, we interrogated all gene sets available through the MSigDB, filtered only to contain at least 15 but no more than 500 of the genes in our RNA-Seq data set (6917 gene sets fulfilled these conditions) as well as four gene sets from our prior characterization of Brg1-dependent

gene expression in RN2 cells (shBrg1_Top100Up or Down, LSC_Signature_Somervaillle and Macrophage_development_(IPA)) [Shi et al., 2013]. Plotting the NES against the familywise-error rate p-value (FWER p-val, a conservative measure of statistical significance), for each of these 6921 gene sets revealed several gene sets with statistically different expression between shRen vs. shBrd9 (Fig. 13a). Notably, among the most enriched gene signatures in this data set (|Normalized Enrichment Score (NES)| > 2 and FWER p-value $= 0$) were the downstream target genes of Myc as well as genes upregulated during myeloid differentiation, which were decreased and increased, respectively, upon Brd9 knockdown (Fig. 13). In addition, a Brg1-dependent gene signature defined previously in RN2 cells was also suppressed following Brd9 knockdown (NES 2.13, FWER p-value 0.015) (Fig. 13b) [Shi et al., 2013].

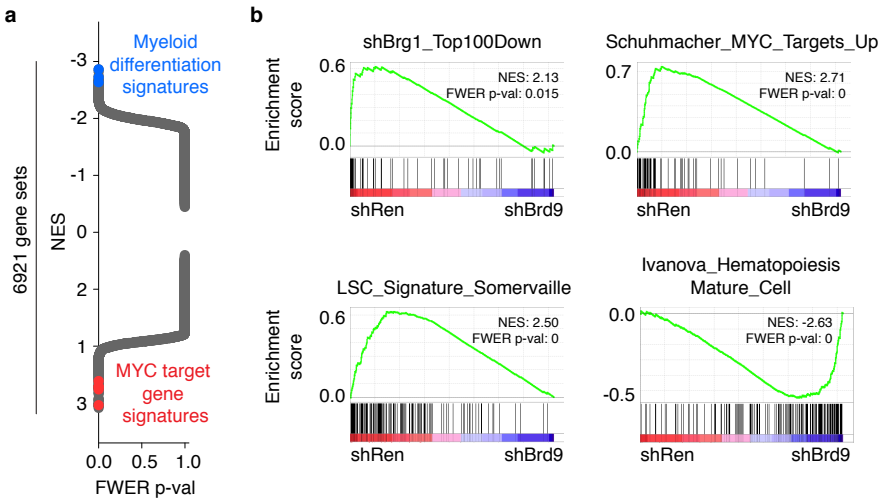

Figure 13. Expression of Myc target gene signatures is decreased, that of myeloid differentiation signatures increased after Brd9 knockdown.
(a) Gene Set Enrichment Analysis (GSEA) of the RNA-Seq data presented in (Fig. 12a). Gene sets available through the Molecular Signatures Database containing 15-500 of the differentially expressed genes in our RNA-Seq dataset (6917 out of 10153 gene sets) were evaluated plus four additional gene sets. (shBrg1_Top100Up or Down, LSC_Signature_Somervaillle and Macrophage_development_(IPA)). A positive Normalized Enrichment Score (NES) reflects enrichment on the left side of the ranked gene list (genes down-regulated with shBrd9), a negative NES reflects enrichment on the right of the ranked gene list (genes up-regulated with shBrd9). FWER p-val, familywise-error rate p-value.
(b) GSEA plots of the top 100 genes downregulated after 4 days of shBrg1 expression in RN2 cells (shBrg1_Top100Down), genes up-regulated in Burkitt's Lymphoma cells induced to express MYC (Schuhmacher_MYC_Targets_Up), genes expressed in leukemia stem cells (LSC_Signature_Somervaille), and genes up-regulated in mature blood cell populations from adult bone marrow and fetal liver (Ivanova_Hematopoiesis_Mature_Cell). shRen targets Renilla luciferase and serves as a negative control.

Importantly, Brd9 knockdown did not influence Myc expression in iMEF cells as tested by RNA-Seq and qRT-PCR (Fig. 14a, b). We also performed an analogous GSEA analysis of shBrd9-induced gene expression changes in iMEF cells. We included two additional gene sets comprising the top 100 up- and down-regulated genes identified after Brd9 knockdown in RN2 cells in this analysis. The NES vs. FWER p-val plot revealed that neither Myc target gene signatures, nor the two Brd9-regulated gene sets from RN2 cells were significantly altered upon Brd9 knockdown in iMEFs, highlighting that Brd9-mediated gene expression is highly context dependent.

Together, these findings show that Brd9, like Brg1, is required to maintain a transcriptional program in AML cells that sustains the Myc pathway and blocks myeloid differentiation.

2.2.2 Brd9 prevents differentiation of AML blasts

To test whether the observed gene expression changes would manifest as a differentiation phenotype, we used flow cytometry to measure cell surface levels of Kit, a tyrosine kinase, which is expressed in undifferentiated hematopoietic cells, and Mac-1 (encoded by *Itgam*), a complement receptor, which is upregulated during myeloid maturation. Three independent Brd9 shRNAs were tested and each provoked a decrease in Kit and an increase in Mac-1, which is consistent with the corresponding gene expression changes in our RNA-seq data (Fig. 15a and Fig. 12a). We also examined May-Grünwald/Giemsa-stained RN2 cells by light microscopy to assess for morphological signs of differentiation. Control RN2 cells showed large nuclei and a round cell shape characteristic of leukemic blasts. In contrast, Brd9-knockdown cells contained multilobulated nuclei and vacuolar structures, and possessed an irregular cell shape, consistent with feature of differentiated myeloid cells, such as neutrophils and macrophages (Fig. 15b).

To discern whether the reduced proliferative capacity of Brd9-knockdown AML cells would be due largely to cell cycle arrest or also to elevated cell deaths, we carried out BrdU incorporation assays and Annexin V stains, respectively. These studies revealed that Brd9 knockdown in RN2 cells resulted in a G1-arrest without a significant effect on apoptosis, which is consistent with the finding that expression of pro-apoptotic genes is not increased in these cells (Fig. 16).

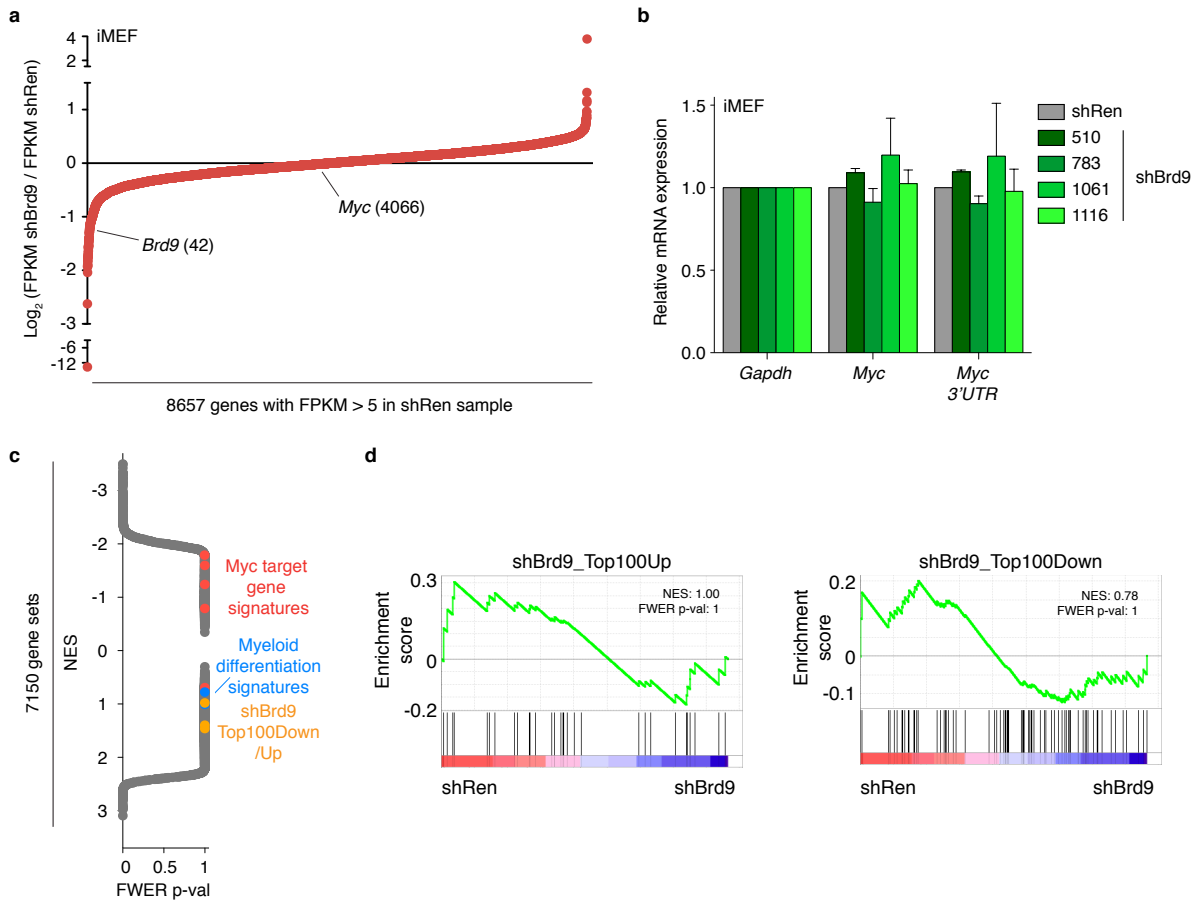

Figure 14. Brd9 knockdown in iMEF cells does not affect Myc expression.
(a) RNA-Seq analysis of gene expression changes in iMEF cells expressing Brd9 shRNAs for 2 days (TRMPV-Neo vector). Averaged FPKM values for two independent Brd9 shRNAs were normalized to mRNA levels in control cells expressing shRen. Genes with FPKM value < 5 in the shRen sample were excluded. Genes are plotted from the most down-regulated genes on the left to the most up-regulated genes on the right.
(b) qRT-PCR analysis to test the effect of Brd9 knockdown on Myc expression in iMEF cells. mRNA levels were examined after 48 hours of shRNA expression (TRMPV-Neo vector). Values were normalized to Gapdh expression within each sample and to shRen values across samples. n = 2
(c) Gene set enrichment analysis (GSEA) on the RNA-Seq data presented in (a). Gene sets available through the Molecular Signatures Database containing 15-500 of the differentially expressed genes in our RNA-Seq dataset (6951 out of 10153 gene sets) were evaluated plus six additional gene sets (shBrg1_Top100Up or Down, LSC_Signature_Somervaillle, Macrophage_development_(IPA), and shBrd9_Top100Up or Down). A positive Normalized Enrichment Score (NES) reflects enrichment on the left side of the ranked gene list (genes down-regulated with shBrd9), a negative NES reflects enrichment on the right of the ranked gene list (genes up-regulated with shBrd9). FWER p-val, familywise-error rate p-value.
(d) GSEA plots of the top 100 genes up- and down-regulated after 2 days of shBrd9 expression in RN2 cells.
shRen targets Renilla luciferase and serves as a negative control. All error bars in this figure represent SEM.

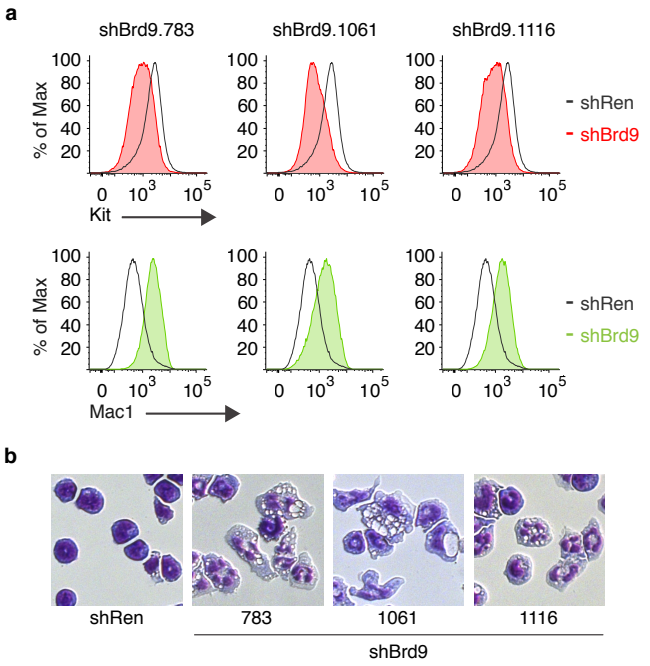

Figure 15. Brd9 supports AML growth by sustaining an undifferentiated cell state.
(a) Flow cytometry analysis of Kit (top) and Mac1 (bottom) cell surface expression after 4 days of shRen or shBrd9 expression (TRMPV-Neo vector) in RN2 cells.
(b) Representative light microscopy images of May-Grünwald/Giemsa-stained RN2 cells expressing shRen or shBrd9 for 4 days (TRMPV-Neo vector) Imaging was performed with a 40X objective.
shRen targets Renilla luciferase and serves as a negative control.

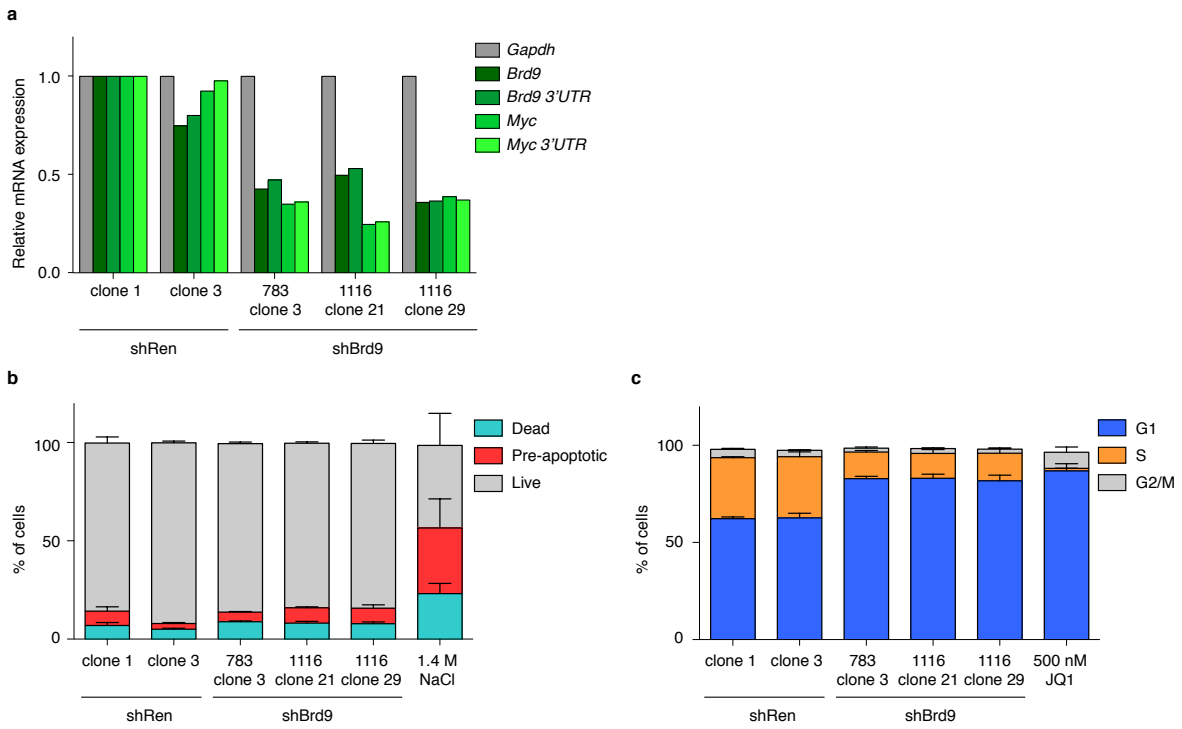

Figure 16. Brd9 knockdown leads to G1 arrest, not apoptosis.
(a) qRT-PCR analysis to test Brd9 knockdown efficiency in RN2-derived shRNA-expressing clones. mRNA levels were examined after 48 hours after dox-induced shRNA expression (TRMPV-Neo vector). Values were normalized to Gapdh expression within each sample and to shRen clone 1 values across samples. n = 1
(b) Cell death assay. Flow cytometry analysis of Annexin V and DAPI stained RN2-derived clones 4 days after induction of shRen or shBrd9 expression (TRMPV-Neo vector). Annexin V-/DAPI- cells were considered live; Annexin V+/DAPI-, cells were considered pre-apoptotic; DAPI+ cells were considered dead. n = 3
(c) Cell cycle assay. Flow cytometry analysis of BrdU labeled; BrdU and DAPI stained RN2-derived clones 4 days after induction of shRen or shBrd9 expression (TRMPV-Neo vector). BrdU-/2N cells were considered to be in G1 phase; BrdU+ cells were considered to be in S phase; BrdU-/4N cells were considered to be in G2/M phase. n = 4
shRen targets Renilla luciferase and serves as a negative control. All error bars in this figure represent SEM.

2.2.3 Myc overexpression suppresses the BRD9 dependence of AML cells

Based on our prior characterization of Brg1-deficient RN2 cells [Shi et al., 2013], we suspected that Myc suppression would be a key contributor to the differentiation phenotype induced upon Brd9 knockdown. We evaluated this hypothesis in cDNA rescue experiments, in which *Myc* cDNA was expressed from a retroviral promoter in RN2 cells prior to expression of Brd9 shRNAs. Similar to the effect of expressing shRNA-insensitive human BRD9 in these cells, Myc expression prevented myeloid differentiation as well as the proliferation arrest induced by Brd9 knockdown (Fig. 17). This suggested that differentiation is the primary cause underlying the growth arrest of Brd9 knockdown cells.

Myc overexpression was previously also found to rescue the differentiation phenotype induced by BRG1 down-regulation [Shi et al., 2013]. Importantly, however, Myc overexpression failed to prevent the apoptosis provoked by Brg1 shRNAs and only modestly slowed the depletion of Brg1 knockdown cells [Shi et al., 2013].

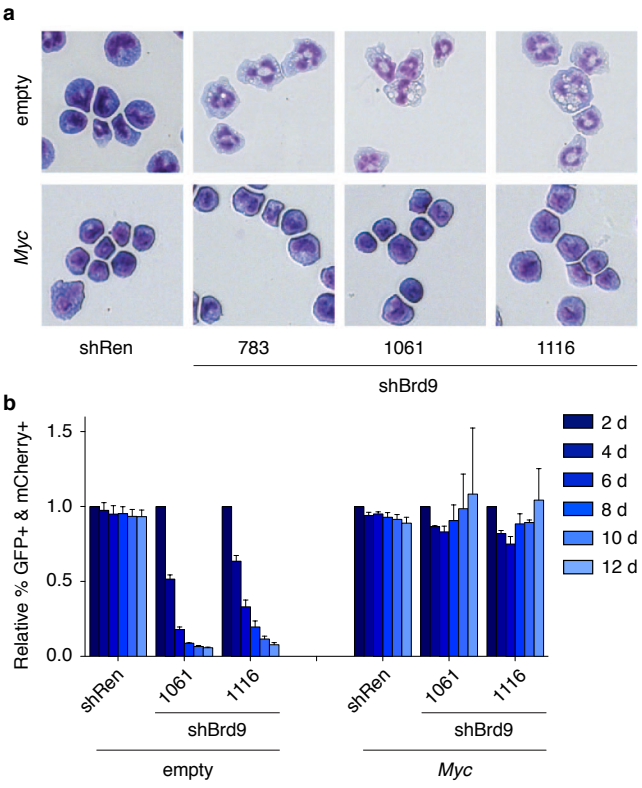

Figure 17. Myc overexpression suppresses the effects of Brd9 knockdown.
(a) Representative light microscopy images of May-Grnwald/Giemsa-stained RN2 cells expressing shRen or shBrd9 for 4 days (TRMPV-Neo vector) in the absence (top) or presence (bottom) of Myc expression (MSCV-based vector). Imaging was performed with a 40X objective.
(b) *Myc* cDNA complementation assay. Myc (linked to GFP, MSCV-based vector) was expressed in RN2 cells prior to expression of shRNAs (linked to mCherry, LMN vector). The percentage of double positive cells was tracked and normalized to day 2 values. n = 3
shRen targets Renilla luciferase and serves as a negative control. All error bars in this figure represent SEM.

The overall similar phenotypic effects of Brd9 and Brg1 knockdown, in concert with the IP-MS and ChIP-seq evidence presented above, provide strong support for Brd9 maintaining the leukemia cell state via its presence in a SWI/SNF complex, although Brg1 also seems to function independently of Brd9 at some sites (e.g. pro-apoptotic genes).

2.3 Analysis of BRD9 domain requirements

2.3.1 BRD9 activity in AML cells requires the DUF and the acetyl-binding capacities of the bromodomain.

Pharmacological inhibition of proteins is generally achieved by designing small-molecule inhibitors against specific, functionally relevant protein domains. Having identified a role for BRD9 in sustaining AML proliferation, we next sought to probe the significance of individual domains within BRD9 for its activity. BRD9 contains two domains - the bromodomain and a domain of unknown function (DUF). While the bromodomain constituted the pharmacologically tractable surface, it was theoretically possible that BRD9 maintained AML proliferation independent of this domain. To assess the importance of both domains for the essential role of BRD9 in leukemia, we employed the shRNA/cDNA complementation assay described above and evaluated the functionality of BRD9 mutants that either lack the bromodomain (BRD9 ΔBD), or the DUF (BRD9 ΔDUF) (Fig. 18a). In contrast to full-length human BRD9, BRD9 ΔBD and BRD9 ΔDUF were unable to support RN2 cell proliferation, despite being expressible at comparable levels to wild-type BRD9 (Fig. 18b, c). To further pinpoint whether the bromodomain was required specifically for its interaction with acetylated lysine residues, we also evaluated a BRD9 mutant which carries an asparagine-to-alanine substitution of a conserved residue that was reported to be a critical mediator of acetyl-lysine binding in related bromodomains (BRD9N216A) (Fig. 18a) [Dhalluin et al., 1999]. Like BRD9 ΔBD, this BRD9N216A mutant was incapable of rescuing the proliferation of Brd9-knockdown cells (Fig. 18b, c).

The cDNA overexpression lines in the above experiment were prepared by retroviral transduction of RN2 cells followed by puromycin selection. During this process we noticed that cells transduced with empty vector, BRD9, or BRD9 ΔDUF selected to above 90 % GFP positive (i.e.

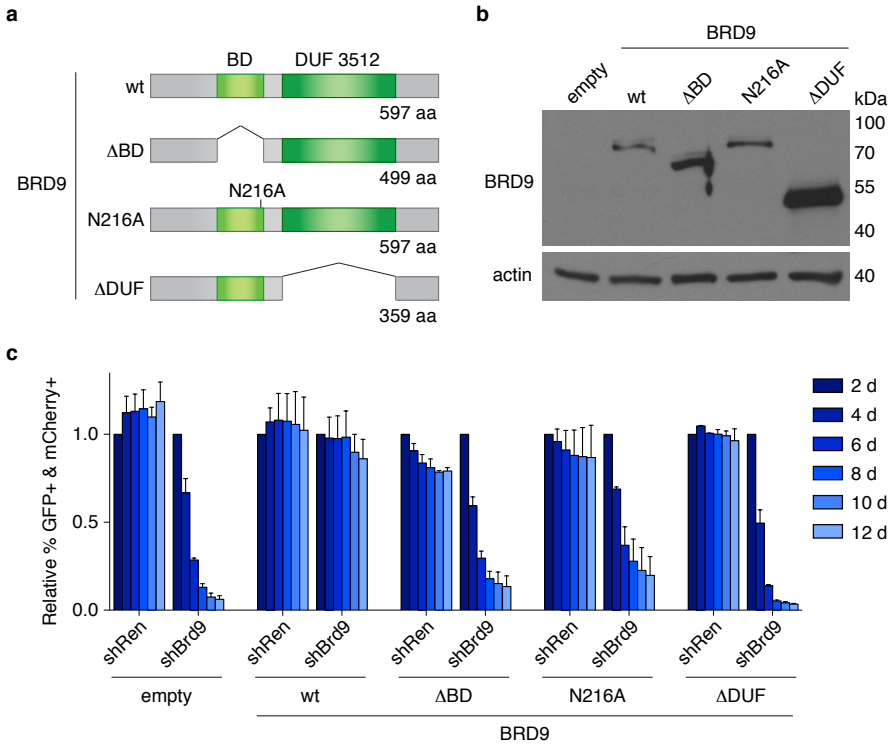

Figure 18. BRD9 requires the bromodomain and DUF for its AML-supporting function.
(a) Domain structure of wild-type (wt) and mutant BRD9. BD: Bromodomain, DUF: Domain of Unknown Function, aa: amino acids.
(b) Western blot to test retroviral expression of wt and mutant BRD9 in 3T3 cells. The antibody recognizes an epitope at the C-terminus of human BRD9 exclusively. For this reason no Brd9 band is observed in the 'empty' lane. An actin blot serves to control for loading.
(c) cDNA complementation assay to test functionality of BRD9 mutants. wt or mutant BRD9 (linked to GFP, MSCV-based vector) was expressed in RN2 cells prior to expression of shRNAs (linked to mCherry, LMN vector). The percentage of double positive cells was tracked and normalized to day 2 values. n = 2
shRen targets Renilla luciferase and serves as a negative control. All error bars in this figure represent SEM.

transgene expressing) cells, while cells transduced with BRD9 ΔBD or BRD9N216A selected to only about 70 %. Additionally, we saw an unexpected, modest depletion of BRD9 ΔBD and BRD9N216A cells expressing the control hairpin against Renilla luciferase. This suggested to us that these two constructs might themselves be negatively selected in these cells. Indeed, we found that overexpression of BRD9 ΔBD or BRD9N216A alone, but not that of full-length wild-type human BRD9 was sufficient to reduce Myc expression (Fig. 19b) and RN2 cell growth (Fig. 19c), yet expression of these cDNAs did not impair the proliferation of Brd9-independent

iMEFs (Fig. 19d). The similarity of these effects to those observed with shRNA-based Brd9 knockdown suggests that bromodomain-mutant alleles of BRD9 exhibit dominant-negative effects on endogenous Brd9. The weaker phenotype of BRD9N216A overexpression compared to BRD9ΔBD in this assay, might be attributed to limited remaining acetyl-binding capacity of

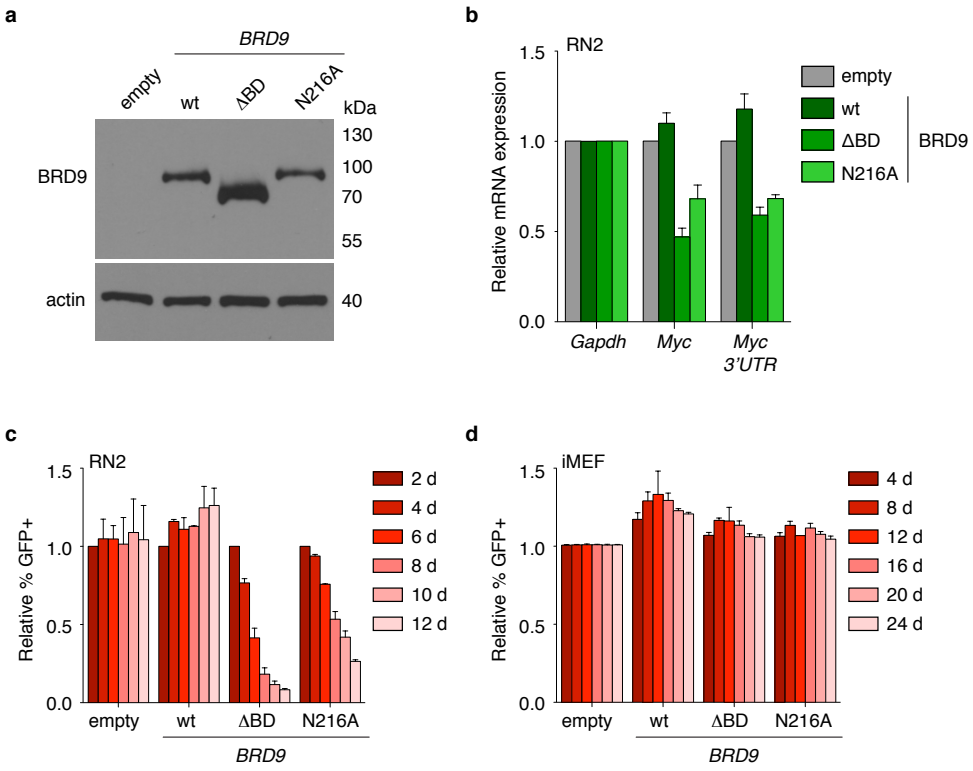

Figure 19. Bromodomain-mutant alleles are negatively selected in AML cells.
(a) Western blot to test retroviral expression of wt and mutant BRD9 in RN2 cells 2 days after transduction. The antibody recognizes an epitope at the C-terminus of human BRD9 exclusively. For this reason no Brd9 band is observed in the 'empty' lane. An actin blot serves to control for loading.
(b) qRT-PCR analysis to test the effect of wt or mutant BRD9 expression (via retrovirus) on Myc mRNA levels in RN2 cells. mRNA expression was examined 48 hours after retroviral transduction of transgenes (MSCV-based vector). Values were normalized to Gapdh expression within each sample and to empty vector values across samples. n = 3-4
(c, d) Competition-based assay to measure the effect of wt or mutant BRD9 expression on the growth of RN2 (c) and iMEF cells (d). Transduced cells were identified by the co-expression of GFP (MSCV-based vector). The percentage of GFP+ cells was tracked and normalized to the GFP percentage on day 2. n = 2 (c), n = 2-3 (d). Data in (d) was collected with help from Jessica Minder.
shRen targets Renilla luciferase and serves as a negative control. All error bars in this figure represent SEM.

the BRD9N216A mutant.

During the course of this project, domain-focussed CRISPR-Cas9-based screening had been developed in our lab [Shi et al., 2015]. Unlike shRNAs, which reduce the expression of their target in the cell by interfering with the translation and/or stability of mRNAs, CRISPR guide RNAs (sgRNAs) induce double strand breaks at their target DNA sites resulting in small indel mutations, which can interfere with the generation of a functional protein product. Indel mutations are particularly likely to generate a phenotype when targeted at functionally significant protein domains and this technique successfully evaluates the requirement of individual protein domains for cancer growth [Shi et al., 2015]. Experiments performed using CRISPR mutagenesis directed at the Brd9 bromodomain-encoding exons lent further support for the role of this domain in maintaining RN2 proliferation (Fig. 20). In agreement with our prior results, the bromodomains of PBRM1 and BRD7 did not score in this assay.

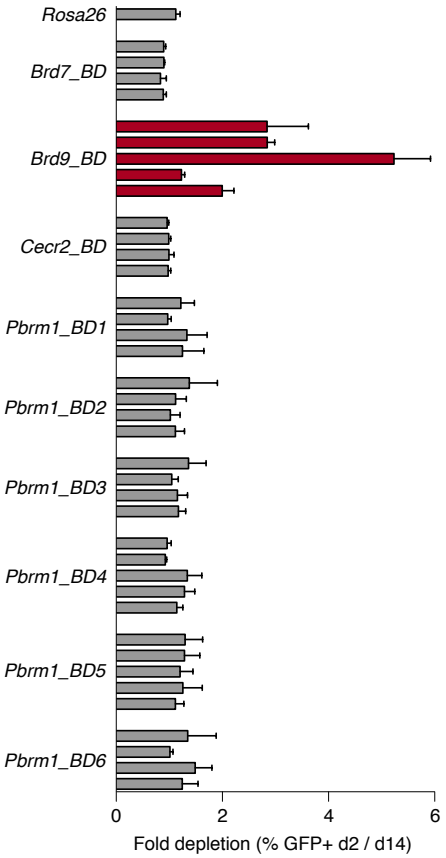

Figure 20. CRISPR-Screen of SWI/SNF bromodomains in AML cells highlights relevance of Brd9.
CRISPR-Cas9 targeting of SWI/SNF bromodomains to assess their relevance for the growth of RN2 cells in a competition-based assay. Transduced (sgRNA-expressing) cells were identified by the co-expression of GFP. The percentage of GFP+ cells on day 2 was divided by the GFP percentage on ∼day 14 to calculate the fold depletion. Higher fold depletion indicates greater anti-proliferative effects of sgRNAs. Each bar represents a different sgRNA. A sgRNA targeting the Rosa26 locus served as a negative control. sgRNAs targeting Brd9 are highlighted in red. Error bars represent SEM. n = 3. Data collected by Joseph Milazzo.

Together, our findings suggest that both bromodomain-mediated acetyl-lysine recognition as well as the DUF are critical for the activity of BRD9 in AML cells.

2.3.2 The BRD9 and BRD7 bromodomains, but not DUFs, are functionally synonymous.

As shown above, unlike Brd9, Brd7 does not support AML proliferation. Like Brd9, however, Brd7 contains a bromodomain and a DUF. To investigate the contribution of the individual domains to the differing functions of the two proteins in leukemia cells, we generated domain-swap mutants of BRD9, in which either the bromodomain or the DUF had been replaced by the corresponding domain of BRD7, and evaluated the functionality of these mutants in the shRNA/cDNA complementation assay (Fig. 21a). Both mutants expressed at similar levels to wild type BRD9 in RN2 cells. To our surprise, a BRD9 mutant containing the bromodomain of BRD7 instead of its own, was fully functional, whereas a mutant expressing the DUF of BRD7 in place of the DUF of BRD9 was not. This result is in agreement with the percent identity of the domains in BRD7 and BRD9 (BD: 66.3 %, DUF: 22 %) and suggests that the specific function of BRD9 in leukemia is at least in part mediated by its unique DUF.

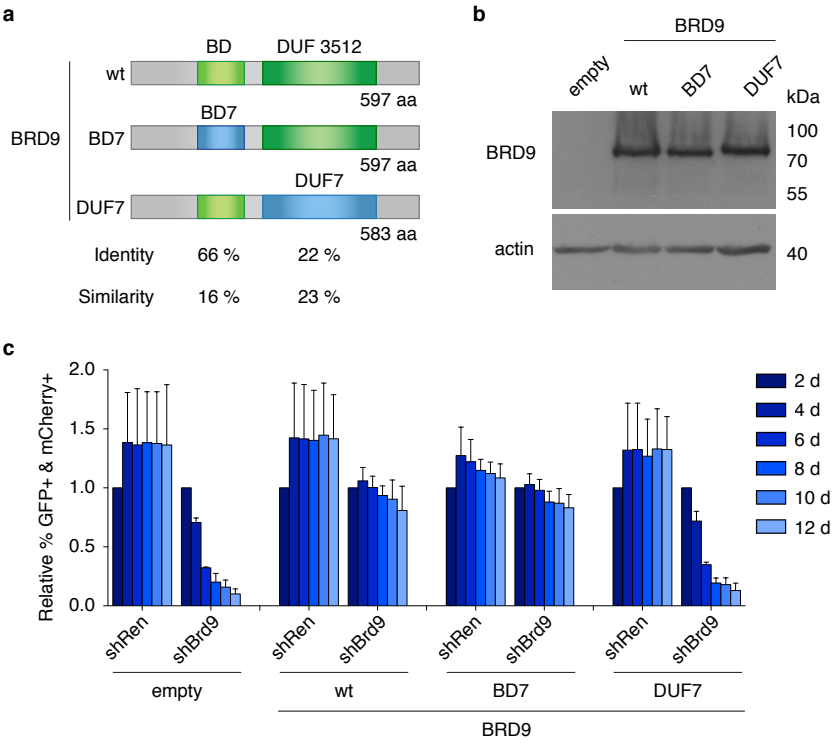

Figure 21. The BRD7 bromodomain, but not the BRD7 DUF can functionally replace the corresponding domain in BRD9.
(a) Domain structure of wild-type (wt) and mutant BRD9. BD: Bromodomain, DUF: Domain of Unknown Function, aa: amino acids.
(b) Western blot to test retroviral expression of wt and mutant BRD9 in RN2 cells. The antibody recognizes an epitope at the C-terminus of human BRD9 exclusively. For this reason no Brd9 band is observed in the 'empty' lane. An actin blot serves to control for loading.
(c) cDNA complementation assay to test functionality of BRD9 mutants. wt or mutant BRD9 (linked to GFP, MSCV-based vector) was expressed in RN2 cells prior to expression of shRNAs (linked to mCherry, LMN vector). The percentage of double positive cells was tracked and normalized to day 2 values. n = 2
shRen targets Renilla luciferase and serves as a negative control. All error bars in this figure represent SEM.

3 Chemical inhibition of the BRD9 bromodomain

3.1 Derivation and characterization of BRD9 bromodomain inhibitors

3.1.1 A large-scale screen identifies chemical inhibitors of the BRD9 bromodomain

Our genetic evidence implicated both the bromodomain and the DUF in the AML maintenance activity of BRD9. The sequence comparison and domain-swap experiments would suggest that targeting the BRD9 DUF could potentially allow for greater selectivity between BRD9 and BRD7. However, the absence of functional and structural insights into this domain prohibited the development of such a probe. In contrast, the BRD9 bromodomain had previously been crystallized, inhibitors for other bromodomains had successfully been generated, and our mutational analysis provided rationale for the development of small molecules that interfere with the acetyl-lysine recognition function of the BRD9 bromodomain.

To this end our collaborators at Boehringer Ingelheim initiated two parallel screening approaches, which led to the identification of BRD9 bromodomain binding compounds (Appendix 1). A generic fragment-based library was screened by differential scanning fluorimetry (DSF), surface plasmon resonance (SPR), and microscale thermophoresis resulting in 77 hits. In parallel, a second library was screened virtually and hits were then tested by DSF and SPR leading to 23 additional candidates. Chemical optimization of the identified hits was guided by co-crystal structures, which were used to improve the shape complementarity of the compounds towards the BRD9 bromodomain. Besides potency for BRD9, these efforts focussed on avoiding binding to the BRD4 bromodomains, which are known to be highly active in supporting leukemia cell proliferation [Zuber et al., 2011b]. Several rounds of optimization resulted in three highly potent compounds for the bromodomain of BRD9 (BI-7271 (**1**), BI-7273 (**2**), and BI-7189 (**3**)) with IC50s < 50 nM and with >1,000 fold selectivity over the bromodomains of BRD4, as determined using AlphaScreen assays, which measure the binding of acetylated histone peptides to recombinant bromodomains in the presence of increasing compound concentrations (Fig. 22). Compound BI-7273 revealed the greatest selectivity over the bromodomains

of BRD4 and was therefore chosen for those downstream analyses in which only one compound was evaluated.

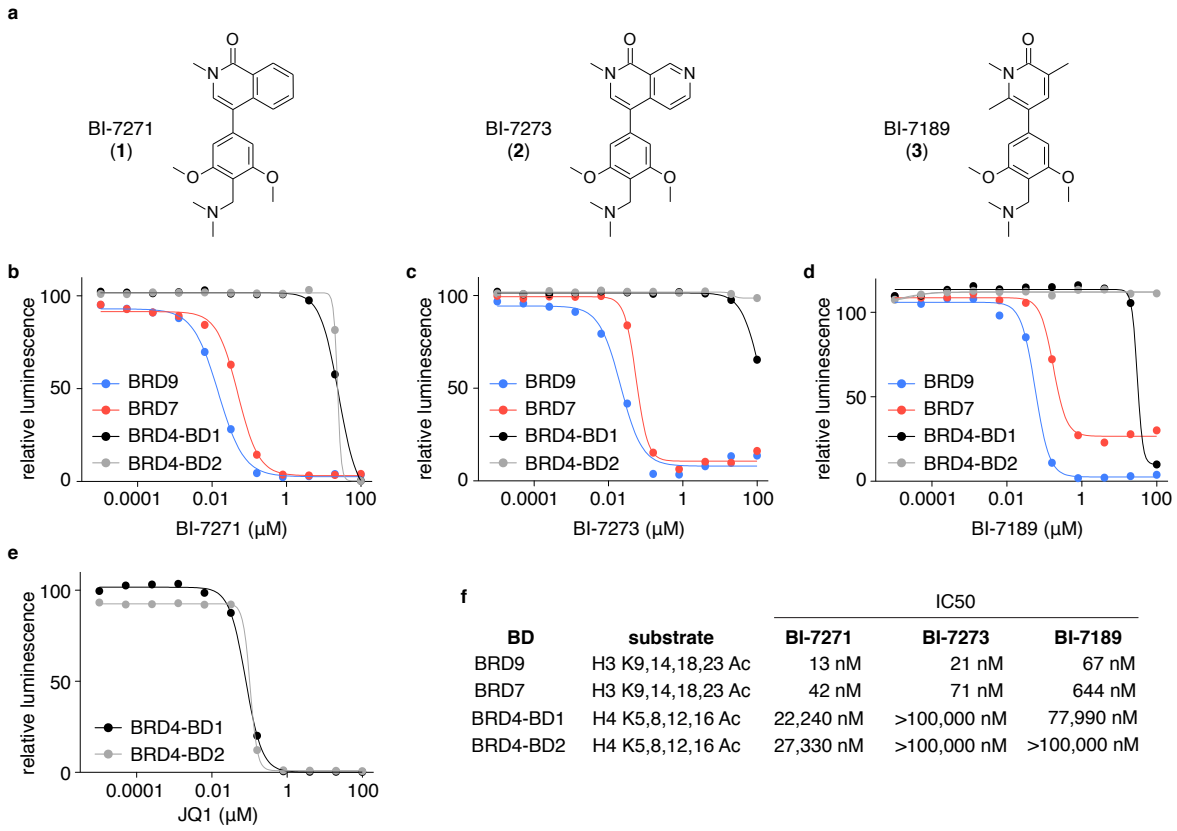

		IC50		
BD	**substrate**	**BI-7271**	**BI-7273**	**BI-7189**
BRD9	H3 K9,14,18,23 Ac	13 nM	21 nM	67 nM
BRD7	H3 K9,14,18,23 Ac	42 nM	71 nM	644 nM
BRD4-BD1	H4 K5,8,12,16 Ac	22,240 nM	>100,000 nM	77,990 nM
BRD4-BD2	H4 K5,8,12,16 Ac	27,330 nM	>100,000 nM	>100,000 nM

Figure 22. A chemical series that inhibits the BRD9 bromodomain.
(a) Chemical structures of the BRD9 bromodomain inhibitor series.
(b, c, d) AlphaScreen assay to determine binding affinities of the compounds in (a) for the bromodomains of BRD9, BRD7 and BRD4. Curves were fit by four parameter non-linear regression using the least squares fitting method. Representative graph out of 2-9 replicates is shown.
(e) Control AlphaScreen assay of JQ1 binding to the bromodomains of BRD4. Curves were fit by four parameter non-linear regression using the least squares fitting method. Representative graph out of 3 replicates is shown.
(f) Summary of IC50 values derived from the AlphaScreen graphs shown in (b, c, and d). IC50 values were obtained from non-linear regression curves with the bottom constrained to 0 and the top constrained to 100.
Compounds were synthesized and data collected at Boehringer Ingelheim.

3.1.2 *In vitro* characterization of BRD9 bromodomain inhibitors

To probe selectivity of the compounds across the bromodomain family, we commissioned bromoMAX and bromoKdELECT assays, which both employ BROMOscan technology [Quinn et al., 2013]. Similar to AlphaScreen assays, BROMOscan technology evaluates binding of test compounds to bromodomains by measuring a compounds' ability to interfere with the interaction between the bromodomain and an immobilized ligand. The bromoMAX assay evaluates binding of the test compound to a preconfigured panel of 32 human bromodomains at a single concentration. 11 bromodomains were identified as binders by bromoMAX and selected for evaluation by bromoKdELECT, which determines a more precise Kd in an 11-point dose response curve. This analysis revealed that all three compounds were highly selective for the homologous bromodomains of BRD9 and BRD7 and, to a 10-fold lesser extent, CECR2, while no binding was detected to any member of the BET family of bromodomains (as shown for BI-7273 in Fig. 23).

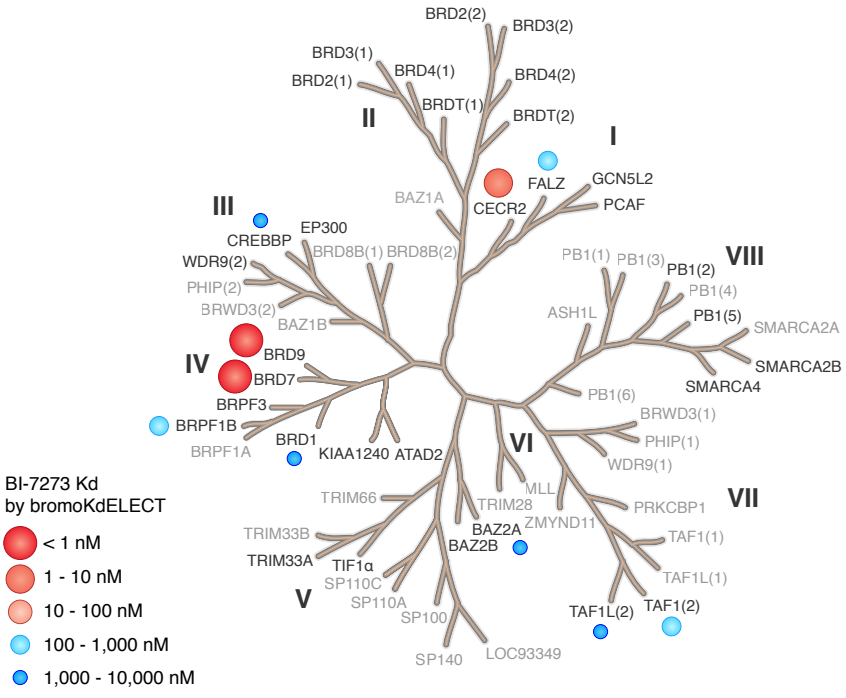

Figure 23. Bromodomain selectivity profiling of BI-7273.
BROMOscan profiling of BI-7273 binding across the bromodomain family. The bromodomains assayed by bromoMAX are shown in black (pre-configured panel). The depicted affinities were determined by bromoKdELECT (assaying those bromodomains identified as binders by bromoMAX). Data collected at DiscoverX.

Co-crystal structures of each of the three compounds and the BRD9 bromodomain were obtained. As evident from the co-crystal structure of BI-7273 bound to the BRD9 bromodomain, the carbonyl group of the isoquinolinone ring interacts with asparagine 216 and further forms a π-stacking interaction with tyrosine 222 (Fig. 24 and Appendix 2). The isoquinolinone ring also interacts with a conserved water molecule bound by tyrosine 173 (not visible in the depicted orientation of the crystal structure). Additionally, the dimethoxyphenyl linker adopts a conformation that permits T-stacking with phenylalanine 160 ((Fig. 24 and Appendix 2). For the purpose of modeling BI-7273 binding to BRD4, the BRD9 bromodomain in this co-crystal structure was computationally aligned with a crystal structure of the first bromodomain of BRD4, and then removed from the visualization (Fig. 25). This model revealed a steric clash of BI-7273 with the BRD4 bromodomain pocket, which can attribute for the lack of binding of this compound to BRD4 (Fig. 25). The synthetic route for all three compounds is provided in Appendix 3.

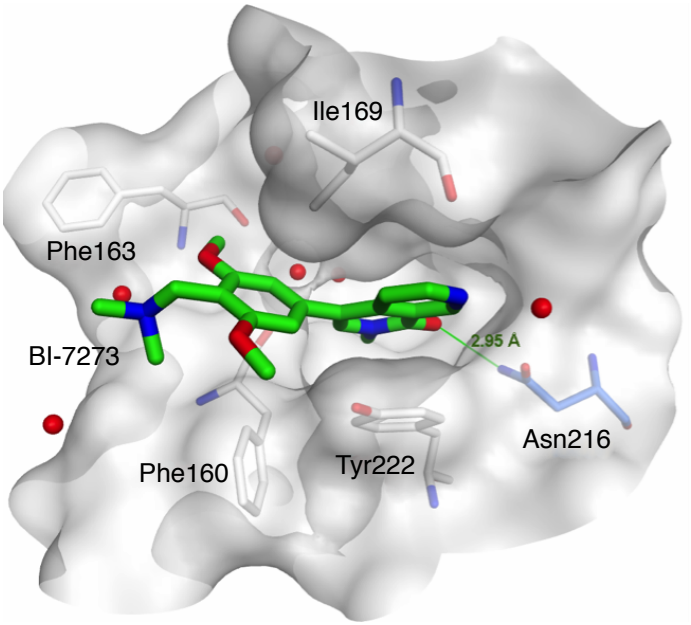

Figure 24. Co-crystal structure of BI-7273 bound to the BRD9 bromodomain.
Co-crystal structure of BI-7273 bound to the BRD9 bromodomain pocket. Key amino acid residues forming the binding pocket are highlighted. The hydrogen bond interaction to Asn216 with 2.95 is key for the correct orientation of the ligand. PDB: 5EU1. Data collected at Boehringer Ingelheim.

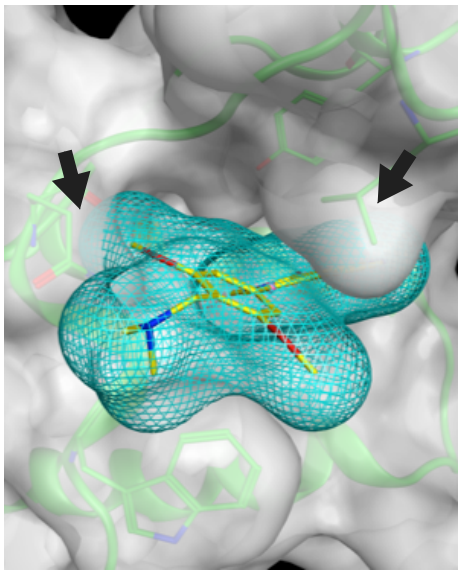

Figure 25. Crystal structure of BI-7273 modeled into a crystal structure of the first bromodomain of BRD4
Co-crystal structure of BI-7273 bound to the BRD9 bromodomain pocket was aligned with a crystal structure of the first bromodomain of BRD4. BI-7273 is shown as a surface representation in green, the first bromodomain of BRD4 is shown as a surface representation in gray, the BRD9 bromodomain pocket is not shown. Computational modeling and visualization performed at Boehringer Ingelheim.

3.2 Evaluation of BRD9 bromodomain inhibitor activity in the cell

3.2.1 BI-7273 perturbs BRD9 and Brg1 chromatin binding.

We next evaluated whether BI-7273 can block the bromodomain function of BRD9 in a cellular environment. We employed a nanoBRET assay, which relies on proximity-dependent bioluminescence resonance energy transfer (BRET) from a nanoLuc luciferase to a long-wavelength fluorophore [Machleidt et al., 2015]. A nanoLuc-BRD9 bromodomain chimera and a histone H3-HaloTag fusion were co-expressed in HEK293T cells. A fluorophore that binds the HaloTag was added to the cells followed by luciferase substrate and BRET was measured at increasing

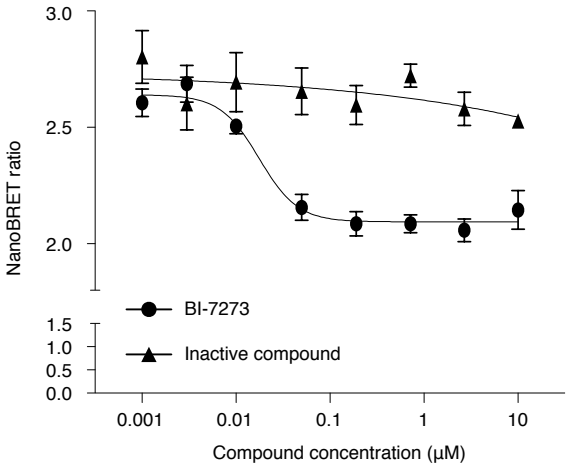

Figure 26. BI-7273 is cell-active.
NanoBRET assay to test binding of BI-7273 to the BRD9 bromodomain expressed in HEK293T cells. As a control the same assay was performed using a compound inactive in BRD9 binding. Error bars in this figure represent SEM. n = 3. Data collected at Boehringer Ingelheim.

concentrations of BI-7273. Using this nanoBRET assay, we confirmed a submicromolar activity of BI-7273 in disrupting the BRD9 bromodomain interaction with histone H3 (Fig. 26).

Additionally, we corroborated the in-cell activity of BI-7273 using ChIP-qPCR studies in RN2 cells. We found that exposure to BI-7273 led to a partial, yet reproducible reduction of FLAG-BRD9[3] and Brg1 occupancy at the *Myc* enhancer elements (Fig. 27a, b). While this effect was of modest magnitude, a ChIP-seq analysis revealed that the *Myc* enhancers were among the genomic regions exhibiting the greatest BRD9 and Brg1 displacement following BI-7273 exposure (Fig. 27 c, d). These findings indicate that BI-7273 inhibits BRD9 in a cellular context, however, it also appears that SWI/SNF complexes are able to associate with chromatin at many genomic regions in a BRD9-independent manner. It was hence unclear, whether the partial SWI/SNF displacement would be sufficient to achieve a reduction in the proliferation of AML cells (Fig. 27d).

[3]A lot change of the antibody against endogenous Brd9 that we had employed in the original ChIP-Seq analysis prevented it from further application in ChIP assays. I tested four additional commercial Brd9 antibodies as well as two homemade Brd9 antibodies generated by PrimmBiotech and identified one commercial antibody which performed well in ChIP-qPCR assays, but unfortunately failed when applied in ChIP-Seq experiments. For this reason we expressed FLAG-tagged BRD9 and performed ChIP-qPCR and -Seq assays using FLAG antibody

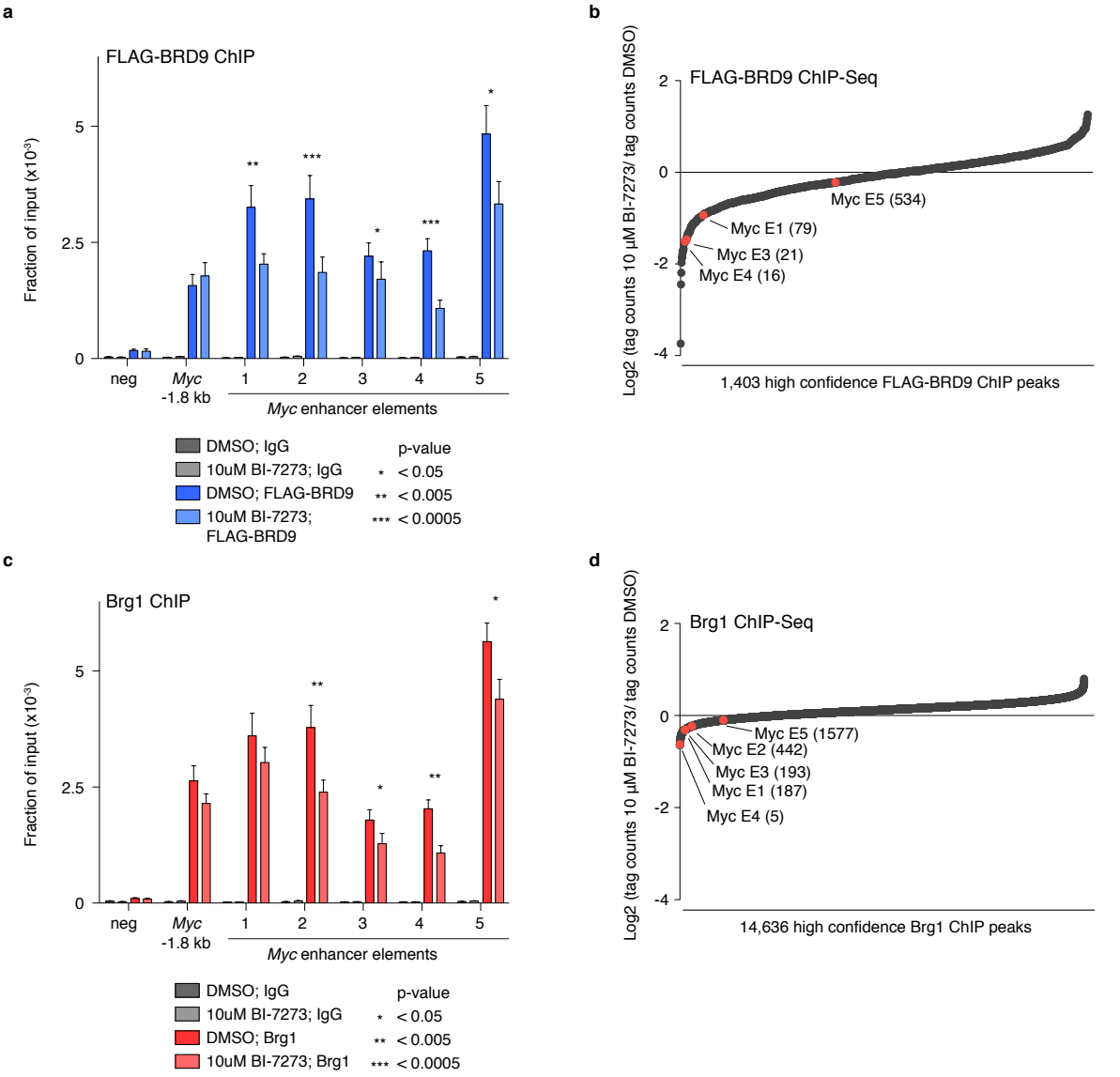

Figure 27. BI-7273 reduces FLAG-BRD9 and Brg1 binding to the *Myc* enhancer in AML cells. (a, c) ChIP-qPCR analysis of FLAG-BRD9 (a) or Brg1 (b) binding to the *Myc* locus in RN2 cells in the presence and absence of BI-7273. Each experiment included a parallel precipitation using an IgG antibody as a negative control. neg = a 'negative' region not bound by Brd9 in RN2 cells. P values were determined using the paired, two-tailed Student's t-Test. Error bars represent SEM. n = 7 (a) n = 6 (b)
(b, d) Ranking of FLAG-BRD9 (c) or Brg1 (d) occupied sites based on fold change of tag counts obtained from ChIP-Seq analysis of BI-7273 vs. DMSO treated FLAG-BRD9 expressing (c) or untransduced (d) RN2 cells. Data collected by Jae-Seok Roe.

3.2.2 Effects of BI-7273 on the proliferation of cancer cell lines

We proceeded to assess the effect of our BRD9 inhibitors on the growth of leukemia cell lines. All three compounds exerted dosage-dependent inhibition of RN2 cell proliferation, with GI50 values ranging from 217-1,784 nM after five days of exposure and these GI50 values correlated with the relative potency of each molecule for BRD9 inhibition in biochemical assays (Fig. 28 and Fig. 22 f). By evaluating BI-7273 in a panel of 62 human cancer cell lines, we found that sensitivity to this compound was largely confined to hematopoietic cancers, with AML cell lines being the most sensitive overall (Fig. 29). These findings are largely in agreement with our genetic profiling of BRD9 dependence in human cancer cell lines (Fig. 8c).

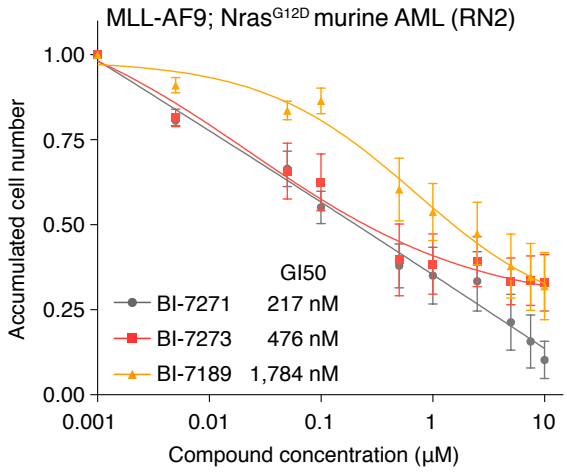

Figure 28. BRD9 inhibitors limit AML cell proliferation.
Anti-proliferative effect of BRD9 bromodomain inhibitors on the growth of RN2 cells. RN2 cells were cultured in the presence of increasing inhibitor concentrations for 5 days before cell numbers were determined and normalized to DMSO control. Curves were fit by four parameter non-linear regression using the least squares fitting method. GI50 values were derived from non-linear regression curves with the bottom constrained to 0 and the top constrained to 1. Error bars represent SEM. n = 3

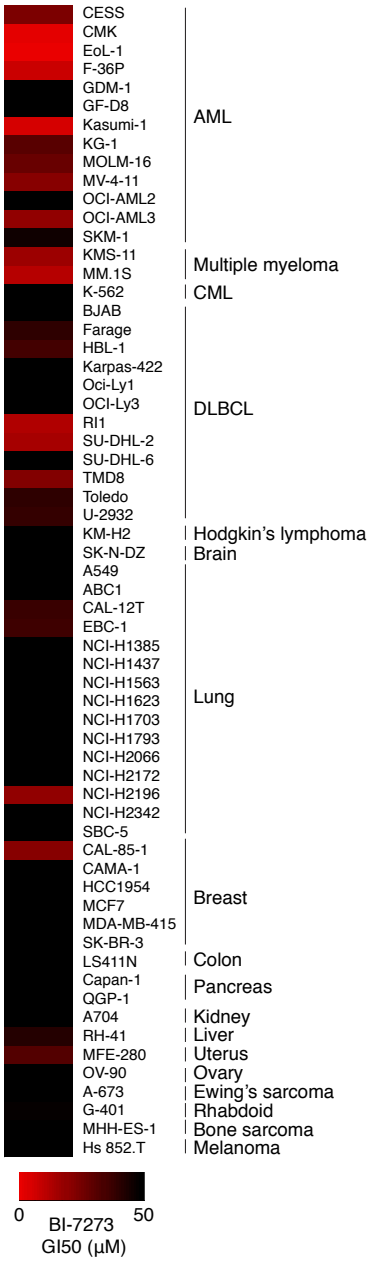

Figure 29. Sensitivity to BI-7273 across human cancer cell lines is confined to hematopoietic cancers.

GI50 measurements for BI-7273 across human cancer cell lines. Cells were cultured in the presence of increasing BI-7273 concentrations for 7 days, then cell proliferation was assessed by CellTiter-Glo and normalized to a DMSO control. Data collected at Boehringer Ingelheim.

4 Validation of BRD9 as the relevant cellular target of our BRD9 inhibitors

4.1 A domain-swap assay for BRD9 inhibitor target validation

4.1.1 Select bromodomains can functionally replace the BRD9 bromodomain

One issue that arises when evaluating the aforementioned compounds lies in determining whether Brd9 is the relevant cellular target that underlies the observed anti-proliferative effects. While our compounds are capable of targeting BRD9, BRD7, and CECR2, our RNAi and CRISPR-Cas9 experiments indicate that only the bromodomain of Brd9 is essential in leukemia cells (Fig. 8, Fig. 10, and Fig. 20). However, BI-7273 mediated BRD9 displacement from chromatin was modest, and RN2 cells have been shown to be highly sensitive to Brd4 bromodomain inhibition [Zuber et al., 2011b]. Hence, we were concerned that even a slight off-target activity of our compound series against Brd4 could account for the observed anti-leukemia effects. Additionally, we could not exclude a contributory off-target activity outside of the bromodomain protein family. We therefore considered it paramount to derive a *BRD9* allele that would be insensitive to chemical inhibition yet retain functionality, in analogy to kinase gatekeeper mutations. Such an allele would allow us to evaluate the contribution of Brd9 to the growth-arrest phenotypes caused by our compound series.

As we had unexpectedly discovered that the bromodomain of BRD9 can be entirely replaced with that of BRD7 without comprising its functionality in leukemia cells, we interrogated whether other bromodomains were functionally synonymous with that of BRD9 as well. Since the closest bromodomain homolog of BRD9 and BRD7 is BRD1 (Fig. 23 and Fig. 30a), we tested the BRD1 bromodomain in the shRNA/cDNA rescue assay. Indeed, like the BRD9 variant harboring the bromodomain of BRD7, the BRD9 mutant carrying the BRD1 bromodomain was expressed and retained full functionality in supporting RN2 proliferation (Fig. 30b, c). To our surprise, we also found that the first bromodomain of BRD4 supported full BRD9 activity in this domain-swap assay, despite its limited sequence and structural similarity to the BRD9

bromodomain (Fig. 30b, c) [Filippakopoulos et al., 2012].

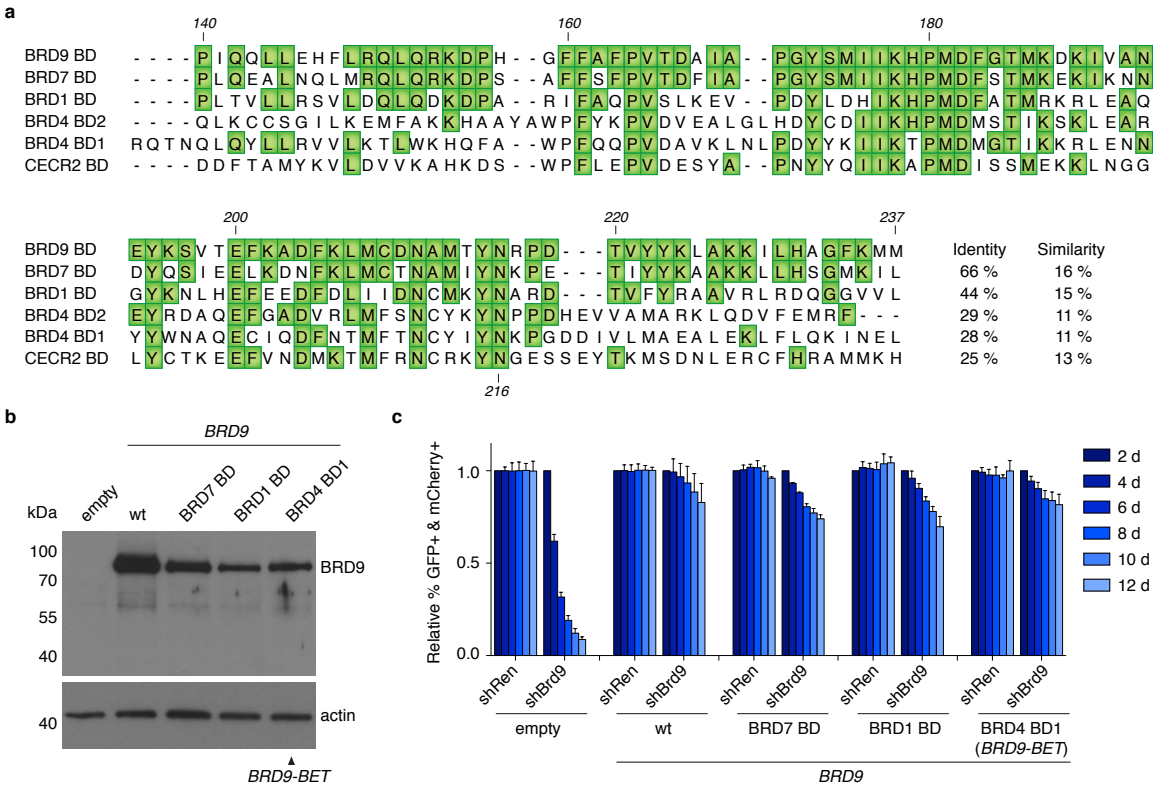

Figure 30. The BRD9 bromodomain can be functionally replaced by the first bromodomain of BRD4.
(a) Protein sequence alignment of the BRD9, BRD7, BRD1, BRD4 and CECR2 bromodomains. Residues in BRD7, BRD1, BRD4, CECR2 that are identical to the corresponding amino acid in BRD9 are highlighted in green boxes. The numbering on top of the alignment corresponds to the residue number in BRD9. Sequence identity and similarity were calculated using the Gonnet similarity matrix in MacVector.
(b) Western blot to test expression of BRD9 wt and bromodomain-swap mutants in RN2 cells. The antibody recognizes an epitope at the C-terminus of human BRD9 exclusively. For this reason no Brd9 band is observed in the 'empty' lane. The actin blot serves to control for loading.
(c) cDNA complementation assay to test functionality of bromodomain-swap alleles. wt or mutant BRD9 (linked to GFP, MSCV-based vector) was expressed in RN2 cells prior to expression of shRNAs (linked to mCherry, LMN vector). The percentage of double positive cells was tracked and normalized to day 2 values. n = 2-5
shRen targets Renilla luciferase and serves as a negative control. All error bars in this figure represent SEM.

In agreement with this finding, ChIP-qPCR analysis revealed that the BRD4 bromodomain allowed localization of the chimeric BRD9 protein (hereafter referred to as BRD9-BET) to the *Myc* enhancer elements at comparable levels to wild-type BRD9 (Fig. 31).

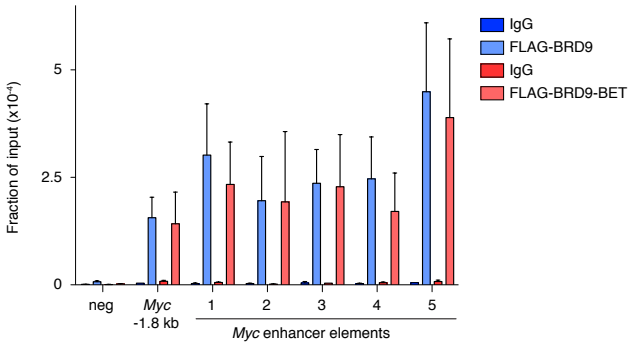

Figure 31. BRD9-BET binds the *Myc* enhancer in AML cells.
ChIP-qPCR analysis of FLAG-BRD9 and FLAG-BRD9-BET binding to the *Myc* locus in RN2 cells. Each experiment included a parallel precipitation using an IgG antibody as a negative control. neg = a 'negative' region not bound by Brd9 in RN2 cells. Error bars represent SEM. n = 2-3

However, other bromodomains (e.g. that of BRG1) failed to support BRD9 function in the domain-swap assay, indicating that only specific bromodomains are interchangeable with that of BRD9 (Fig. 32). These observations define a domain-swap strategy for producing a functional BRD9 protein possessing a radically altered amino acid composition of its bromodomain module.

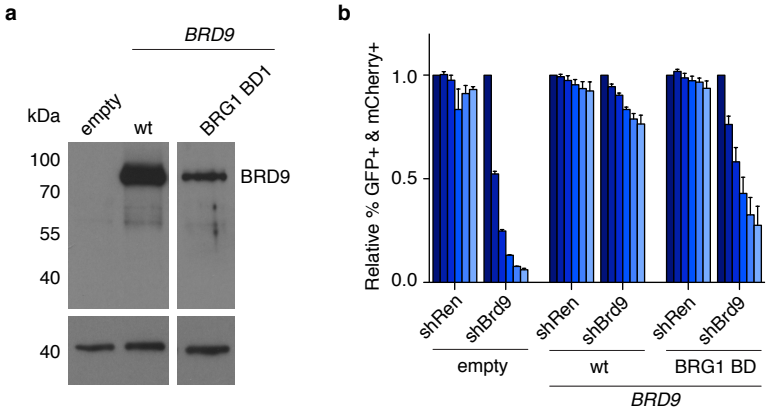

Figure 32. The BRG1 bromodomain cannot functionally substitute the BRD9 bromodomain.
(a) Western blot to test expression of BRD9 wt and BRG1-bromodomain-swap mutant in RN2 cells. The antibody recognizes an epitope at the C-terminus of human BRD9 exclusively. For this reason no Brd9 band is observed in the 'empty' lane. The actin blot serves to control for loading. Same Western Blot as shown in 30
(b) cDNA complementation assay to test functionality of BRG1-bromodomain-swap allele. wt or mutant BRD9 (linked to GFP, MSCV-based vector) was expressed in RN2 cells prior to expression of shRNAs (linked to mCherry, LMN vector). The percentage of double positive cells was tracked and normalized to day 2 values. n = 3
shRen targets Renilla luciferase and serves as a negative control. All error bars in this figure represent SEM.

4.1.2 A bromodomain-swap allele of *BRD9* can rescue the anti-proliferative effects of BRD9 bromodomain inhibition

In vitro selectivity profiling had shown that our compound series exhibits minimal affinity for BRD4 bromodomains, and therefore should have reduced affinity for BRD9-BET relative to wild type BRD9 (Fig. 22 b - d, f and Fig. 23). We reasoned that if Brd9 is the relevant target underlying the anti-proliferative effects of our inhibitors, expression of BRD9-BET should reduce the sensitivity of RN2 cells to these compounds. To evaluate this possibility, we compared the effect of the inhibitors on the proliferation of RN2 cells expressing either wild-type BRD9 or BRD9-BET. Remarkably, BRD9-BET expression reduced the sensitivity of RN2 cells to all three compounds (Fig. 33). In the case of BI-7271 and, to a lesser extent, BI-7189, the rescue effect was partial at higher inhibitor concentrations (Fig. 33a, c). In contrast, BRD9-BET expressing cells were completely resistant to BI-7273 at even the highest concentrations tested (Fig. 33b). These findings establish Brd9 as the sole target underlying the anti-proliferative effects of this molecule in RN2 cells. In addition, use of this allele reveals the superiority of BI-7273 within our chemical series in achieving potent and selective Brd9 inhibition.

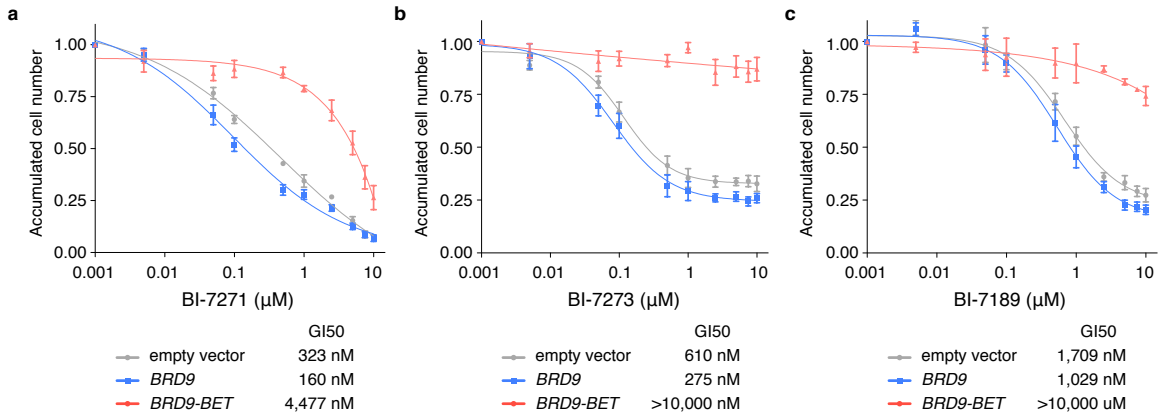

Figure 33. BRD9-BET validates on-target activity of our BRD9 inhibitors.
(a, b, c) Cell counts to measure the effect of BRD9 bromodomain inhibitors on the growth of RN2 cells transduced with and selected for empty vector, BRD9 or BRD9-BET (MSCV-based vector). Cells were cultured in the presence of increasing inhibitor concentrations for 5 days before cell numbers were determined and normalized to DMSO control. Curves were fit by four parameter non-linear regression using the least squares fitting method. GI50 values were derived from non-linear regression curves with the bottom constrained to 0 and the top constrained to 1. Error bars represent SEM. n=3

4.1.3 Evaluation of published BRD9 inhibitors in the bromodomain-swap assay

This assay also allowed us to evaluate the on-target activity of two other recently described BRD9 bromodomain inhibitors, LP99 and I-BRD9 [Clark et al., 2015, Theodoulou et al., 2015]. Expression of BRD9-BET partially alleviated the growth-arrest caused by I-BRD9, but only minimally influenced the sensitivity of RN2 cells to LP99 (Fig. 34). This finding was in agreement with the relative effect of these compounds on the proliferation of BRD9-dependent (HL60) versus BRD9-independent (Jurkat) human cell lines (Fig. 35). Taken together, these findings highlight the utility of a bromodomain-swap allele in evaluating on-target effects within a compound series.

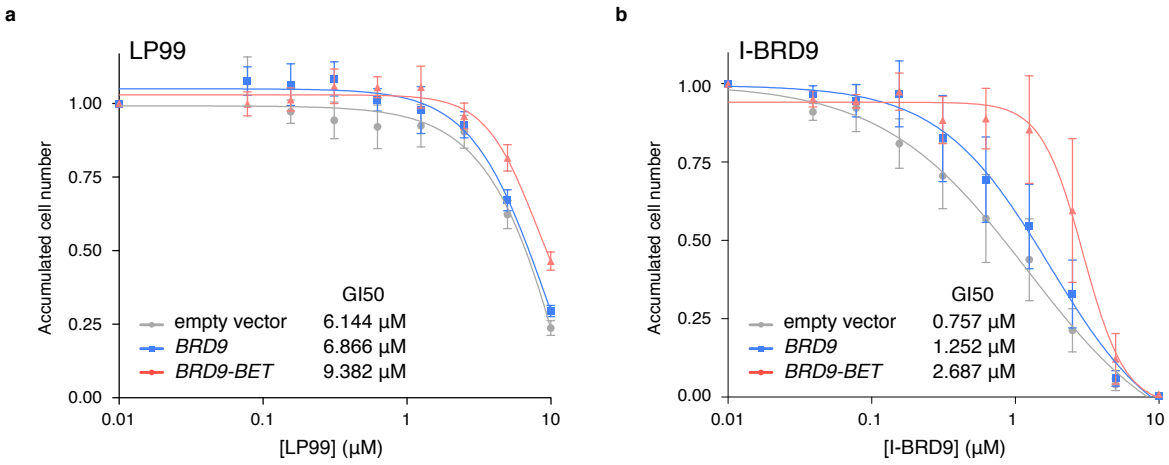

Figure 34. Evaluation of BRD9 inhibitors LP99 and I-BRD9 in the bromodomain-swap assay. (a, b) Cell counts to measure the effect of BRD9 bromodomain inhibitors LP99 (a) and I-BRD9 (b) on the growth of RN2 cells transduced with and selected for empty vector, BRD9 or BRD9-BET (MSCV-based vector). Cells were cultured in the presence of increasing inhibitor concentrations for 7 days (LP99, a) or 5 days (I-BRD9, b) before cell numbers were determined and normalized to DMSO control. Curves were fit by four parameter non-linear regression using the least squares fitting method. IC50 values were derived from non-linear regression curves with the bottom constrained to 0 and the top constrained to 1. Error bars represent SEM. n = 4 (a); n = 3 (b)

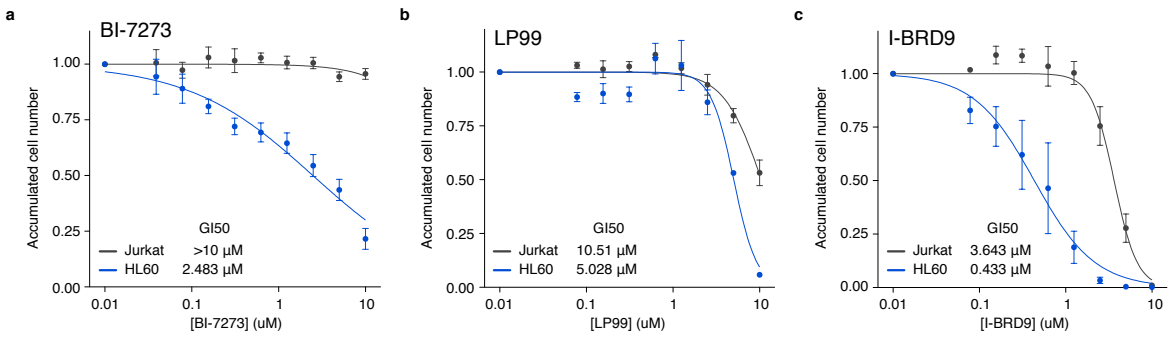

Figure 35. Comparison of the effect of BRD9 inhibitors on BRD9-dependent and -independent human cancer lines.
(a, b, c) Cell counts to measure the effect of BRD9 bromodomain inhibitors on the growth of human cancer cell lines. Cells were cultured in the presence of increasing BI-7273 (a), LP99 (b), or I-BRD9 (c) concentrations for 7 days before cell numbers were determined and normalized to DMSO control. Curves were fit by four parameter non-linear regression using the least squares fitting method with the bottom constrained to 0 and the top constrained to 1. Error bars represent SEM. n = 3-6

4.2 Gene expression changes after chemical vs. genetic BRD9 targeting

4.2.1 Treating AML cells with BI-7273 mimics the transcriptional changes associated with genetic targeting of Brd9

The results of our bromodomain-swap assay could be independently corroborated using a complementary approach. If a BRD9 targeting compound achieves its primary effect in RN2 cells via Brd9 inhibition, the transcriptional changes induced by inhibitor administration should mimic those observed with genetic targeting of Brd9. To evaluate this, we performed RNA-seq analysis following exposure of RN2 cells to 1.25 µM BI-7273 for 24 hours. Overall, the gene expression changes after chemical BRD9 inhibition were of more modest magnitude than those observed with genetic BRD9 targeting. However, among the most altered genes were *Myc*, *Mpo*, *Ccr2*, and *Itgam*, which resembled the gene expression changes observed following Brd9 knockdown (Fig. 36 and Fig. 12a). To further evaluate the similarity of genetic and chemical Brd9 inhibition, we performed GSEA as described above, with the inclusion of the gene sets containing the top 100 up- and down-regulated genes identified in our prior RNA-seq analysis in RN2 cells experiencing Brd9 knockdown (Fig. 36b, c). Among this large group of gene sets, the

two Brd9-dependent gene signatures were outliers with regard to the magnitude of perturbation following BI-7273 treatment (Fig. 36b, c). In addition, BI-7273 altered Myc target gene sets and myeloid differentiation signatures similarly to Brd9 knockdown (Fig. 36b, d).

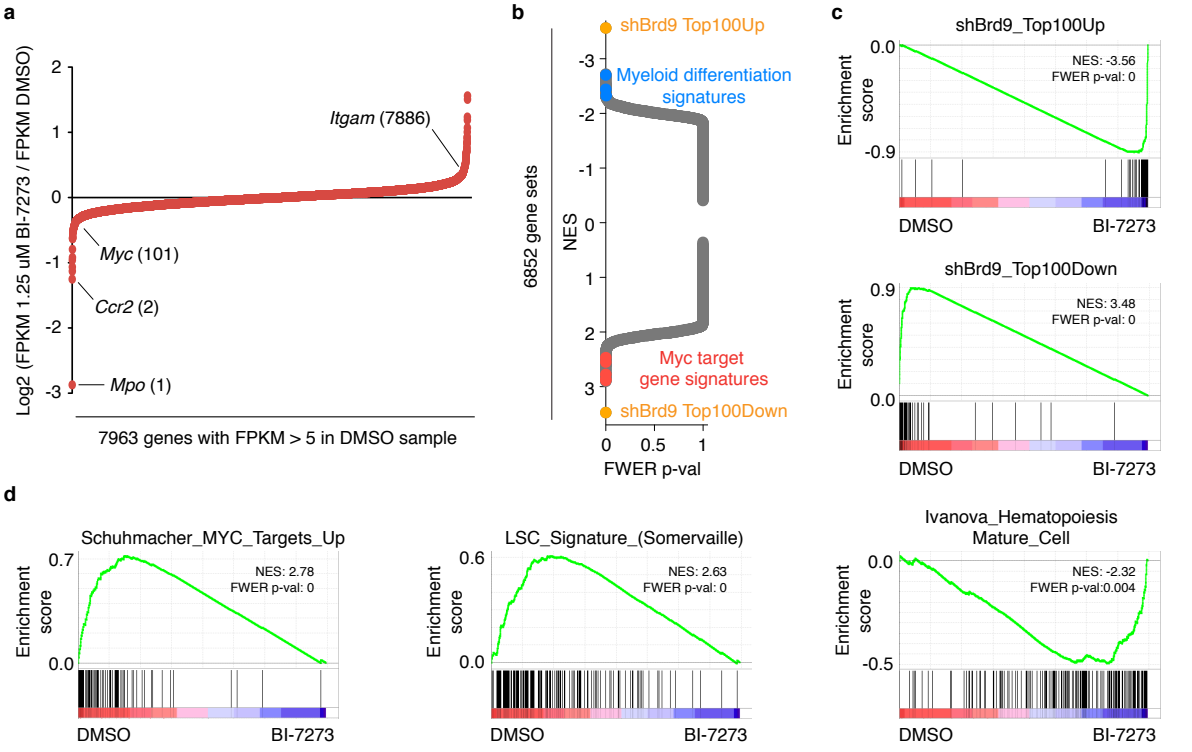

Figure 36. BI-7273-mediated chemical Brd9 inhibition mimics the transcriptional effects of Brd9 knockdown

(a) RNA-Seq analysis of gene expression changes in RN2 cells after 24 hours of 1.25 μM BI-7273 exposure. FPKM values from treated cells were normalized to FPKM values recorded in cells cultured in the presence of DMSO. Genes with a FPKM value < 5 in the DMSO sample were excluded. Genes are plotted from the most down-regulated genes on the left to the most up-regulated genes on the right.

(b) Gene set enrichment analysis (GSEA) of the RNA-Seq data presented in (a). Evaluated all gene sets available through the Molecular Signatures Database containing 15-500 of the differentially expressed genes in our RNA-Seq dataset (6846 out of 10153 gene sets) plus six additional gene sets (shBrg1_Top100Up or Down, LSC_Signature_Somervaille, Macrophage_development_(IPA), shBrd9_Top100Up or Down). A positive Normalized Enrichment Score (NES) reflects enrichment on the left side of the ranked gene list (genes down-regulated with BI-7273), a negative NES reflects enrichment on the right of the ranked gene list (genes up-regulated with BI-7273). FWER p-val, familywise-error rate p-value.

(c, d) GSEA plots of the top 100 genes up- and down-regulated after 2 days of shBrd9 expression in RN2 cells (shBrd9_Top100Up and shBrd9_Top100Down), genes up-regulated in Burkitt's Lymphoma cells induced to express MYC (Schuhmacher_MYC_Targets_Up), genes expressed in leukemia stem cells (LSC_Signature_Somervaille), and genes up-regulated in mature blood cell populations from adult bone marrow and fetal liver (Ivanova_Hematopoiesis_Mature_Cell).

Importantly, like shRNA-mediated knockdown of Brd9 in iMEFs, BI-7273 did not influence the expression of the shBrd9_Top100Up, shBrd9_Top100Down, and Myc target gene signatures in these cells (Fig. 37).

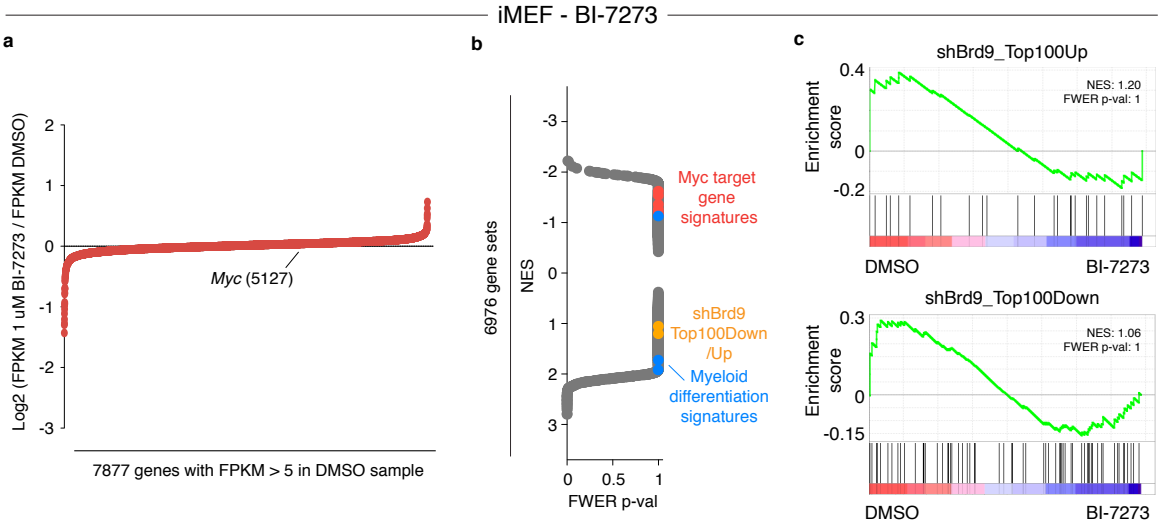

Figure 37. BI-7273 does not perturb Myc expression in iMEF cells.
(a) RNA-Seq analysis of gene expression changes in iMEF cells treated with after 24 hours of 1 μM BI-7273 treatment. FPKM values from treated cells were normalized to FPKM values recorded in cells cultured in the presence of DMSO. Genes with a FPKM value < 5 in the DMSO sample were excluded. Genes are plotted from the most down-regulated genes on the left to the most up-regulated genes on the right.
(b) Gene set enrichment analysis (GSEA) on the RNA-Seq data presented in (a). Evaluated all gene sets available through the Molecular Signatures Database containing 15-500 of the differentially expressed genes in our RNA-Seq dataset (6970 out of 10153 gene sets in both cases) plus six additional gene sets (shBrg1_Top100Up or Down, LSC_Signature_Somervaille, Macrophage_development_(IPA), shBrd9_Top100Up or Down). A positive Normalized Enrichment Score (NES) reflects enrichment on the left side of the ranked gene list (genes down-regulated with BI-7273), a negative NES reflects enrichment on the right of the ranked gene list (genes up-regulated with BI-7273). FWER p-val, familywise-error rate p-value.
(c) GSEA plots of the top 100 genes up- and down-regulated after 2 days of shBrd9 expression in RN2 cells (shBrd9_Top100Up and shBrd9_Top100Down).

Using RNA-seq, we also observed a similar context-dependent pattern of MYC suppression upon treating human BRD9-dependent AML cell lines HL-60 and MV4-11 with BI-7273, while no such effect was found in BRD9-independent HeLa cells (Fig. 38).

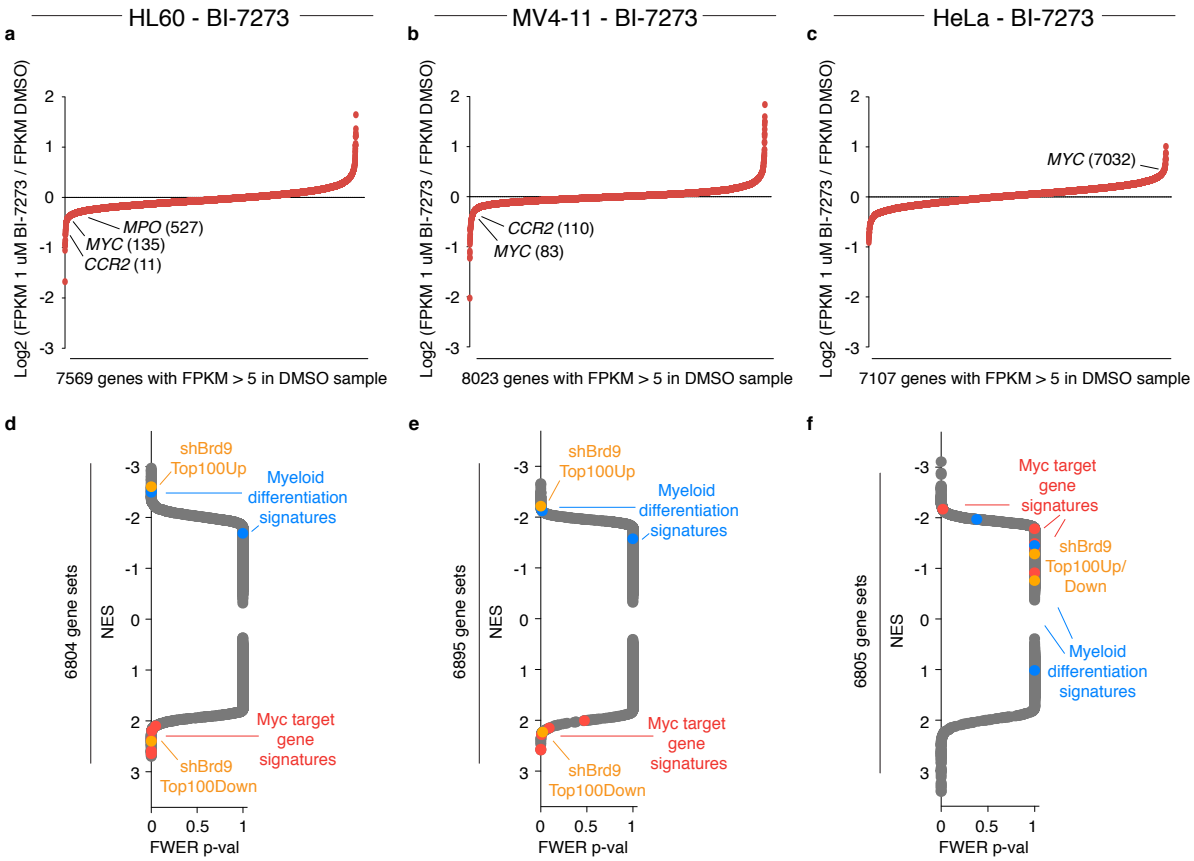

Figure 38. BI-7273-induced gene expression changes in HL60, MV4-11, HeLa cells highlights context-dependent effect on MYC expression.
(a, b, c) RNA-Seq analysis of gene expression changes in HL60 (a), MV4-11 (b) and HeLa (c) cells after 24 hours of 1 μBI-7273 exposure. FPKM values from treated cells were normalized to FPKM values recorded in cells cultured in the presence of DMSO. Genes with a FPKM value $<$ 5 in the DMSO sample were excluded. Genes are plotted from the most down-regulated genes on the left to the most up-regulated genes on the right.
(d, e, f) Gene set enrichment analysis (GSEA) on the RNA-Seq data presented in (d), (e) and (f), respectively. Evaluated all gene sets available through the Molecular Signatures Database containing 15-500 of the differentially expressed genes in our RNA-Seq dataset (6798, 6889, 6799 out of 10153 gene sets, respectively) plus six additional gene sets (shBrg1_Top100Up or Down, LSC_Signature_Somervaille, Macrophage_development_(IPA), shBrd9_Top100Up or Down). A positive Normalized Enrichment Score (NES) reflects enrichment on the left side of the ranked gene list (genes down-regulated with BI-7273), a negative NES reflects enrichment on the right of the ranked gene list (genes up-regulated with BI-7273). FWER p-val, familywise-error rate p-value.

In addition, retroviral overexpression of Myc reduced the sensitivity of RN2 cells to BI-7273, in accord with Myc suppression being a major consequence of both chemical and genetic targeting of Brd9 (Fig. 39 and Fig. 17). Collectively, these findings independently support the identification of BRD9 as the relevant cellular target of BI-7273, and further indicate that on-target chemical inhibition of Brd9 leads to AML-specific Myc suppression and a consequent arrest of rapid cell proliferation.

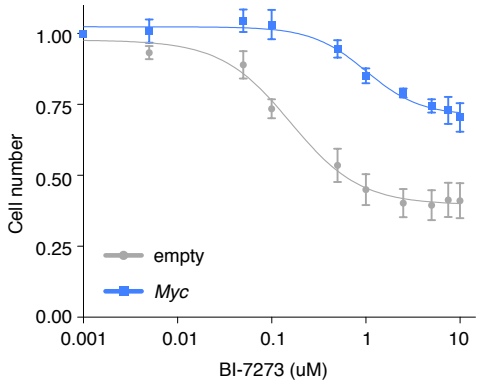

Figure 39. Myc overexpression reduces the sensitivity of AML cells to BI-7273.
Cell counts to measure the effect of the BRD9 bromodomain inhibitor BI-7273 on the growth of RN2 cells transduced with and selected for empty vector or Myc (MSCV-based vector). Cells were cultured in the presence of increasing inhibitor concentrations for 5 days before cell numbers were determined and normalized to DMSO control. Curves were fit by four parameter non-linear regression using the least squares fitting method. Error bars represent SEM. n=3

4.2.2 Evaluation of gene expression changes induced by published BRD9 inhibitors

We also applied RNA-Seq and GSEA analysis to evaluate gene expression changes induced by the two published BRD9 inhibitors in RN2 cells. While 1 μM I-BRD9 provoked a similar pattern of gene expression changes as BI-7273, 1 μM LP99 only minimally influenced Brd9-dependent gene expression (Fig. 40). These findings are in agreement with results of the bromodomain-swap assay, which revealed on-target effects of I-BRD9, but not LP99, at the 1 μM concentration (Fig. 34).

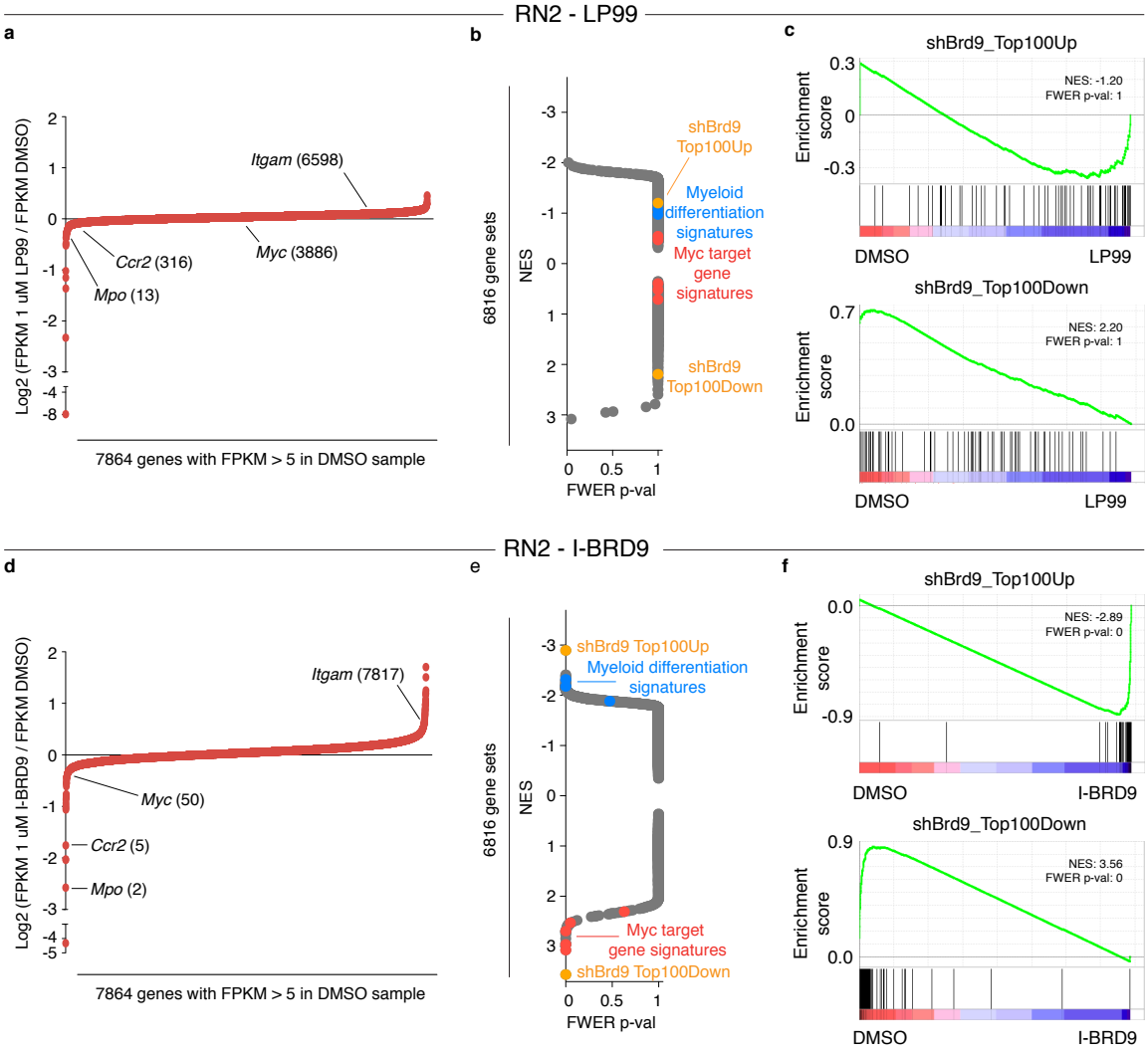

Figure 40. Evaluation of gene expression changes induced by published BRD9 inhibitors.
(a, d) RNA-Seq analysis of gene expression changes in RN2 cells treated with LP99 (a) or I-BRD9 (d) at 1 μM for 24 hours. FPKM values from treated cells were normalized to FPKM values recorded in cells cultured in the presence of DMSO. Genes with a FPKM value < 5 in the DMSO sample were excluded. Genes are plotted from the most down-regulated genes on the left to the most up-regulated genes on the right.
(b, e) Gene set enrichment analysis (GSEA) of the RNA-Seq data presented in (a) and (d), respectively. Evaluated all gene sets available through the Molecular Signatures Database containing 15-500 of the differentially expressed genes in our RNA-Seq dataset (6810 out of 10153 gene sets in both cases) plus six additional gene sets (shBrg1_Top100Up or Down, LSC_Signature_Somervaille, Macrophage_development_(IPA), shBrd9_Top100Up or Down). A positive Normalized Enrichment Score (NES) reflects enrichment on the left side of the ranked gene list (genes down-regulated with BI-7273), a negative NES reflects enrichment on the right of the ranked gene list (genes up-regulated with BI-7273). FWER p-val, familywise-error rate p-value.
(c, f) GSEA plots of the top 100 genes up- and down-regulated after 2 days of shBrd9 expression in RN2 cells (shBrd9_Top100Up and shBrd9_Top100Down) based on the RNA-Seq data presented in (a) and (d), respectively.

5 Broader utility of the domain-swap assay in target validation

5.1 A SET domain-swap allele of *EZH2* can rescue the anti-proliferative effects of the EZH2 SET domain inhibitor GSK126

Having recognized the utility of the domain-swap allele of BRD9 in distinguishing on-target from off-target effects of different BRD9 inhibitors, we next explored whether the domain-swap strategy could be applied to evaluate the activities of other chromatin-modulating chemical probes. Recent studies have characterized small-molecule inhibitors of the EZH1 and EZH2 SET domains, which catalyze H3K27 methylation to repress transcription [McCabe and Creasy, 2014, Margueron and Reinberg, 2011]. One such molecule, GSK126, exhibits > 150-fold selectivity for EZH2 versus EZH1, despite the 94% identity of their two SET domains (Fig. 41a) [McCabe et al., 2012]. Moreover, it has previously been established that MLL-AF9-transformed AML cells are dependent on EZH2, and undergo growth-arrest following exposure to GSK126 [Neff et al., 2012, Kim et al., 2013]. Based on this, we considered the possibility that expressing a variant of EZH2 harboring the SET domain of EZH1 (hereafter termed EZH2$^{\text{EZH1-SET}}$) in RN2 cells might confer resistance to GSK126. To this end, we transduced RN2 cells with wild-type human EZH2 or EZH2$^{\text{EZH1-SET}}$ and compared the effect of GSK126 on the proliferation of these cells (Fig. 41b, c). While overexpression of wild-type EZH2 minimally influenced the sensitivity of RN2 cells to GSK126, we found that overexpression of EZH2$^{\text{EZH1-SET}}$ rendered the cells resistant to GSK126 at concentrations up to 10 μM (Fig. 41c). These results confirm the specificity of GSK126 for EZH2 versus EZH1, and establish EZH2 as the single target underlying the effects of this molecule under these experimental conditions. Collectively, the findings in this study suggest a broader utility for domain-swap alleles in establishing on-target effects of chemical probes in cells.

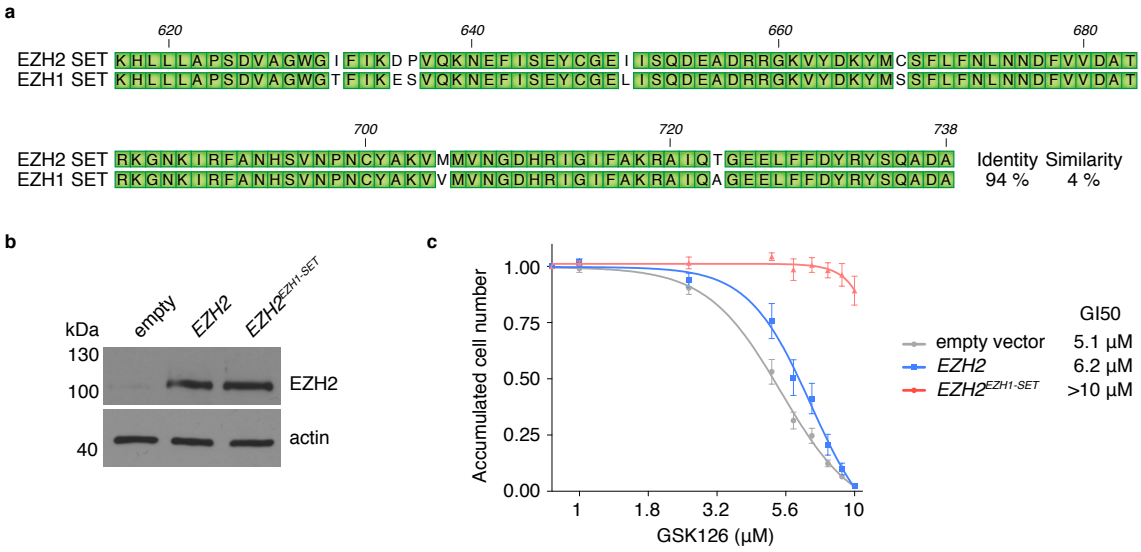

Figure 41. A SET domain-swap allele validates on-target activity of the EZH2 inhibitor GSK126.

(a) Protein sequence alignment of the EZH2 and EZH1 SET domains. Residues in EZH1 that are identical to the corresponding amino acid in EZH2 are highlighted in green boxes. The numbering on top of the alignment corresponds to the residue number in EZH2. Sequence identity and similarity were calculated using the gonnet similarity matrix in MacVector. EZH2 sequence corresponds to isoform A (NM_001203249.1/NP_001190178.1).

(b) Western blot to test expression of EZH2 wt and EZH2EZH1-SET in RN2 cells. The antibody recognizes human EZH2 exclusively. For this reason no Ezh2 band is observed in the 'empty' lane. The actin blot serves to control for loading.

(c) Cell counts to measure the effect of EZH2 inhibitor GSK126 on the growth of RN2 cells transduced with and selected for empty vector, EZH2 or EZH2EZH1-SET (MSCV-based vector). Cells were cultured in the presence of increasing inhibitor concentrations for 7 days before cell numbers were determined and normalized to DMSO control. Curves were fit by four parameter non-linear regression using the least squares fitting method. GI50 values were derived from non-linear regression curves with the bottom constrained to 0 and the top constrained to 1. Error bars represent SEM. n = 5

6 Discussion and perspectives

6.1 Potential and limitations of BRD9 inhibition for SWI/SNF targeting in AML

Our investigation into the role of BRD9 in leukemia was motivated by its existence as a SWI/SNF subunit. Our IP-MS and ChIP-Seq data imply that BRD9 associates with BRG1 and co-occurs with the SWI/SNF complex across the AML genome. Our results also indicate, however, that Brd9 is present only in a subset of SWI/SNF complexes in AML cells. The exact identity of BRD9-SWI/SNF complexes in AML remains to be defined. BRD9 IP-MS experiments would prove useful in identifying BRD9 associated factors and defining the composition of BRD9-SWI/SNF complexes in these cells. Our BRG1 IP-MS experiments in NOMO-1 cells precipitated not just SWI/SNF-A subunits such as ARID1A, ARID1B, BRD9, and BAF45D, but also SWI/SNF-B subunits ARID2 and BAF54A, further supporting the notion that distinct SWI/SNF assemblies may co-exist in this cell type. While heterogeneity is a defining feature of the mammalian SWI/SNF complex, it complicates the targeting of BRG1-mediated SWI/SNF functions through accessory subunits. The phenotype of Brd9 knockdown cells shows several close parallels to that observed after Brg1 knockdown, which is in concert with Brd9 being part of the tumorigenic Brg1-SWI/SNF complex that regulates *Myc* expression in AML cells. However, it is noteworthy that the Brd9 requirement in RN2 cells can be entirely bypassed by overexpressing Myc, whereas Myc overexpression only minimally alleviates the Brg1 requirement in this context. This suggests that while Brd9 acts primarily through activating *Myc*, Brg1 has *Myc*-independent means of sustaining AML, which cannot be targeted through Brd9 inhibition. Consistently, our comparison of gene expression changes after Brd9 and Brg1 knockdown revealed that Brg1, but not Brd9, plays a role in the regulation of pro-apoptotic genes. This result, in conjunction with our Brg1 ChIP-seq analysis in BI-7273 treated RN2 cells, implies that the bromodomain functionality of Brd9 is only relevant at a subset of SWI/SNF-dependent genes, which, in leukemia cells, includes *Myc*.

6.2 Insights into targeting the SWI/SNF complex in cancer

How best to attack the SWI/SNF complex for cancer therapy remains an ongoing discussion. One important implication of our findings is that targeting individual subunits is likely to only affect SWI/SNF localization at a subset of *cis* elements, which can be explained by the presence of multiple chromatin binding modules within highly heterogeneous SWI/SNF complex assemblies. Therefore, it is likely that combined targeting of multiple SWI/SNF surfaces will be necessary to achieve complete complex eviction from chromatin. Since chemical modulation of SWI/SNF holds considerable promise as a therapeutic avenue in cancer, future efforts should be directed at defining the full complement of chromatin-binding modules in SWI/SNF and how such surfaces act in a redundant/compensatory manner with one another. Such an approach may reveal opportunities for combining BRD9 inhibitors with other small-molecules to achieve potent SWI/SNF displacement and consequent therapeutic effects in cancer. An alternative approach might be to target SWI/SNF complexes for proteasome-mediated destruction, which has recently been achieved for bromodomain-containing proteins by conjugating bromodomain inhibitors to phthalimide derivatives [Lu et al., 2015, Winter et al., 2015, Zengerle et al., 2015]. Compounds aiming to provoke SWI/SNF disassembly would also be worth investigating. So far, the only subunit identified for maintaining the structural integrity of SWI/SNF complexes is ARID1A/B [Helming et al., 2014]. In analogy to the stapled EZH2 peptide, stabilized peptides mimicking ARID1A/B domains could be assessed in this regard [Kim et al., 2013].

In the case of AML, it further remains to be seen if a therapeutic window exists for inhibition of the BRG1 ATPase. In support of this approach, BRG1-mutant animals retain an intact hematopoietic stem cell compartment [Buscarlet et al., 2014]. Indeed, even dual inactivation of BRG1/BRM in adult mice was found to cause minimal effects on the abundance of hematopoietic stem cells and multipotent progenitors [Willis et al., 2012]. The risk of carcinogenesis as a potential on-target consequence and the developmental abnormalities associated with BRG1 mutations in mice and in humans indicate the potential limitations to this approach.

6.3 BRD9 - a context-specific dependency in cancer

Synthetic lethal interactions within the SWI/SNF complex were a breakthrough discovery for many previously intractable SWI/SNF mutant cancers. A key question that arose from these studies was whether these cancers depend exclusively on the paralogs of the inactivated subunit or if the entirety of the residual SWI/SNF complex represents a cancer-specific dependency. In our study, we found that BRG1-deficient lung cancers are insensitive to BRD9 knockdown and to chemical BRD9 inhibition, despite being dependent on residual SWI/SNF complexes. While the exact subunit composition of the residual SWI/SNF complex in these lung cancers remains to be established, our result suggests that SWI/SNF-mutant cancers do not rely on all remaining subunits. This finding also indicates that Brd9 is not a universal requirement for SWI/SNF function in supporting cancer growth. Instead, our study reveals a context-specific role for BRD9 in cancer. While several genetically distinct subtypes of AML are sensitive to BRD9 inhibition, we discovered no such BRD9 dependence in solid cancers. Interestingly, the Brd9-dependent *Myc* enhancers are only active in the hematopoietic lineage [Shi et al., 2013]. This raises the possibility that a cell type-specific enhancer configuration present in leukemia cells may underlie the selective Brd9 dependency for cell proliferation in this context. Additionally, we detected no BRD9 dependence in breast cancer cells that carry a BRD9 amplification and express elevated BRD9 mRNA levels. This suggests that the amplification of BRD9 in solid cancers might be a passenger rather than a driver of oncogenesis - a hypothesis that seems particularly likely given the close chromosomal proximity of BRD9 to the TERT gene.

6.4 Implications of the functional redundancy of certain bromodomains

The on-target effects of chemical Brd9 inhibition in our study were established by using the *BRD9-BET* bromodomain-swap allele, which replaces the BRD9 bromodomain with that of the first bromodomain of BRD4. The interchangeability of the BRD9 and BRD4 bromodomains in these experiments was highly unexpected, since recombinant bromodomains were reported to have varying affinity for acetylated lysines at distinct positions in histone tails and it is believed that bromodomains have selective targeting potential [Filippakopoulos et al., 2012]. BRD9 and

BRD4, in particular, exhibit markedly different binding preferences for acetylated peptides in biochemical assays and belong to different phylogenetic subfamilies of bromodomain modules [Filippakopoulos et al., 2012]. Interestingly however, Brd4, Brd9, and BRD9-BET are each highly enriched at the *Myc* enhancers in AML cells [Shi et al., 2013]. Given the importance of the *Myc* gene among the Brd9 target genes, it is conceivable that any bromodomain that localizes to the *Myc* enhancer - independent of histone tail preference - will allow BRD9 to perform its function. This leads us to speculate that the distinct ligands of the BRD4 and BRD9 bromodomains in the cell are likely to coexist at the distal *Myc* enhancers in AML cells, which would allow two otherwise divergent reader domain modules to be functionally synonymous. In order to evaluate this latter possibility, insights into the binding pattern of BRD7 and BRD1 in leukemia would be informative, as their bromodomains were similarly capable of functionally replacing that of BRD9.

6.5 A necessity for drug mechanism of action assays

Original efforts to identify pharmaceutical agents for cancer therapy date back to the 1940s, when knowledge about cellular components and their functions in health and disease was limited. Nonetheless, cytotoxic drugs with surprising efficacy in certain cancers were discovered and, specifically through combination chemotherapy, patient outcome could be drastically improved. A major drawback of conventional chemotherapy is the limited specificity of its cytotoxic effects for cancer cells, such that severe side effects limit tolerable doses. With the recognition of genetic mutations as critical drivers of tumorigenesis, targeted cancer therapies were successfully developed to affect cancer cells with higher selectivity. Traditionally, the initial stages of a chemotherapeutic development program included a high-throughput phenotypic screen of a large library of chemical compounds to identify those molecules that provoked the desired cellular phenotypes. In the pursuit of targeted cancer therapies, drug development approaches have shifted to reverse chemical genetics, in which a protein target is selected prior to the generation of small-molecule inhibitors [Schenone et al., 2013]. While these therapies hold great promise in light of our growing understanding of the alterations underlying human malignancies, they rely on our ability to interfere with target protein function in a highly se-

lective manner to allow efficacy and tolerability. Achieving selectivity of small-molecules is a formidable challenge and can sometimes be impossible, in particular when targeting conserved protein domains. Although recent advances in polypharmacology have highlighted that hitting more than a single protein target can have beneficial consequences in terms of efficacy, it also bears the risk of unintended off-target effects. The high attrition rate of chemical inhibitors in clinical development highlights the need for better tools to understand a compound's mechanism of action early during the drug development process [Frigault and Barrett, 2014].

6.6 The potential of domain-swap alleles

Assessing the risk of a compound's off-target effects necessitates profiling its binding activities in the cell. To elucidate a compound's cellular mechanism of action, however, identifying its binding partners in the cell is not sufficient. Instead, to interpret compound-induced cellular phenotypes and to guide probe or drug development, it is critical to differentiate physiologically irrelevant compound-protein interactions from those binding events that are responsible for the observed phenotypic changes. In the field of epigenetic target validation, common approaches include structure-activity relationship assays of analogous small molecules as well as comparisons of cellular effects of structurally dissimilar compounds against the same target. Additionally, correlation analysis between genetic perturbations of a presumed target and compound-provoked phenotypes can be elucidating, as is highlighted in our analysis of BRD9 inhibitors. However, to our knowledge, so far it has not been possible to extend the development of resistance alleles, which have proven useful for validating various signaling molecules as relevant drug targets, to the field of epigenetic compound validation.

Our study highlights the use of domain-swap alleles as a chemical-genetic strategy with potential for broad utility in establishing the relevant protein target underlying the biological effects of a chromatin modulating small-molecule. Such a reagent may aid our interpretation of effects of existing chemical probes, particularly those with only partially characterized target selectivity in biochemical assays. The approach may further prove useful in our evaluation and optimization of chemical probes during the drug development process, particularly for chromatin regulator drug targets. Since minimal biochemical and structural insight into a protein target is required

to generate a domain-swap allele, this approach can be readily expanded to many targets of small-molecules. A large-scale effort to define functionally synonymous members within domain families may have potential to greatly expand our chemical-genetic toolkit.

7 Future directions

7.1 Unraveling the detailed cellular activities of BRD9

When we started this project, BRD9 was an essentially unstudied protein. In the course of this study, we have learned that BRD9 associates with the SWI/SNF complex in AML, that it binds to chromatin and regulates gene expression. One aspect of its cellular activity that remains to be investigated is the dedication of BRD9 to the SWI/SNF complex in AML cells. Our ChIP-Seq analysis revealed a majority of Brd9 and Brg1 co-occupied regions, however we also observed examples of peaks to which only one of the two proteins localized. 'Brg1 only' peaks are in agreement with our hypothesis that Brd9 is present only in a subset of SWI/SNF complexes in leukemia cells, but we were intrigued to find regions bound by Brd9 alone. Previously, BRD9 was identified as a dedicated component of SWI/SNF-A complexes in a human T-cell line [Kadoch et al., 2013]. Whether this is equally true in AML cells remains to be investigated. BRD9 precipitation followed by density sedimentation would allow assessment of the dedication of BRD9 to the SWI/SNF complex, and might reveal a potential existence of BRD9 outside of the SWI/SNF complex. Additionally, a ChIP-Seq repeat with an independent Brd9 antibody in RN2 cells would help to eliminate any peaks caused by non-specific antibody binding. However, any remaining 'Brd9 only' peaks would indicate SWI/SNF-independent functions of Brd9. A comparison of the location of such peaks to the list of genes whose expression changes following Brd9 knockdown would allow us to assess whether binding at these locations is relevant for the leukemia maintenance function of Brd9.

The activities of the Domain of Unknown Function (DUF) represent another open question that remains to be answered. Our ChIP-qPCR analysis in the presence of BI-7273 revealed that inhibition of the bromodomain reduces BRD9 occupancy on chromatin. If we therefore assume that the bromodomain constitutes BRD9's chromatin interaction module, the DUF might form the point of contact with the SWI/SNF complex. Our mutational analysis showed that the DUF is critical for BRD9 function in AML and that the BRD9 and BRD7 DUFs are not interchangeable. As BRD9 and BRD7 have been reported to be associated with SWI/SNF-A (BAF) and SWI/SNF-B (PBAF), respectively, it is possible that their unique DUFs facilitate

incorporation into these different SWI/SNF assemblies. To explore this possibility, it will be illuminating to compare the interactome of BRD9 to that of the BRD9 ΔDUF mutant, as well as to that of BRD7.

7.2 Enhancing the anti-leukemic effects of BRD9 bromodomain inhibition

The BRD9 bromodomain inhibitors identified in this study limit the proliferation of AML cells through their on-target engagement of BRD9 in the cell. However, in comparison to published inhibitors of other chromatin modifiers with efficacy in AML models (e.g. BRD4 or DOT1L inhibitors), the reduction in proliferative capacity of AML cells in response to BI-7273 is of modest magnitude. Efforts to enhance the anti-leukemia effects of this inhibitor should be explored.

Unlike BRD4, which is almost completely displaced from chromatin in the presence of JQ1, SWI/SNF binding to chromatin was only modestly reduced by our BRD9 inhibitors. Based on the assumption that the SWI/SNF complex fulfills its leukemia maintenance function predominantly through its association with chromatin, achieving greater SWI/SNF eviction is desirable. As SWI/SNF likely associates with chromatin through several of its subunits, simultaneous inhibition of two or more of these chromatin-binding modules is worth investigating. In a pilot study, we found that a combination of JQ1, the BRG1/BRM bromodomain inhibitor PFI-3, and our BRD9 inhibitor BI-7273 did not increase SWI/SNF displacement. However, several other SWI/SNF-subunits remain to be investigated for their contribution to SWI/SNF chromatin binding. In the absence of chemical inhibitors of these proteins, we could leverage domain-focussed CRISPR screening, which was recently established in our lab. To this end, a sgRNA library targeting all domains found in SWI/SNF subunits could be constructed. Evaluating the effects of this library in AML cells in the presence and absence of BI-7273, could reveal potential synergistic interactions.

It is further possible that the anti-leukemic effects of BRD9 bromodomain inhibitors could be augmented by combination with compounds targeting proteins outside of the SWI/SNF

complex. In recognition of the importance of epigenetic modifiers in the pathogenesis of AML, it would be interesting to investigate potential synergistic effects within this class of proteins. A domain-focused CRISPR-screening library targeting various epigenetic writers, erasers and readers exists in our lab, and the effect of these libraries on leukemia cells could be compared in the presence and absence of BI-7273.

7.3 Extending the use of the domain-swap assay

While the functional interchangeability of chromatin-modifying domains could not have been anticipated, our study has demonstrated two cases in which a domain-swap allele was successfully expressed and adopted the function of its wild-type counterpart, thereby allowing the relevant cellular target of a chromatin-targeted compound to be revealed. An important shortcoming of epigenetic therapies currently in the clinic (DNMTi and HDACi) is the limited understanding of their mechanisms of action, which has been listed as one of the obstacles to their broader application in cancer therapy thus far. Identifying the relative contributions to individual DNMTs and HDACs to the phenotypes provoked by these inhibitors could be an important step towards a more defined molecular mechanism with implications for clinical response predictions.

Additionally, it would be interesting to explore the extent of functionally synonymous domains within the class of epigenetic regulators. Although the generation of libraries of domain-swap alleles is not trivial, positive selection screens in the presence of chromatin-modifying compounds could discern on-target from off-target phenotypic contribution in a previously unprecedented manner.

8 Conclusions

The aim of this study was to evaluate the possibility of interfering with SWI/SNF function in AML through inhibition of the non-ATPase bromodomain-containing subunits PBRM1, BRD7, or BRD9. We have shown that unlike PBRM1 and BRD7, BRD9 is an essential and targetable component of SWI/SNF complexes in AML. Like the SWI/SNF ATPase Brg1, Brd9 is required to sustain *Myc* transcription, rapid cell proliferation, and a block in differentiation. In collaboration with Boehringer Ingelheim, we have developed nanomolar affinity BRD9 bromodomain inhibitors that selectively impair proliferation of AML cells. The modest, yet reproducible Brg1 displacement from chromatin in the presence of these inhibitors is a promising result and an important proof-of-concept for the ability to target SWI/SNF through accessory subunits.

Additionally, we have engineered a bromodomain-swap allele of *BRD9* that retains functionality despite a radically altered bromodomain pocket. To our knowledge, this constitutes the first engineered resistance allele of a chromatin reader target. We employed this allele to validate BRD9 as the relevant cellular target of our BRD9 inhibitors in AML. We further revealed the ability of this assay to identify the superior compound among a series of chemical inhibitors against the same target. Additionally, we have demonstrated a broader utility of the domain-swap approach for generating resistance alleles of chromatin modulators, as we were able to engineer a resistant version of EZH2 using the same strategy.

Our study demonstrates a previously unrecognized role of BRD9 in cancer and reveals a simple genetic assay to probe on-target activity of chromatin-modulating chemical probes in cells (Fig. 42).

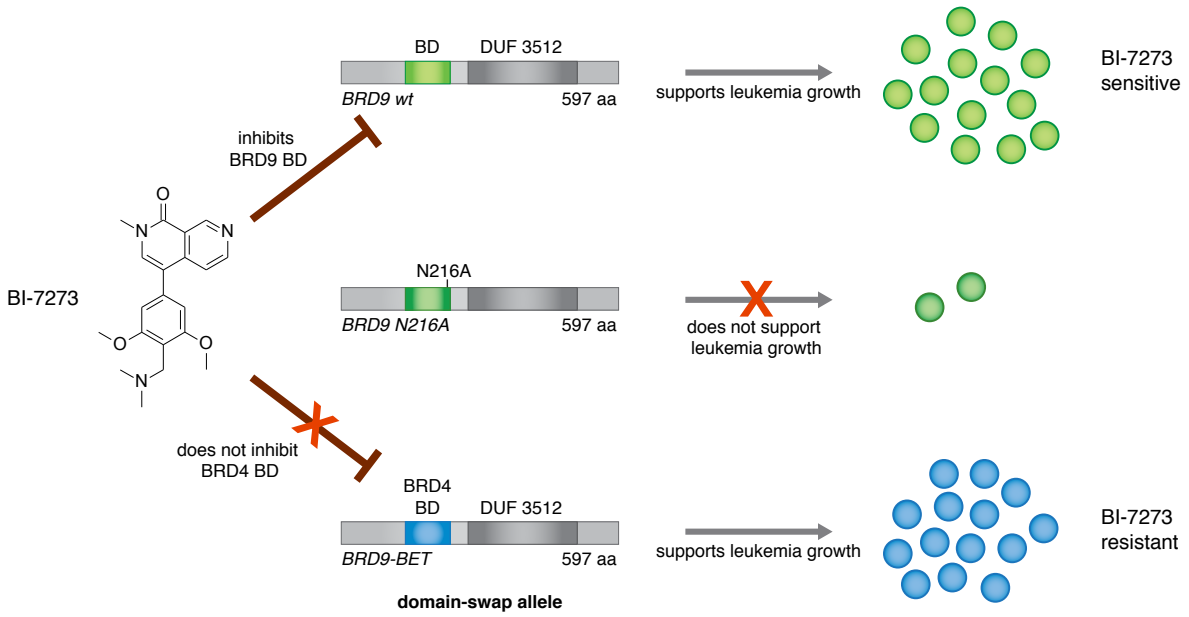

Figure 42. Graphical Summary: A bromodomain-swap allele demonstrates that on-target chemical inhibition of BRD9 limits the proliferation of acute myeloid leukemia cells.
BRD9 constitutes a specific requirement for the rapid proliferation of AML cells. The bromodomain is essential for the leukemia-supporting function of BRD9, and AML cells are sensitive to the BRD9 bromodomain inhibitor BI-7273. A domain-swap allele of *BRD9*, which carries the first bromodomain of BRD4 instead of its own, is functional in AML cells and insensitive to BI-7273 binding. Overexpression of this *BRD9-BET* allele renders AML cells resistant to BI-7273, thereby validating BRD9 as the relevant target underlying the BI-7273 sensitivity of these cells.

9 Materials and Methods

9.1 Immunoprecipitation

To isolate nuclear extracts, NOMO-1 cell pellets were washed in PBS, resuspended in Buffer A2 (10 mM Hepes-KOH pH 7.9, 1.5 mM $MgCl_2$, 10 mM KCL) and incubated on ice for 30 min to allow cell lysis to occur. Nuclei were separated by centrifugation, resuspended in Buffer C2 (20 mM Hepes-KOH pH 7.9, 25 % glycerol, 420 mM NaCl, 1.5 mM $MgCl_2$, 0.2 mM EDTA) and incubated on ice for 30 min, prior to spinning in a table-top centrifuge at 16,100 g, 4 °C for 10 min. The resulting supernatant was dialyzed against Buffer D (20 mM Tris pH 8.0, 20 % glycerol, 0.2 mM EDTA, 100 mM KCl) using a 3,500 molecular weight cutoff dialysis bag overnight. To immunoprecipitate the SWI/SNF complex, 1 ug BRG1 antibody (Santa Cruz #sc-17796) or control IgG antibody were incubated with ∼1 mg dialyzed nuclear extract for 2 hrs at 4 °C. The antibody-antigen complex was pulled down in a 2 hr incubation with BSA pre-blotted dynabeads (protein G). To remove any non-specific binders, the dynabeads were washed three times with Tris buffer pH 7.5 containing 300 mM NaCl and 0.5 % NP-40. Before subjecting to iTRAQ MS, the samples were washed one time with 1x PBS and one time with 1/2x PBS. All buffers contained protease inhibitors (Roche) and 1 mM DTT.

9.2 iTRAQ mass spectrometry[4]

9.2.1 Tryptic digestion and iTRAQ labeling

The beads for BRG1 and IgG control samples were reconstituted with 20 uL of 50 mM triethylammonium bicarbonate buffer (TEAB). Protease Max Surfactant was added to a final concentration of 0.1 % and tris(2-carboxyethyl)phosphine (TCEP) was added to a final concentration of 5 mM. Samples were then heated to 55 °C for 20 min, allowed to cool to room temperature and methyl methanethiosulfonate (MMTS) was added to a final concentration of 10 mM. Samples were incubated at room temperature for 20 min to complete blocking of free sulfhydryl groups. 2 ug of sequencing grade trypsin (Promega) was then added to the sam-

[4]performed at Cold Spring Harbor Laboratory's Proteomics Shared Resource

ples and they were digested overnight at 37 °C. After digestion the supernatant was removed from the beads and was dried *in vacuo*. Peptides were reconstituted in 50 uL of 0.5 M TEAB, 70 % ethanol and labeled with 8-plex iTRAQ reagent for 2 hrs at room temperature [Ross et al., 2004]. Labeled samples were then acidified to pH 4 using formic acid, combined and concentrated *in vacuo* until ∼10 uL remained.

9.2.2 2-dimensional fractionation

Peptides were fractionated using a high-low pH reverse phase separation strategy [Gilar et al., 2005]. For the first (high pH) dimension, peptides were fractionated on a 10 cm × 1.0 mm column packed with Gemini 3u C18 resin (Phenomenex, Ventura, CA) at a flow rate of 100 ul/min. Mobile phase A consisted of 20 mM ammonium formate pH 10 and mobile phase B consisted of 90 % acetonitrile, 20 mM ammonium formate pH 10. Samples were reconstituted with 50 uL of mobile phase A and the entire sample injected onto the column. Peptides were separated using a 35 min linear gradient from 5 % B to 70 % B and then increasing mobile phase to 95 % B for 10 min. Fractions were collected every minute for 40 min and were then combined into 8 fractions using the concatenation strategy [Wang et al., 2011b]. Each of the 8 fractions was then separately injected into the mass spectrometer using capillary reverse phase LC at low pH.

9.2.3 Mass spectrometry

An Orbitrap Velos Pro mass spectrometer (Thermo Scientific), equipped with a nano-ion spray source was coupled to an EASY-nLC system (Thermo Scientific). The nano-flow LC system was configured with a 180 μm id fused silica capillary trap column containing 3 cm of Aqua 5 μm C18 material (Phenomenex), and a self-pack PicoFrit^{TM} 100 μm analytical column with an 8 μm emitter (New Objective, Woburn, MA) packed to 15 cm with Aqua 3 μm C18 material (Phenomenex). Mobile phase A consisted of 2 % acetonitrile, 0.1 % formic acid and mobile phase B consisted of 90 % acetonitrile, 0.1 % formic Acid. 3 uL of each sample dissolved in mobile phase A, were injected through the autosampler onto the trap column. Peptides were

then separated using the following linear gradient steps at a flow rate of 400 nL/min: 5 % B for 1 min, 5 % B to 35 % B over 70 min, 35 % B to 75 % B over 15 min, held at 75 % B for 8 min, 75 % B to 8 % B over 1 min and the final 5 min held at 8 % B. Eluted peptides were directly electrosprayed into the Orbitrap Velos Pro mass spectrometer with the application of a distal 2.3 kV spray voltage and a capillary temperature of 275 °C. Each full-scan mass spectrum (Res=60,000; 380-1700 m/z) was followed by MS/MS spectra for the top 12 masses. High-energy collisional dissociation (HCD) was used with the normalized collision energy set to 35 for fragmentation, the isolation width set to 1.2 and activation time of 0.1. A duration of 70 sec was set for the dynamic exclusion with an exclusion list size of 500, repeat count of 1 and exclusion mass width of 10 ppm. We used monoisotopic precursor selection for charge states 2+ and greater, and all data were acquired in profile mode.

9.2.4 Database searching

Peaklist files were generated by Mascot Distiller (Matrix Science). Protein identification and quantification was carried using Mascot 2.548 against the UniProt human sequence database (89,005 sequences; 35,230,190 residues). Methylthiolation of cysteine and N-terminal and lysine iTRAQ modifications were set as fixed modifications, methionine oxidation and deamidation (NQ) as variable. Trypsin was used as cleavage enzyme with one missed cleavage allowed. Mass tolerance was set at 30 ppm for intact peptide mass and 0.3 Da for fragment ions. Search results were rescored to give a final 1 % FDR using a randomized version of the same Uniprot Human database. Protein-level iTRAQ ratios were calculated as intensity weighted, using only peptides with expectation values <0.05. As this was a protein IP experiment, no global ratio normalization was applied. Protein enrichment was then calculated by dividing the true sample protein ratios by the corresponding control sample ratios.

9.3 ChIP-Seq

9.3.1 Library preparation and Illumina sequencing

50 - 100 million cells were crosslinked by adding formaldehyde to a final concentration of 1 % and shaking at room temperature for 20 min. Crosslinking was quenched by incubating with 0.125 M glycine for 10 min. ChIP was performed as previously described [Steger et al., 2008]. Immunoprecipitated DNA was purified using a QIAquick Gel Extraction Kit (Qiagen) and ChIP-Seq libraries were generated using the TruSeq ChIP Sample Prep Kit (Illumina) following the manufacturer's instructions. The quality of each library was determined using a Bioanalyzer and High Sensitivity chip (Agilent). Library DNA sizes ranged from 250 to 300 bp. Barcoded libraries were multiplexed at equal molar ratio (two to six libraries per lane) and sequenced using an Illumina HiSeq 2000 platform as single end reads of 50 bases.

9.3.2 Data analysis

Sequencing reads of 50 bp were mapped to the murine genome assembly mm9 or the human genome assembly hg19 using Bowtie. The MACS peak finding algorithm version 1.4.2 was used to identify ChIP-Seq peaks. H3K27ac and H3K4me3 ChIP-Seq data in RN2 cells was obtained from GSE52277.

9.3.3 Density map generation

In the generation of density plots, all Brg1 peaks with an FDR <0.05 % and a minimal fold enrichment of 5 over input were used. Brg1 peaks were considered as promoters if the peak showed at least 1 bp overlap with a +/- 200 bp window surrounding RefSeq gene transcription start sites (TSSs). If Brg1-enriched peaks showed no overlap with the +/- 200 bp window surrounding RefSeq gene TSSs, they were considered enhancer-bound peaks. Heatmap matrices were created by counting tags using the indicated window size with 50 bp bins. Heatmap matrices were visualized by Java TreeView 1.1.6r4.

9.3.4 Quantifying FLAG-BRD9 and Brg1 chromatin occupancy after BI-2 treatment

High confidence peaks (FDR <10 %; minimal fold enrichment of 10 over input) were identified among the DMSO treated FLAG-BRD9 and Brg1 ChIP-Seq data sets. Tag counts for these locations were then re-calculated from uniquely mapped reads in both, DMSO and BI-7273 treated samples, and normalized to the total number of uniquely mapped reads in each data set (to control for differences in sequencing depth). Changes in FLAG-BRD9 and Brg1 chromatin occupancy after BI-7273 exposure were then quantified as the fold change of normalized tag counts between BI-7273 and DMSO treated samples for each of the identified high confidence peaks. To exclude regions of minimal occupancy, peaks with tag counts below 40 and 200 were excluded from the analysis of FLAG-BRD9 and Brg1 binding alterations, respectively.

9.4 Plasmids

For competition assays in RN2 cells, LMN-GFP or LMN-mCherry shRNA retroviral vectors were used (MSCV-miR30-shRNA-PGK-NeoR-IRES-GFP/mCherry). For competition assays in human cell lines, shRNAs were expressed from the MLS-E GFP vector (MSCV-miRE-shRNA-SV40-GFP) [Fellmann et al., 2013]. Conditional RNAi experiments in RN2 cells employed the TRMPV-Neo shRNA vector (MSCV-TRE-dsRed-miR30-shRNA-PGK-GFP-IRES-NeoR)[Zuber et al., 2011a]. cDNA constructs were expressed from an MSCV-based vector containing a puromycin resistance gene and a GFP reporter (MSCV-transgene-PGK-Puro-IRES-GFP). CRISPR experiments were performed using an MSCV-based vector for hCas9 expression (MSCV-hCas9-PGK-Puro) and a lentiviral vector for sgRNA expression (U6-sgRNA-EFS-GFP).

9.5 Cell culture

The murine AML line used here (RN2) was derived from a mouse model of MLL-AF9/Nras^{G12D} AML as previously described [Zuber et al., 2011a]. Other cell lines used in this study were obtained from the ATCC or the DSMZ. Murine and human leukemia cells were cultured in

RPMI-1640 supplemented with 10 % fetal bovine serum (FBS) and penicillin/streptomycin. iMEF, human solid cancer cell lines, HEK293T and Plat-E cells were cultured in DMEM supplemented with 10 % FBS and penicillin/streptomycin. Cell lines were tested for Mycoplasma contamination once a month.

9.6 Virus production

Transient transfection was performed using PEI transfection methods. All retroviral packaging was performed using Plat-E cells in 10 cm plates according to established protocols. Virus was collected 48-72 hrs post transfection. For CRISPR-mediated evaluation of bromodomain requirements, lentiviral packaging of sgRNA plasmids was achieved by transfecting HEK293T cells in 96-well plates with lentiviral sgRNA, pVSVg, and psPAX2 plasmids in a 4:2:3 ratio. Virus was collected 36-72 hrs post transfection.

9.7 Competition assay to measure cellular effects of shRNAs

Cells were retrovirally transduced with LMN- or MLS-E shRNA vectors in which shRNA expression is linked to GFP expression through an IRES. The percentage of GFP expressing cells was then measured over various days post infection using a Guava Easycyte (Millipore). Forward and side scatter were used to gate on live cells before assessing GFP percentage. The rate at which the percentage of GFP positive cells declined over time was used to infer the growth disadvantage conferred by a given shRNA relative to the uninfected cells in the same culture. For cDNA rescue experiments, RN2 cells were first transduced with an MSCV-based vector carrying a transgene and GFP and cultured in the presence of puromycin (1 ug/ml) to select infected cells. Cells were subsequently transduced with LMN-mCherry shRNA vectors. Double GFP/mCherry positivity was tracked using a BD LSR2 flow cytometer. Forward and side scatter were used to gate on live, single cells before assessing GFP percentage. Data analysis was performed using Flowjo software.

9.8 Inducible shRNA expression

Cells were retrovirally transduced with TRMPV-Neo shRNA vectors, which constitutively express GFP. Cells were then cultured in the presence of neomycin (G418, to 10 ug/ml) until > 95 % of cells were GFP positive. shRNA expression was induced by the addition of doxycycline to a final concentration of 0.1 ug/ml. shRNA induction efficiency was evaluated by measuring the co-expression of dsRed. For BrdU and Annexin V assays, single cell-derived clones were generated by serial dilution. Clones were evaluated for their shRNA induction efficiency by measuring the percentage of double GFP/dsRed positive cells upon doxycycline addition.

9.9 RT-qPCR

Total RNA was extracted from cells using TRIzol (Invitrogen) according to the manufacturer's instructions. Isolated RNA was treated with DNase I to eliminate contaminating genomic DNA. For cDNA synthesis, SuperScript III reverse transcriptase (Life Technologies) was used according to the manufacturer's protocol. All results were quantified by qPCR performed using SYBR green (ABI) on an ABI 7900HT Fast Real-Time PCR machine, and normalized using Gapdh as a control gene.

9.10 RNA-Seq

9.10.1 Library preparation and Illumina sequencing

Total RNA was extracted using TRIzol reagent (Invitrogen) according to the manufacturer's instructions. RNA-Seq libraries were constructed using the TruSeq sample Prep Kit V2 (Illumina) according to the manufacturer's instructions. Briefly, 2 ug of total RNA were selected with the Poly-A selection procedure and fragmented enzymatically. Poly A-selected and fragmented RNA was further used as template for cDNA synthesis using the Super Script II master mix (Life Technologies). End repairing, dA tailing, adapter ligation and final library amplification steps were subsequently performed. RNA-Seq libraries were sequenced using the Illumina HiSeq 2000 platform. Barcoded libraries were sequenced in a multiplexed fashion of two to six

libraries at equal molar ratios, with single end reads of 50 bases.

9.10.2 Data analysis

For the RNAi data set (but not the BI-7273 data set), reads were trimmed to 28 bases corresponding to the 9th to 36th position from the 5' end of the reads for quality purposes. Reads were mapped to mouse genome assembly mm9 using Tophat. Differentially expressed genes were identified using Cuffdiff. During this step, structural RNAs (e.g., ribosomal or mitochondrial RNA) were masked. Only genes with FPKM values greater than 5 in the control (shRen or DMSO) sample and FPKM values > 0 in the test sample were included in the analysis. For the RNAi data set, the average FPKM value per gene of three independent Brd9 shRNAs was used to calculate the fold change to the shRen control sample. For BRD9 inhibitor datasets, two independent replicates (with DMSO and test compound samples each) were analyzed and then averaged. Only those genes were included in the plotted data that had FPKM > 5 in the DMSO sample and FPKM > 0 in test sample in both of the independent replicates.

9.10.3 Gene Set Enrichment Analysis (GSEA)

Gene set enrichment analyses were performed using the weighted GSEAPreranked mode according to the instructions at www.broadinstitute.org/gsea/index.jsp. Gene sets available through the Molecular Signatures Database containing 15-500 of the differentially expressed genes in the investigated RNA-Seq dataset were evaluated plus four to six additional custom gene sets (shBrg1_Top100Up or Down, LSC_Signature_Somervaillle and Macrophage_development_(IPA), shBrd9_Top100Up or Down). The Normalized Enrichment Score (NES) was used to quantify the extent of gene set enrichment along the ranked list of genes. The familywise-error rate p-value (FWER p-val) was chosen as the statistical measure as it corrects for multiple hypothesis testing and prevents false-positive results [Subramanian et al., 2005].

9.11 Cell surface marker staining and flow cytometry

RN2 cells transduced with TRMPV-Neo constructs were treated with 0.1 ug/ml doxycycline for 4 days to induce shRNA expression. Cells were then incubated with APC-conjugated Kit (1:200) or Mac-1 (1:200) antibodies in FACS buffer (5 % FBS, 0.05 % NaN3 in PBS) for 1 hr at 4 °C in the dark. Cells were washed 3x in FACS buffer and then analyzed on a BD LSR2 flow cytometer. Cell surface marker staining was evaluated in GFP+/dsRed+ (i.e. shRNA+) cell populations. Data analysis was performed using Flowjo software.

9.12 May-Grünwald-Giemsa cytospin staining

RN2 cells transduced with TRMPV-Neo constructs were treated with 0.1 ug/ml doxycyclin for 4 days to induce shRNA expression. 50,000 cells were then resuspended in 100 µl FACS buffer (5 % FBS, 0.05 % NaN3 in PBS) and cytospun onto glass slides using a Shandon Cytospin 2 Centrifuge at 500 rpm for 5 min. May-Grünwald (Sigma) and Giemsa (Sigma) staining was performed according to manufacturer's protocols. Images were collected using a Zeiss Observer Microscope with a 40x objective.

9.13 Annexin V staining

Clones derived from RN2 cells transduced with TRMPV-Neo constructs were treated with 0.1 ug/ml doxycycline for 4 days to induce shRNA expression. Annexin V apoptosis staining was then performed according to the manufacturer's protocol (BD, APC Annexin V Apoptosis Detection Kit) and cells were analyzed on a BD LSR2 flow cytometer. Early apoptotic (Annexin V+/DAPI-) cells were differentiated from live (Annexin V-/DAPI-) and dead (DAPI+) cells. Data analysis was performed using Flowjo software.

9.14 BrdU incorporation assay

Clones derived from RN2 cells transduced with TRMPV-Neo constructs were treated with 0.1 ug/ml doxycycline for 4 days to induce shRNA expression. Cells were then pulsed with BrdU

for 30 min and the BrdU incorporation assay was performed according to the manufacturer's protocol (BD, APC BrdU Flow Kit) with DAPI co-staining to measure DNA content. BrdU incorporation and DAPI staining was evaluated in GFP+/dsRed+ (i.e. shRNA+) cell populations. Data analysis was performed using Flowjo software.

9.15 Whole cell lysate preparation and Western blotting

Cell pellets were washed with PBS, resuspended in SDS-PAGE Sample Buffer and passed through a 26.5 gauge needle for 15x prior to boiling at 95 °C for 7 min. The equivalent of 25,000 cells was loaded per lane. Proteins were separated by SDS-PAGE and transferred to a nitrocellulose membrane. The membrane was blocked in 5 % milk for 1 hr at room temperature and then incubated in 1 antibody at 4 °C overnight. The membrane was washed 3x in TBS-T, incubated in 2 antibody for 2 hrs at room temperature, washed another 3x in TBS-T, incubated in ECL, and developed.

9.16 CRISPR-Screening

CRISPR-Cas9 screening was performed as previously described [Shi et al., 2015]. Briefly, RN2 cells were retrovirally transduced with MSCV-hCas9-PGK-Puro and cultured in the presence of puromycin (1 ug/ml) to select infected cells. Single cell-derived clones were then obtained by serial dilution, assayed for Cas9 expression by Western Blot (anti-FLAG) and clone RN2c was chosen to perform sgRNA competition assays. RN2c cells were plated in 96-well plates and lentivirally transduced with U6-sgRNA-EFS-GFP plasmids. The percentage of GFP expressing cells was then measured over various days post infection using a Guava Easycyte (Millipore). Forward and side scatter were used to gate on live cells before assessing GFP percentage. The extent to which the percentage of GFP positive cells declined over time was used to infer the growth disadvantage conferred by a given sgRNA relative to the uninfected cells in the same culture.

9.17 Chemical high-throughput screen

The Boehringer Ingelheim proprietary fragment library of ∼1700 compounds was screened against the BRD9 bromodomain using three different assays in parallel: a differential scanning fluorimetry (DSF) assay, a surface plasmon resonance (SPR) assay and a microscale thermophoresis assay. The hits coming from these three screening methods were validated in an orthogonal binding assay using 15N HSQC NMR (Heteronuclear Single Quantum Coherence Nuclear Magnetic Resonance). 77 hits showed significant cross peak shifts in the 15N HSQC NMR spectra and 55 of these compounds were succsessully co-crystallised with the bromodomain of BRD9. The binding affinity of the compounds was quantified by SPR with 12 compounds displaying a dissociation constant (KD) of below 100 μM. Additionally our proprietary high concentration screening (HiCoS) library of ∼74,500 compounds was screened virtually with a Glide docking model, followed by BRD9 bromodomain pharmacophore mapping and finally filtering based on molecular weight (MW <280), lipophilicity (clogP <2) and compound availability. This virtual screening led to the selection of 208 compounds, which were measured in both our DSF and SPR assays. The binding affinity of the hits was quantified by determination of KD using SPR. This led to the discovery of 23 additional hits. The binding mode of 11 of these compounds was elucidated by Xray crystallography. In contrast to our fragment library, our HiCoS library is not fully quality controlled for purity, solubility and aggregation; hence all compounds with a KD below 100 μM were resynthesized and all 11 compounds had their affinities reconfirmed by SPR. Thus 23 fragments with affinity of under 100 μM and Xray co-crystal structures were obtained as a starting point for structure based medicinal chemistry.

9.18 Chemical synthesis and characterization

Unless otherwise indicated all reactions were carried out in standard commercially available glassware using standard synthetic chemistry methods. Air-sensitive and moisture-sensitive reactions were performed under an atmosphere of dry nitrogen or argon with dried glassware. Commercial starting materials were used without further purification. Solvents used for reactions were of commercial dry- or extra-dry or analytical grade. All other solvents used were

reagent grade. Preperative RP-HPLC were carried out on Agilent or Gilson systems using columns from Waters (Sunfire C18 OBD, 5 or 10 µm, 20×50 mm, 30×50 mm or 50×150 mm; X-Bridge C18 OBD, 5 or 10 µm, 20×50, 30×50, or 50×150 mm) or YMC (Triart C18, 5 or 10 µm, 20×50 mm, or 30×50 mm). Compounds were eluted with different MeCN/water gradients using either acidic (0.2 % HCOOH or TFA) or basic water (5 mL 2 M NH4HCO3 + 2 mL NH3 (32 %) made up to 1 L with water). NMR experiments were recorded on Bruker Avance 400 MHz and 500 MHz spectrometers at 298K. Samples were dissolved in 600 µL DMSO-d6 or CDCl3 and TMS was added as an internal standard. 1D 1H spectra were acquired with 30° excitation pulses and an interpulse delay of 4.2 sec with 64,000 datapoints and 20 ppm sweep width. 1D 13C spectra were acquired with broadband composite pulse decoupling (WALTZ16) and an interpulse delay of 3.3 sec with 64,000 datapoints and a sweep width of 240 ppm. Processing and analysis of 1D spectra was performed with Bruker Topspin 2.0 software. No zero filling was performed and spectra were manually integrated after automatic baseline correction. Chemical shifts are reported in ppm on the x scale. Analytical LC/MS data [LC/MS(BAS1)] were measured on an Agilent HPLC 1100 Series with Agilent LC/MSD SL detector using a Waters X-Bridge C18, 2.5 µm, 2.1×20 mm column (Part.No. 186003201) and solvent A [20 mM NH4HCO3/ NH3 (pH 9)] and solvent B [acetonitrile HPLC grade] as eluent (additional settings: flow 1 ml/min; injection volume 5 µl; column temp. 60 °C). Standard gradient: 0.00 min: 10 % B; 0.00 - 1.50 min: 10 % to 95 % B; 1.50 - 2.00 min: 95 % B; 2.00 - 2.10 min: 95 % to 10 % B. HRMS data were recorded using a Thermo Scientific Orbitrap Elite Hybrid Ion Trap/Orbitrap Spectrometer system with an Ultimate 3000 Series LPG-3400XRS Pump system. The mass calibration was performed using the Pierce LTQ Velos ESI positive ion calibration solution from Thermo Scientific (Lot PF200011, Prod.Nr. 88323). The synthetic route for BI-7271, BI-7273 and BI-7189 is shown in full in Appendix 3.

9.19 AlphaScreen

This assay was used to identify compounds, which inhibit the interaction of the bromodomain of BRD9 with a tetra-acetylated peptide based on the sequence of histone H3 (H3 K9/14/18/23Ac (1-28)). The sequence of the H3 K9/14/18/23Ac(1-28) peptide is Biotin-

ARTKQTARK(Ac)STGGK(Ac)APRK(Ac)QLATK(Ac)AARKS, MW: 3392. BRD9 (aa 130 - 259 that contain the bromodomain of BRD9 (accession number NM_023924.4)) was expressed in *E. coli* with an amino-terminal GST tag. Control BRD4 AlphaScreen assays were performed using a tetra-acetylated H4 tail, which was potently inhibited by JQ1 in control experiments. The assay was performed in a darkened room below 100 Lux. Compounds are dispensed onto assay plates (Proxiplate-384 PLUS, white, PerkinElmer) using an Access Labcyte Workstation with the Labcyte Echo 550 from a DMSO solution. For the chosen highest assay concentration of 100 µM, 150 nl of compound solution are transferred from a 10 mM DMSO compound stock solution. A series of 11 concentrations is transferred for each compound at which each concentration is five fold lower than the previous one. DMSO is added such that every well has a total of 150 nl compound solution. 10 µl of a mix containing 4 nM GST-BRD9 protein (aa 130 - 259) and 12 nM biotinylated H3 K9/14/18/23Ac(1-28) peptide prepared in assay buffer (50 mM HEPES pH=7.3; 25 mM NaCl; 0.1 % Tween 20; 0.1 % bovine serum albumin (BSA); 2 mM dithiothreitol (DTT)) and 5 µl of bead mix (AlphaLISA Glutathione Acceptor Beads and AlphaScreen Streptavidin Donor Beads mixed in assay buffer at a concentration of 10 µg/ml each) were added to the assay plate that contain 150 nl of the compound solution. After 60 minutes at room temperature the signal was measured in a PerkinElmer Envision HTS Multilabel Reader using the AlphaScreen specifications from PerkinElmer. Each plate contained negative controls where biotinylated H3 K9/14/18/23Ac(1-28) peptide and GST-BRD9 were left out and replaced by assay buffer. Negative control values were entered as low basis for normalization. IC50 values were calculated using a four parameter non-linear regression model.

9.20 BROMOscan

Bromodomain profiling was provided by DiscoverX Corp. using their BROMOscan platform (http://www.discoverx.com/services/drug-discovery-development-services/epigenetic-profiling/bromoscan). The bromoMAX screen was used to profile BRD9 inhibitors against a preconfigured panel of 32 human bromodomains. Inhibitors were added at a single concentration and profiled for their ability to compete with the binding of a reference immobilized ligand (readout was percent of control - % ctrl binding, with lower values representing

greater competition (i.e. binding) by the test compound). BromoKdELECT was employed to determine the Kd between BRD9 inhibitors and 11 selected bromodomains. Kd were obtained by evaluating an 11-point series of test compound concentration for binding competition against a reference immobilized ligand.

9.21 NanoBRET

The interactions of the bromodomains of BRD9 with Histone H3.3 were measured by nanoBRET according to the manufacturer's instructions (Promega, products N1830 and N1840). In brief, two chimeric proteins were transiently expressed in HEK293 cells: nanoLuc luciferase fused to the C-terminus of the bromodomain of BRD9, and HaloTag fused to the C-terminus of histone H3.3. Transfected cells were plated in two sets of triplicates. To the first set of cells, HaloTag 618 ligand was added, a fluorescent small molecule that selectively binds the HaloTag, The second set of cells did not receive HaloTag 618 ligand. Luciferase substrate was added to all cells. If the bromodomain comes in close proximity of histone H3.3, light emitted at 460 nM by nanoLuc luciferase excites the HaloTag 618 ligand, which then emits at 618 nM. To calculate nanoBRET signals, emission at 618 nM was normalized for emission at 460 nM and divided by the same ratio from cells that did not receive the HaloTag 618 ligand.

9.22 Protein purification and crystallization

The bromodomain of human BRD9 (residues 14-134 of isoform 5, Uniprot identifier Q9H8M2-1) was obtained from the SGC (Structural Genomics Consortium) and has been expressed and purified as previously described [Filippakopoulos et al., 2012]. Protein crystallization was done using the hanging drop method by mixing 2.0 µL of apo BRD9 (10 mg/mL in 25 mM HEPES pH 7.5, 300 mM NaCl, 0.5 mM TCEP) with 2 µL of reservoir solution (30 % glycerol ethoxylate, 100 mM Tris pH 8.3) at 4 °C. Crystals grew within a few days to a final size of 150-200 µm). Apo crystals were transferred to a soaking buffer containing 33 % glycerol ethoxylate and soaked overnight by adding 0.1 µL of a 100 mM DMSO stock solution of BI-7273. Crystals were frozen in liquid nitrogen and data were collected at the SLS beam line

X06SA (Swiss Light Source, Paul Scherrer Institute, λ= 1.000 Å) using the PILATUS 6M detector. The crystals belonged to space group P21212 with unit cell parameters a = 70.80, b = 125.34, c = 29.92 and α, β, γ= 90 and contained 2 monomers per asymmetric unit. Images were processed with autoPROC [Vonrhein et al., 2011]. The resolution limit was set to 1.605 Å using default autoPROC settings. The structure was solved by molecular replacement using the BRD9 structure 3HME as a search model. Subsequent model building and refinement was done with standard protocols using CCP454, COOT55 and autoBUSTER (Global Phasing Ltd.). The structure was refined to R and Rfree values of 17.8 % and 19.2 %, respectively, with 100 % of the residues in Ramachandran favoured regions as validated with Molprobity [Chen et al., 2010]. Statistics for data collection and refinement can be found in Appendix 2. PDB: 5EU1.

9.23 GI50 measurements

Cells were counted and equal cell numbers were plated per cell line and grown in the presence of increasing inhibitor concentrations for 5-7 days in a 24-well plate. The accumulated cell numbers were then measured using a Guava Easycyte (Millipore) and normalized to cell numbers in DMSO control wells. For profiling of BI-7273 sensitivities across human cancer cell lines, cell viability was assayed using the CellTiter-Glo assay (Promega). GI50 values were calculated using a four parameter non-linear regression model.

9.24 ChIP-qPCR

Five million cells were crosslinked using 1 % formaldehyde at room temperature for 20 min with shaking. Crosslinking was quenched by incubating with 0.125 M glycine for 10 min. ChIP-qPCR assays were performed as described [Steger et al., 2008]. Immunoprecipitated DNA was purified using a QIAquick Gel Extraction Kit (Qiagen). All results were quantified by qPCR performed using SYBR green (ABI) on an ABI 7900HT Fast Real-Time PCR machine. Each IP signal was referenced to an input standard curve dilution series (IP/Input) to normalize for differences in starting cell number and for primer amplification efficiency.

9.25 Antibodies

Anti-BRG1 (Santa Cruz #sc-17796), Anti-Brg1 (Abcam #ab110641), Anti-Brd9 (Abcam #ab66443), Anti-BRD9 (#ab137245; Bethyl #A303-781A) Anti-β-actin HRP antibody (Sigma #A3854), APC anti-mouse B220 (BioLegend #103212), APC anti-mouse Mac-1/Cd11b (BioLegend #101211), Anti-FLAG (Sigma #F1804), control rabbit IgG (Sigma #I8140)

References

[Álvarez-Errico et al., 2015] Álvarez-Errico, D., Vento-Tormo, R., Sieweke, M., and Ballestar, E. (2015). Epigenetic control of myeloid cell differentiation, identity and function. *Nature Reviews Immunology*, 15(1):7–17.

[Arrowsmith et al., 2015] Arrowsmith, C. H., Audia, J. E., Austin, C., Baell, J., Bennett, J., Blagg, J., Bountra, C., Brennan, P. E., Brown, P. J., Bunnage, M. E., et al. (2015). The promise and peril of chemical probes. *Nature Chemical Biology*, 11(8):536–541.

[Balzano et al., 2011] Balzano, D., Santaguida, S., Musacchio, A., and Villa, F. (2011). A general framework for inhibitor resistance in protein kinases. *Chemistry and Biology*, 18(8):966–975.

[Bannister and Kouzarides, 2011] Bannister, A. J. and Kouzarides, T. (2011). Regulation of chromatin by histone modifications. *Cell Research*, 21(3):381–395.

[Baylin and Jones, 2011] Baylin, S. B. and Jones, P. A. (2011). A decade of exploring the cancer epigenome—biological and translational implications. *Nature Reviews Cancer*, 11(10):726–734.

[Becker and Hörz, 2002] Becker, P. B. and Hörz, W. (2002). Atp-dependent nucleosome remodeling. *Annual Review of Biochemistry*, 71(1):247–273.

[Bennett et al., 2015] Bennett, J., Fedorov, O., Tallant, C., Monteiro, O., Meier, J., Gamble, V., Savitsky, P., Nunez-Alonso, G. A., Haendler, B., Rogers, C., et al. (2015). Discovery of a chemical tool inhibitor targeting the bromodomains of trim24 and brpf. *Journal of Medicinal Chemistry*.

[Berger, 2007] Berger, S. L. (2007). The complex language of chromatin regulation during transcription. *Nature*, 447(7143):407–412.

[Bernstein et al., 2006] Bernstein, B. E., Mikkelsen, T. S., Xie, X., Kamal, M., Huebert, D. J., Cuff, J., Fry, B., Meissner, A., Wernig, M., Plath, K., et al. (2006). A bivalent chromatin structure marks key developmental genes in embryonic stem cells. *Cell*, 125(2):315–326.

[Bernt et al., 2011] Bernt, K. M., Zhu, N., Sinha, A. U., Vempati, S., Faber, J., Krivtsov, A. V., Feng, Z., Punt, N., Daigle, A., Bullinger, L., et al. (2011). Mll-rearranged leukemia is dependent on aberrant h3k79 methylation by dot1l. *Cancer Cell*, 20(1):66–78.

[Bianconi et al., 2013] Bianconi, E., Piovesan, A., Facchin, F., Beraudi, A., Casadei, R., Frabetti, F., Vitale, L., Pelleri, M. C., Tassani, S., Piva, F., et al. (2013). An estimation of the number of cells in the human body. *Annals of Human Biology*, 40(6):463–471.

[Biegel et al., 1999] Biegel, J. A., Zhou, J.-Y., Rorke, L. B., Stenstrom, C., Wainwright, L. M., and Fogelgren, B. (1999). Germ-line and acquired mutations of ini1 in atypical teratoid and rhabdoid tumors. *Cancer Research*, 59(1):74–79.

[Bonifer, 2005] Bonifer, C. (2005). Epigenetic plasticity of hematopoietic cells. *Cell Cycle*, 4(2):214–217.

[Boulais and Frenette, 2015] Boulais, P. E. and Frenette, P. S. (2015). Making sense of hematopoietic stem cell niches. *Blood*, 125(17):2621–2629.

[Brand et al., 2014] Brand, M., Measures, A. M., Wilson, B. G., Cortopassi, W. A., Alexander, R., Höss, M., Hewings, D. S., Rooney, T. P., Paton, R. S., and Conway, S. J. (2014). Small molecule inhibitors of bromodomain–acetyl-lysine interactions. *ACS Chemical Biology*, 10(1):22–39.

[Brock et al., 2008] Brock, M. V., Hooker, C. M., Ota-Machida, E., Han, Y., Guo, M., Ames, S., Glöckner, S., Piantadosi, S., Gabrielson, E., Pridham, G., et al. (2008). Dna methylation markers and early recurrence in stage i lung cancer. *New England Journal of Medicine*, 358(11):1118–1128.

[Brown, 2002] Brown, T. (2002). *Genomes*, volume Chapter 1, The Human Genome. Oxford: Wiley-Liss, 2nd edition edition.

[Bultman et al., 2000] Bultman, S., Gebuhr, T., Yee, D., La Mantia, C., Nicholson, J., Gilliam, A., Randazzo, F., Metzger, D., Chambon, P., Crabtree, G., et al. (2000). A brg1 null mutation in the mouse reveals functional differences among mammalian swi/snf complexes. *Molecular Cell*, 6(6):1287–1295.

[Buscarlet et al., 2014] Buscarlet, M., Krasteva, V., Ho, L., Simon, C., Hébert, J., Wilhelm, B., Crabtree, G. R., Sauvageau, G., Thibault, P., and Lessard, J. A. (2014). Essential role of brg, the atpase subunit of baf chromatin remodeling complexes, in leukemia maintenance. *Blood*, 123(11):1720–1728.

[Cai et al., 2015] Cai, S. F., Chen, C.-W., and Armstrong, S. A. (2015). Drugging chromatin in cancer: Recent advances and novel approaches. *Molecular Cell*, 60(4):561–570.

[Cairns et al., 1994] Cairns, B. R., Kim, Y.-J., Sayre, M. H., Laurent, B. C., and Kornberg, R. D. (1994). A multisubunit complex containing the swi1/adr6, swi2/snf2, swi3, snf5, and snf6 gene products isolated from yeast. *Proceedings of the National Academy of Sciences*, 91(5):1950–1954.

[Cedar and Bergman, 2011] Cedar, H. and Bergman, Y. (2011). Epigenetics of haematopoietic cell development. *Nature Reviews Immunology*, 11(7):478–488.

[Cerami et al., 2012] Cerami, E., Gao, J., Dogrusoz, U., Gross, B. E., Sumer, S. O., Aksoy, B. A., Jacobsen, A., Byrne, C. J., Heuer, M. L., Larsson, E., et al. (2012). The cbio cancer genomics portal: an open platform for exploring multidimensional cancer genomics data. *Cancer discovery*, 2(5):401–404.

[Chan and Majeti, 2013] Chan, S. M. and Majeti, R. (2013). Role of dnmt3a, tet2, and idh1/2 mutations in pre-leukemic stem cells in acute myeloid leukemia. *International Journal of Hematology*, 98(6):648–657.

[Chen et al., 2015a] Chen, C.-W., Koche, R. P., Sinha, A. U., Deshpande, A. J., Zhu, N., Eng, R., Doench, J. G., Xu, H., Chu, S. H., Qi, J., Wang, X., Delaney, C., Bernt, K. M., Root, D. E., Hahn, W. C., Bradner, J. E., and Armstrong, S. A. (2015a). Dot1l inhibits sirt1-mediated epigenetic silencing to maintain leukemic gene expression in mll-rearranged leukemia. *Nature Medicine*, 21(4):335–43.

[Chen et al., 2015b] Chen, P., Chaikuad, A., Bamborough, P., Bantscheff, M., Bountra, C., Chung, C.-w., Fedorov, O., Grandi, P., Jung, D., Lesniak, R., et al. (2015b). Discovery

and characterization of gsk2801, a selective chemical probe for the bromodomains baz2a and baz2b. *Journal of Medicinal Chemistry*.

[Chen et al., 2010] Chen, V. B., Arendall, W. B., Headd, J. J., Keedy, D. A., Immormino, R. M., Kapral, G. J., Murray, L. W., Richardson, J. S., and Richardson, D. C. (2010). Molprobity: all-atom structure validation for macromolecular crystallography. *Acta Crystallographica Section D: Biological Crystallography*, 66(1):12–21.

[Chi et al., 2003] Chi, T. H., Wan, M., Lee, P. P., Akashi, K., Metzger, D., Chambon, P., Wilson, C. B., and Crabtree, G. R. (2003). Sequential roles of brg, the atpase subunit of baf chromatin remodeling complexes, in thymocyte development. *Immunity*, 19(2):169–82.

[Clapier and Cairns, 2009] Clapier, C. R. and Cairns, B. R. (2009). The biology of chromatin remodeling complexes. *Annual Review of Biochemistry*, 78:273–304.

[Clark et al., 2015] Clark, P. G., Vieira, L. C., Tallant, C., Fedorov, O., Singleton, D. C., Rogers, C. M., Monteiro, O. P., Bennett, J. M., Baronio, R., Müller, S., et al. (2015). Lp99: Discovery and synthesis of the first selective brd7/9 bromodomain inhibitor. *Angewandte Chemie International Edition*, 54(21):6217–6221.

[Côté et al., 1994] Côté, J., Quinn, J., Workman, J. L., and Peterson, C. L. (1994). Stimulation of gal4 derivative binding to nucleosomal dna by the yeast swi/snf complex. *Science*, 265(5168):53–60.

[Cui et al., 2009] Cui, K., Zang, C., Roh, T.-Y., Schones, D. E., Childs, R. W., Peng, W., and Zhao, K. (2009). Chromatin signatures in multipotent human hematopoietic stem cells indicate the fate of bivalent genes during differentiation. *Cell Stem Cell*, 4(1):80–93.

[Dawson and Kouzarides, 2012] Dawson, M. A. and Kouzarides, T. (2012). Cancer epigenetics: from mechanism to therapy. *Cell*, 150(1):12–27.

[Dawson et al., 2012] Dawson, M. A., Kouzarides, T., and Huntly, B. J. (2012). Targeting epigenetic readers in cancer. *New England Journal of Medicine*, 367(7):647–657.

[Delmore et al., 2011] Delmore, J. E., Issa, G. C., Lemieux, M. E., Rahl, P. B., Shi, J., Jacobs, H. M., Kastritis, E., Gilpatrick, T., Paranal, R. M., Qi, J., et al. (2011). Bet bromodomain

inhibition as a therapeutic strategy to target c-myc. *Cell*, 146(6):904–917.

[Dhalluin et al., 1999] Dhalluin, C., Carlson, J. E., Zeng, L., He, C., Aggarwal, A. K., and Zhou, M.-M. (1999). Structure and ligand of a histone acetyltransferase bromodomain. *Nature*, 399(6735):491–496.

[Doan et al., 2004] Doan, D. N., Veal, T. M., Yan, Z., Wang, W., Jones, S. N., and Imbalzano, A. N. (2004). Loss of the ini1 tumor suppressor does not impair the expression of multiple brg1-dependent genes or the assembly of swi/snf enzymes. *Oncogene*, 23(19):3462–3473.

[Doulatov et al., 2012] Doulatov, S., Notta, F., Laurenti, E., and Dick, J. E. (2012). Hematopoiesis: a human perspective. *Cell Stem Cell*, 10(2):120–136.

[Drost et al., 2010] Drost, J., Mantovani, F., Tocco, F., Elkon, R., Comel, A., Holstege, H., Kerkhoven, R., Jonkers, J., Voorhoeve, P. M., Agami, R., et al. (2010). Brd7 is a candidate tumour suppressor gene required for p53 function. *Nature Cell Biology*, 12(4):380–389.

[Dundr and Misteli, 2001] Dundr, M. and Misteli, T. (2001). Functional architecture in the cell nucleus. *Biochem. J.*, 356:297–310.

[Dykhuizen et al., 2013] Dykhuizen, E. C., Hargreaves, D. C., Miller, E. L., Cui, K., Korshunov, A., Kool, M., Pfister, S., Cho, Y.-J., Zhao, K., and Crabtree, G. R. (2013). Baf complexes facilitate decatenation of dna by topoisomerase ii. *Nature*, 497(7451):624–7.

[Eroglu et al., 2014] Eroglu, E., Burkard, T. R., Jiang, Y., Saini, N., Homem, C. C. F., Reichert, H., and Knoblich, J. A. (2014). Swi/snf complex prevents lineage reversion and induces temporal patterning in neural stem cells. *Cell*, 156(6):1259–73.

[Essers et al., 2009] Essers, M. A. G., Offner, S., Blanco-Bose, W. E., Waibler, Z., Kalinke, U., Duchosal, M. A., and Trumpp, A. (2009). Ifnalpha activates dormant haematopoietic stem cells in vivo. *Nature*, 458(7240):904–8.

[Feinberg and Tycko, 2004] Feinberg, A. P. and Tycko, B. (2004). The history of cancer epigenetics. *Nature Reviews Cancer*, 4(2):143–153.

[Fellmann et al., 2013] Fellmann, C., Hoffmann, T., Sridhar, V., Hopfgartner, B., Muhar, M., Roth, M., Lai, D. Y., Barbosa, I. A., Kwon, J. S., Guan, Y., et al. (2013). An optimized microrna backbone for effective single-copy rnai. *Cell Reports*, 5(6):1704–1713.

[Filippakopoulos and Knapp, 2014] Filippakopoulos, P. and Knapp, S. (2014). Targeting bromodomains: epigenetic readers of lysine acetylation. *Nature Reviews Drug discovery*, 13(5):337–356.

[Filippakopoulos et al., 2012] Filippakopoulos, P., Picaud, S., Mangos, M., Keates, T., Lambert, J.-P., Barsyte-Lovejoy, D., Felletar, I., Volkmer, R., Müller, S., Pawson, T., et al. (2012). Histone recognition and large-scale structural analysis of the human bromodomain family. *Cell*, 149(1):214–231.

[Filippakopoulos et al., 2010] Filippakopoulos, P., Qi, J., Picaud, S., Shen, Y., Smith, W. B., Fedorov, O., Morse, E. M., Keates, T., Hickman, T. T., Felletar, I., Philpott, M., Munro, S., McKeown, M. R., Wang, Y., Christie, A. L., West, N., Cameron, M. J., Schwartz, B., Heightman, T. D., La Thangue, N., French, C. A., Wiest, O., Kung, A. L., Knapp, S., and Bradner, J. E. (2010). Selective inhibition of bet bromodomains. *Nature*, 468(7327):1067–73.

[Fiskus et al., 2014] Fiskus, W., Sharma, S., Shah, B., Portier, B., Devaraj, S., Liu, K., Iyer, S. P., Bearss, D., and Bhalla, K. (2014). Highly effective combination of lsd1 (kdm1a) antagonist and pan-histone deacetylase inhibitor against human aml cells. *Leukemia*, 28(11):2155–2164.

[Fiskus et al., 2009] Fiskus, W., Wang, Y., Sreekumar, A., Buckley, K. M., Shi, H., Jillella, A., Ustun, C., Rao, R., Fernandez, P., Chen, J., et al. (2009). Combined epigenetic therapy with the histone methyltransferase ezh2 inhibitor 3-deazaneplanocin a and the histone deacetylase inhibitor panobinostat against human aml cells. *Blood*, 114(13):2733–2743.

[Flowers et al., 2009] Flowers, S., Nagl, N. G., Beck, G. R., and Moran, E. (2009). Antagonistic roles for brm and brg1 swi/snf complexes in differentiation. *Journal of Biological Chemistry*, 284(15):10067–10075.

[Frigault and Barrett, 2014] Frigault, M. M. and Barrett, J. C. (2014). Is target validation all we need? *Current Opinion in Pharmacology*, 17:81–86.

[Gao et al., 2013] Gao, J., Aksoy, B. A., Dogrusoz, U., Dresdner, G., Gross, B., Sumer, S. O., Sun, Y., Jacobsen, A., Sinha, R., Larsson, E., et al. (2013). Integrative analysis of complex cancer genomics and clinical profiles using the cbioportal. *Science signaling*, 6(269):pl1.

[Gibney and Nolan, 2010] Gibney, E. and Nolan, C. (2010). Epigenetics and gene expression. *Heredity*, 105(1):4–13.

[Gilar et al., 2005] Gilar, M., Olivova, P., Daly, A. E., and Gebler, J. C. (2005). Two-dimensional separation of peptides using rp-rp-hplc system with different ph in first and second separation dimensions. *Journal of Separation Science*, 28(14):1694–1703.

[Hargreaves and Crabtree, 2011] Hargreaves, D. C. and Crabtree, G. R. (2011). Atp-dependent chromatin remodeling: genetics, genomics and mechanisms. *Cell Research*, 21(3):396–420.

[Harte et al., 2010] Harte, M. T., O'Brien, G. J., Ryan, N. M., Gorski, J. J., Savage, K. I., Crawford, N. T., Mullan, P. B., and Harkin, D. P. (2010). Brd7, a subunit of swi/snf complexes, binds directly to brca1 and regulates brca1-dependent transcription. *Cancer Research*, 70(6):2538–2547.

[Hay et al., 2014] Hay, D. A., Fedorov, O., Martin, S., Singleton, D. C., Tallant, C., Wells, C., Picaud, S., Philpott, M., Monteiro, O. P., Rogers, C. M., et al. (2014). Discovery and optimization of small-molecule ligands for the cbp/p300 bromodomains. *Journal of the American Chemical Society*, 136(26):9308–9319.

[Helin and Dhanak, 2013] Helin, K. and Dhanak, D. (2013). Chromatin proteins and modifications as drug targets. *Nature*, 502(7472):480–488.

[Helming et al., 2014] Helming, K. C., Wang, X., Wilson, B. G., Vazquez, F., Haswell, J. R., Manchester, H. E., Kim, Y., Kryukov, G. V., Ghandi, M., Aguirre, A. J., et al. (2014). Arid1b is a specific vulnerability in arid1a-mutant cancers. *Nature Medicine*, 20(3):251–254.

[Hirschhorn et al., 1992] Hirschhorn, J. N., Brown, S. A., Clark, C. D., and Winston, F. (1992). Evidence that snf2/swi2 and snf5 activate transcription in yeast by altering chromatin struc-

ture. *Genes and Development*, 6(12a):2288–2298.

[Ho and Crabtree, 2010] Ho, L. and Crabtree, G. R. (2010). Chromatin remodelling during development. *Nature*, 463(7280):474–484.

[Hoffman et al., 2014] Hoffman, G. R., Rahal, R., Buxton, F., Xiang, K., McAllister, G., Frias, E., Bagdasarian, L., Huber, J., Lindeman, A., Chen, D., et al. (2014). Functional epigenetics approach identifies brm/smarca2 as a critical synthetic lethal target in brg1-deficient cancers. *Proceedings of the National Academy of Sciences*, 111(8):3128–3133.

[Imbalzano et al., 1994] Imbalzano, A. N., Kwon, H., Green, M. R., and Kingston, R. E. (1994). Facilitated binding of tata-binding protein to nucleosomal dna. *Nature*, 370(6489):481–5.

[Imielinski et al., 2012] Imielinski, M., Berger, A. H., Hammerman, P. S., Hernandez, B., Pugh, T. J., Hodis, E., Cho, J., Suh, J., Capelletti, M., Sivachenko, A., et al. (2012). Mapping the hallmarks of lung adenocarcinoma with massively parallel sequencing. *Cell*, 150(6):1107–1120.

[Jaenisch and Bird, 2003] Jaenisch, R. and Bird, A. (2003). Epigenetic regulation of gene expression: how the genome integrates intrinsic and environmental signals. *Nature Genetics*, 33:245–254.

[Jagani et al., 2010] Jagani, Z., Mora-Blanco, E. L., Sansam, C. G., McKenna, E. S., Wilson, B., Chen, D., Klekota, J., Tamayo, P., Nguyen, P. T. L., Tolstorukov, M., Park, P. J., Cho, Y.-J., Hsiao, K., Buonamici, S., Pomeroy, S. L., Mesirov, J. P., Ruffner, H., Bouwmeester, T., Luchansky, S. J., Murtie, J., Kelleher, J. F., Warmuth, M., Sellers, W. R., Roberts, C. W. M., and Dorsch, M. (2010). Loss of the tumor suppressor snf5 leads to aberrant activation of the hedgehog-gli pathway. *Nature Medicine*, 16(12):1429–33.

[Juergens et al., 2011] Juergens, R. A., Wrangle, J., Vendetti, F. P., Murphy, S. C., Zhao, M., Coleman, B., Sebree, R., Rodgers, K., Hooker, C. M., Franco, N., et al. (2011). Combination epigenetic therapy has efficacy in patients with refractory advanced non–small cell lung cancer. *Cancer Discovery*, 1(7):598–607.

[Kadam and Emerson, 2003] Kadam, S. and Emerson, B. M. (2003). Transcriptional specificity of human swi/snf brg1 and brm chromatin remodeling complexes. *Molecular Cell*, 11(2):377–389.

[Kadoch et al., 2013] Kadoch, C., Hargreaves, D. C., Hodges, C., Elias, L., Ho, L., Ranish, J., and Crabtree, G. R. (2013). Proteomic and bioinformatic analysis of mammalian swi/snf complexes identifies extensive roles in human malignancy. *Nature Genetics*, 45(6):592–601.

[Kaelin, 2005] Kaelin, Jr, W. G. (2005). The concept of synthetic lethality in the context of anticancer therapy. *Nature Reviews Cancer*, 5(9):689–98.

[Kandoth et al., 2013] Kandoth, C., McLellan, M. D., Vandin, F., Ye, K., Niu, B., Lu, C., Xie, M., Zhang, Q., McMichael, J. F., Wyczalkowski, M. A., et al. (2013). Mutational landscape and significance across 12 major cancer types. *Nature*, 502(7471):333–339.

[Khavari et al., 1993] Khavari, P. A., Peterson, C. L., Tamkun, J. W., Mendel, D. B., and Crabtree, G. R. (1993). Brg 1 contains a conserved domain of the swi 2/snf 2 family necessary for normal mitotic growth and transcription. *Nature*, 366(6451):170–174.

[Kim et al., 2015] Kim, K. H., Kim, W., Howard, T. P., Vazquez, F., Tsherniak, A., Wu, J. N., Wang, W., Haswell, J. R., Walensky, L. D., Hahn, W. C., et al. (2015). Swi/snf-mutant cancers depend on catalytic and non-catalytic activity of ezh2. *Nature Medicine*, 21(12):1491–1496.

[Kim et al., 2013] Kim, W., Bird, G. H., Neff, T., Guo, G., Kerenyi, M. A., Walensky, L. D., and Orkin, S. H. (2013). Targeted disruption of the ezh2–eed complex inhibits ezh2-dependent cancer. *Nature Chemical Biology*, 9(10):643–650.

[Kimura, 2013] Kimura, H. (2013). Histone modifications for human epigenome analysis. *Journal of Human Genetics*, 58(7):439–445.

[Knutson et al., 2013] Knutson, S. K., Warholic, N. M., Wigle, T. J., Klaus, C. R., Allain, C. J., Raimondi, A., Porter Scott, M., Chesworth, R., Moyer, M. P., Copeland, R. A., Richon, V. M., Pollock, R. M., Kuntz, K. W., and Keilhack, H. (2013). Durable tumor regression in genetically altered malignant rhabdoid tumors by inhibition of methyltransferase

ezh2. *Proceedings of the National Academy of Sciences of the United States of America*, 110(19):7922–7.

[Kornberg and Lorch, 1999] Kornberg, R. D. and Lorch, Y. (1999). Twenty-five years of the nucleosome, fundamental particle of the eukaryote chromosome. *Cell*, 98(3):285–294.

[Kouzarides, 2007] Kouzarides, T. (2007). Chromatin modifications and their function. *Cell*, 128(4):693–705.

[Kumar et al., 2014] Kumar, V., Abbas, A. K., Fausto, N., and Aster, J. C. (2014). *Robbins and Cotran pathologic basis of disease*. Elsevier Health Sciences.

[Kuo and Allis, 1998] Kuo, M.-H. and Allis, C. D. (1998). Roles of histone acetyltransferases and deacetylases in gene regulation. *Bioessays*, 20(8):615–626.

[Kwon et al., 1994] Kwon, H., Imbalzano, A. N., Khavari, P. A., Kingston, R. E., and Green, M. R. (1994). Nucleosome disruption and enhancement of activator binding by a human sw1/snf complex. *Nature*.

[Lessard et al., 2007] Lessard, J., Wu, J. I., Ranish, J. A., Wan, M., Winslow, M. M., Staahl, B. T., Wu, H., Aebersold, R., Graef, I. A., and Crabtree, G. R. (2007). An essential switch in subunit composition of a chromatin remodeling complex during neural development. *Neuron*, 55(2):201–215.

[Li and Gilmour, 2011] Li, J. and Gilmour, D. S. (2011). Promoter proximal pausing and the control of gene expression. *Current Opinion in Genetics and Development*, 21(2):231–235.

[Love et al., 2012] Love, C., Sun, Z., Jima, D., Li, G., Zhang, J., Miles, R., Richards, K. L., Dunphy, C. H., Choi, W. W., Srivastava, G., et al. (2012). The genetic landscape of mutations in burkitt lymphoma. *Nature Genetics*, 44(12):1321–1325.

[Lowenberg et al., 1999] Lowenberg, B., Downing, J. R., and Burnett, A. (1999). Acute myeloid leukemia. *New England Journal of Medicine*, 341(14):1051–1062.

[Lu et al., 2015] Lu, J., Qian, Y., Altieri, M., Dong, H., Wang, J., Raina, K., Hines, J., Winkler, J. D., Crew, A. P., Coleman, K., et al. (2015). Hijacking the e3 ubiquitin ligase cereblon to

efficiently target brd4. *Chemistry and Biology*, 22(6):755–763.

[Machleidt et al., 2015] Machleidt, T., Woodroofe, C. C., Schwinn, M. K., Méndez, J., Robers, M. B., Zimmerman, K., Otto, P., Daniels, D. L., Kirkland, T. A., and Wood, K. V. (2015). Nanobret–a novel bret platform for the analysis of protein-protein interactions. *ACS chemical biology*.

[Margueron and Reinberg, 2011] Margueron, R. and Reinberg, D. (2011). The polycomb complex prc2 and its mark in life. *Nature*, 469(7330):343–349.

[Martens and Winston, 2002] Martens, J. A. and Winston, F. (2002). Evidence that swi/snf directly represses transcription in s. cerevisiae. *Genes and Development*, 16(17):2231–2236.

[McCabe and Creasy, 2014] McCabe, M. T. and Creasy, C. L. (2014). Ezh2 as a potential target in cancer therapy. *Epigenomics*, 6(3):341–351.

[McCabe et al., 2012] McCabe, M. T., Ott, H. M., Ganji, G., Korenchuk, S., Thompson, C., Van Aller, G. S., Liu, Y., Graves, A. P., Diaz, E., LaFrance, L. V., et al. (2012). Ezh2 inhibition as a therapeutic strategy for lymphoma with ezh2-activating mutations. *Nature*, 492(7427):108–112.

[Medina et al., 2008] Medina, P. P., Romero, O. A., Kohno, T., Montuenga, L. M., Pio, R., Yokota, J., and Sanchez-Cespedes, M. (2008). Frequent brg1/smarca4–inactivating mutations in human lung cancer cell lines. *Human Mutation*, 29(5):617–622.

[Mertz et al., 2011] Mertz, J. A., Conery, A. R., Bryant, B. M., Sandy, P., Balasubramanian, S., Mele, D. A., Bergeron, L., and Sims, R. J. (2011). Targeting myc dependence in cancer by inhibiting bet bromodomains. *Proceedings of the National Academy of Sciences*, 108(40):16669–16674.

[Middeljans et al., 2012] Middeljans, E., Wan, X., Jansen, P. W., Sharma, V., Stunnenberg, H. G., and Logie, C. (2012). Ss18 together with animal-specific factors defines human baf-type swi/snf complexes. *PLoS One*, 7(3):e33834.

[Mora-Blanco et al., 2014] Mora-Blanco, E. L., Mishina, Y., Tillman, E. J., Cho, Y.-J., Thom, C. S., Pomeroy, S. L., Shao, W., and Roberts, C. W. M. (2014). Activation of -catenin/tcf

targets following loss of the tumor suppressor snf5. *Oncogene*, 33(7):933–8.

[Nagl et al., 2007] Nagl, N. G., Wang, X., Patsialou, A., Van Scoy, M., and Moran, E. (2007). Distinct mammalian swi/snf chromatin remodeling complexes with opposing roles in cell-cycle control. *The EMBO Journal*, 26(3):752–763.

[Narlikar et al., 2013] Narlikar, G. J., Sundaramoorthy, R., and Owen-Hughes, T. (2013). Mechanisms and functions of atp-dependent chromatin-remodeling enzymes. *Cell*, 154(3):490–503.

[Neff et al., 2012] Neff, T., Sinha, A. U., Kluk, M. J., Zhu, N., Khattab, M. H., Stein, L., Xie, H., Orkin, S. H., and Armstrong, S. A. (2012). Polycomb repressive complex 2 is required for mll-af9 leukemia. *Proceedings of the National Academy of Sciences*, 109(13):5028–5033.

[Neigeborn and Carlson, 1984] Neigeborn, L. and Carlson, M. (1984). Genes affecting the regulation of suc2 gene expression by glucose repression in saccharomyces cerevisiae. *Genetics*, 108(4):845–858.

[Network et al., 2013] Network, C. G. A. R. et al. (2013). Genomic and epigenomic landscapes of adult de novo acute myeloid leukemia. *The New England Journal of Medicine*, 368(22):2059.

[Nicodeme et al., 2010] Nicodeme, E., Jeffrey, K. L., Schaefer, U., Beinke, S., Dewell, S., Chung, C.-w., Chandwani, R., Marazzi, I., Wilson, P., Coste, H., et al. (2010). Suppression of inflammation by a synthetic histone mimic. *Nature*, 468(7327):1119–1123.

[Nie et al., 2000] Nie, Z., Xue, Y., Yang, D., Zhou, S., Deroo, B. J., Archer, T. K., and Wang, W. (2000). A specificity and targeting subunit of a human swi/snf family-related chromatin-remodeling complex. *Molecular and Cellular Biology*, 20(23):8879–8888.

[Oike et al., 2013] Oike, T., Ogiwara, H., Tominaga, Y., Ito, K., Ando, O., Tsuta, K., Mizukami, T., Shimada, Y., Isomura, H., Komachi, M., et al. (2013). A synthetic lethality–based strategy to treat cancers harboring a genetic deficiency in the chromatin remodeling factor brg1. *Cancer Research*, 73(17):5508–5518.

[Orphanides and Reinberg, 2002] Orphanides, G. and Reinberg, D. (2002). A unified theory of gene expression. *Cell*, 108(4):439–451.

[Peng et al., 2007] Peng, C., Liu, H. Y., Zhou, M., Zhang, L. M., Li, X. L., Shen, S. R., and Li, G. Y. (2007). Brd7 suppresses the growth of nasopharyngeal carcinoma cells (hne1) through negatively regulating β-catenin and erk pathways. *Molecular and Cellular Biochemistry*, 303(1-2):141–149.

[Peterson et al., 1994] Peterson, C. L., Dingwall, A., and Scott, M. P. (1994). Five swi/snf gene products are components of a large multisubunit complex required for transcriptional enhancement. *Proceedings of the National Academy of Sciences*, 91(8):2905–2908.

[Peterson and Herskowitz, 1992] Peterson, C. L. and Herskowitz, I. (1992). Characterization of the yeast swi1, swi2, and swi3 genes, which encode a global activator of transcription. *Cell*, 68(3):573–583.

[Phelan et al., 1999] Phelan, M. L., Sif, S., Narlikar, G. J., and Kingston, R. E. (1999). Reconstitution of a core chromatin remodeling complex from swi/snf subunits. *Molecular Cell*, 3(2):247–253.

[Popovic and Licht, 2012] Popovic, R. and Licht, J. D. (2012). Emerging epigenetic targets and therapies in cancer medicine. *Cancer discovery*, 2(5):405–413.

[Quinn et al., 2013] Quinn, E., Wodicka, L., Ciceri, P., Pallares, G., Pickle, E., Torrey, A., Floyd, M., Hunt, J., and Treiber, D. (2013). Bromoscan-a high throughput, quantitative ligand binding platform identifies best-in-class bromodomain inhibitors from a screen of mature compounds targeting other protein classes. *Cancer Research*, 73(8 Supplement):4238–4238.

[Reisman et al., 2003] Reisman, D. N., Sciarrotta, J., Wang, W., Funkhouser, W. K., and Weissman, B. E. (2003). Loss of brg1/brm in human lung cancer cell lines and primary lung cancers: correlation with poor prognosis. *Cancer Research*, 63(3):560–566.

[Reyes et al., 1998] Reyes, J., Barra, J., Muchardt, C., Camus, A., Babinet, C., and Yaniv, M. (1998). Altered control of cellular proliferation in the absence of mammalian brahma (snf2α). *The EMBO Journal*, 17(23):6979–6991.

[Rius and Lyko, 2012] Rius, M. and Lyko, F. (2012). Epigenetic cancer therapy: rationales, targets and drugs. *Oncogene*, 31(39):4257–4265.

[Robinson et al., 2012] Robinson, G., Parker, M., Kranenburg, T. A., Lu, C., Chen, X., Ding, L., Phoenix, T. N., Hedlund, E., Wei, L., Zhu, X., et al. (2012). Novel mutations target distinct subgroups of medulloblastoma. *Nature*, 488(7409):43–48.

[Roesch et al., 2010] Roesch, A., Fukunaga-Kalabis, M., Schmidt, E. C., Zabierowski, S. E., Brafford, P. A., Vultur, A., Basu, D., Gimotty, P., Vogt, T., and Herlyn, M. (2010). A temporarily distinct subpopulation of slow-cycling melanoma cells is required for continuous tumor growth. *Cell*, 141(4):583–594.

[Romero et al., 2012] Romero, O. A., Setien, F., John, S., Gimenez-Xavier, P., Gómez-López, G., Pisano, D., Condom, E., Villanueva, A., Hager, G. L., and Sanchez-Cespedes, M. (2012). The tumour suppressor and chromatin-remodelling factor brg1 antagonizes myc activity and promotes cell differentiation in human cancer. *EMBO Molecular Medicine*, 4(7):603–16.

[Ross et al., 2004] Ross, P. L., Huang, Y. N., Marchese, J. N., Williamson, B., Parker, K., Hattan, S., Khainovski, N., Pillai, S., Dey, S., Daniels, S., et al. (2004). Multiplexed protein quantitation in saccharomyces cerevisiae using amine-reactive isobaric tagging reagents. *Molecular and Cellular Proteomics*, 3(12):1154–1169.

[Schenone et al., 2013] Schenone, M., Dančík, V., Wagner, B. K., and Clemons, P. A. (2013). Target identification and mechanism of action in chemical biology and drug discovery. *Nature Chemical Biology*, 9(4):232–240.

[Seligson et al., 2005] Seligson, D. B., Horvath, S., Shi, T., Yu, H., Tze, S., Grunstein, M., and Kurdistani, S. K. (2005). Global histone modification patterns predict risk of prostate cancer recurrence. *Nature*, 435(7046):1262–1266.

[Shain and Pollack, 2013] Shain, A. H. and Pollack, J. R. (2013). The spectrum of swi/snf mutations, ubiquitous in human cancers. *PloS One*, 8(1):e55119.

[Sharma et al., 2010] Sharma, S. V., Lee, D. Y., Li, B., Quinlan, M. P., Takahashi, F., Maheswaran, S., McDermott, U., Azizian, N., Zou, L., Fischbach, M. A., et al. (2010).

A chromatin-mediated reversible drug-tolerant state in cancer cell subpopulations. *Cell*, 141(1):69–80.

[Shi et al., 2015] Shi, J., Wang, E., Milazzo, J. P., Wang, Z., Kinney, J. B., and Vakoc, C. R. (2015). Discovery of cancer drug targets by crispr-cas9 screening of protein domains. *Nature Biotechnology*, 33(6):661–667.

[Shi et al., 2013] Shi, J., Whyte, W. A., Zepeda-Mendoza, C. J., Milazzo, J. P., Shen, C., Roe, J.-S., Minder, J. L., Mercan, F., Wang, E., Eckersley-Maslin, M. A., et al. (2013). Role of swi/snf in acute leukemia maintenance and enhancer-mediated myc regulation. *Genes and Development*, 27(24):2648–2662.

[Steger et al., 2008] Steger, D. J., Lefterova, M. I., Ying, L., Stonestrom, A. J., Schupp, M., Zhuo, D., Vakoc, A. L., Kim, J.-E., Chen, J., Lazar, M. A., et al. (2008). Dot1l/kmt4 recruitment and h3k79 methylation are ubiquitously coupled with gene transcription in mammalian cells. *Molecular and Cellular Biology*, 28(8):2825–2839.

[Stern et al., 1984] Stern, M., Jensen, R., and Herskowitz, I. (1984). Five swi genes are required for expression of the ho gene in yeast. *Journal of Molecular Biology*, 178(4):853–868.

[Strahl and Allis, 2000] Strahl, B. D. and Allis, C. D. (2000). The language of covalent histone modifications. *Nature*, 403(6765):41–45.

[Strobeck et al., 2002] Strobeck, M. W., Reisman, D. N., Gunawardena, R. W., Betz, B. L., Angus, S. P., Knudsen, K. E., Kowalik, T. F., Weissman, B. E., and Knudsen, E. S. (2002). Compensation of brg-1 function by brm insight into the role of the core swi· snf subunits in retinoblastoma tumor suppressor signaling. *Journal of Biological Chemistry*, 277(7):4782–4789.

[Subramanian et al., 2005] Subramanian, A., Tamayo, P., Mootha, V. K., Mukherjee, S., Ebert, B. L., Gillette, M. A., Paulovich, A., Pomeroy, S. L., Golub, T. R., Lander, E. S., et al. (2005). Gene set enrichment analysis: a knowledge-based approach for interpreting genome-wide expression profiles. *Proceedings of the National Academy of Sciences of the United States of America*, 102(43):15545–15550.

[Theodoulou et al., 2015] Theodoulou, N. H., Bamborough, P., Bannister, A. J., Becher, I., Bit, R. A., Che, K. H., Chung, C.-w., Dittmann, A., Drewes, G., Drewry, D. H., et al. (2015). Discovery of i-brd9, a selective cell active chemical probe for bromodomain containing protein 9 inhibition. *Journal of Medicinal Chemistry*.

[Tsai and Baylin, 2011] Tsai, H.-C. and Baylin, S. B. (2011). Cancer epigenetics: linking basic biology to clinical medicine. *Cell Research*, 21(3):502–517.

[Vangamudi et al., 2015] Vangamudi, B., Paul, T. A., Shah, P. K., Kost-Alimova, M., Nottebaum, L., Shi, X., Zhan, Y., Leo, E., Mahadeshwar, H. S., Protopopov, A., et al. (2015). The smarca2/4 atpase domain surpasses the bromodomain as a drug target in swi/snf-mutant cancers: Insights from cdna rescue and pfi-3 inhibitor studies. *Cancer Research*, 75(18):3865–3878.

[Varela et al., 2011] Varela, I., Tarpey, P., Raine, K., Huang, D., Ong, C. K., Stephens, P., Davies, H., Jones, D., Lin, M.-L., Teague, J., et al. (2011). Exome sequencing identifies frequent mutation of the swi/snf complex gene pbrm1 in renal carcinoma. *Nature*, 469(7331):539–542.

[Versteege et al., 1998] Versteege, I., Sévenet, N., Lange, J., Rousseau-Merck, M.-F., Ambros, P., Handgretinger, R., Aurias, A., and Delattre, O. (1998). Truncating mutations of hsnf5/ini1 in aggressive paediatric cancer. *Nature*, 394(6689):203–206.

[Viré et al., 2006] Viré, E., Brenner, C., Deplus, R., Blanchon, L., Fraga, M., Didelot, C., Morey, L., Van Eynde, A., Bernard, D., Vanderwinden, J.-M., et al. (2006). The polycomb group protein ezh2 directly controls dna methylation. *Nature*, 439(7078):871–874.

[Vonrhein et al., 2011] Vonrhein, C., Flensburg, C., Keller, P., Sharff, A., Smart, O., Paciorek, W., Womack, T., and Bricogne, G. (2011). Data processing and analysis with the autoproc toolbox. *Acta Crystallographica Section D: Biological Crystallography*, 67(4):293–302.

[Waddington, 1956] Waddington, C. H. (1956). Genetic assimilation of the bithorax phenotype. *Evolution*, pages 1–13.

[Wang et al., 1996a] Wang, W., Cote, J., Xue, Y., Zhou, S., Khavari, P., Biggar, S., Muchardt, C., Kalpana, G., Goff, S., Yaniv, M., et al. (1996a). Purification and biochemical heterogeneity of the mammalian swi-snf complex. *The EMBO Journal*, 15(19):5370.

[Wang et al., 1996b] Wang, W., Xue, Y., Zhou, S., Kuo, A., Cairns, B. R., and Crabtree, G. R. (1996b). Diversity and specialization of mammalian swi/snf complexes. *Genes and Development*, 10(17):2117–2130.

[Wang et al., 2009] Wang, X., Sansam, C. G., Thom, C. S., Metzger, D., Evans, J. A., Nguyen, P. T. L., and Roberts, C. W. M. (2009). Oncogenesis caused by loss of the snf5 tumor suppressor is dependent on activity of brg1, the atpase of the swi/snf chromatin remodeling complex. *Cancer Research*, 69(20):8094–101.

[Wang et al., 2011a] Wang, X., Werneck, M. B. F., Wilson, B. G., Kim, H.-J., Kluk, M. J., Thom, C. S., Wischhusen, J. W., Evans, J. A., Jesneck, J. L., Nguyen, P., Sansam, C. G., Cantor, H., and Roberts, C. W. M. (2011a). Tcr-dependent transformation of mature memory phenotype t cells in mice. *The Journal of Clinical Investigation*, 121(10):3834–45.

[Wang et al., 2004] Wang, X., Wilsker, D., Van, M., Pacchione, S., Yaciuk, P., Peter, B., Moran, E., et al. (2004). Two related arid family proteins are alternative subunits of human swi/snf complexes. *Biochemical Journal*, 383(2):319–325.

[Wang et al., 2011b] Wang, Y., Yang, F., Gritsenko, M. A., Wang, Y., Clauss, T., Liu, T., Shen, Y., Monroe, M. E., Lopez-Ferrer, D., Reno, T., et al. (2011b). Reversed-phase chromatography with multiple fraction concatenation strategy for proteome profiling of human mcf10a cells. *Proteomics*, 11(10):2019–2026.

[Weishaupt et al., 2010] Weishaupt, H., Sigvardsson, M., and Attema, J. L. (2010). Epigenetic chromatin states uniquely define the developmental plasticity of murine hematopoietic stem cells. *Blood*, 115(2):247–256.

[Willis et al., 2012] Willis, M. S., Homeister, J. W., Rosson, G. B., Annayev, Y., Holley, D., Holly, S. P., Madden, V. J., Godfrey, V., Parise, L. V., and Bultman, S. J. (2012). Functional

redundancy of swi/snf catalytic subunits in maintaining vascular endothelial cells in the adult heart. *Circulation Research*, 111(5):e111–e122.

[Wilson et al., 2014] Wilson, B. G., Helming, K. C., Wang, X., Kim, Y., Vazquez, F., Jagani, Z., Hahn, W. C., and Roberts, C. W. (2014). Residual complexes containing smarca2 (brm) underlie the oncogenic drive of smarca4 (brg1) mutation. *Molecular and Cellular Biology*, 34(6):1136–1144.

[Wilson and Roberts, 2011] Wilson, B. G. and Roberts, C. W. (2011). Swi/snf nucleosome remodellers and cancer. *Nature Reviews Cancer*, 11(7):481–492.

[Wilson et al., 2010] Wilson, B. G., Wang, X., Shen, X., McKenna, E. S., Lemieux, M. E., Cho, Y.-J., Koellhoffer, E. C., Pomeroy, S. L., Orkin, S. H., and Roberts, C. W. (2010). Epigenetic antagonism between polycomb and swi/snf complexes during oncogenic transformation. *Cancer Cell*, 18(4):316–328.

[Winter et al., 2015] Winter, G. E., Buckley, D. L., Paulk, J., Roberts, J. M., Souza, A., Dhe-Paganon, S., and Bradner, J. E. (2015). Phthalimide conjugation as a strategy for in vivo target protein degradation. *Science*, 348(6241):1376–1381.

[Wong et al., 2000] Wong, A. K., Shanahan, F., Chen, Y., Lian, L., Ha, P., Hendricks, K., Ghaffari, S., Iliev, D., Penn, B., Woodland, A.-M., et al. (2000). Brg1, a component of the swi-snf complex, is mutated in multiple human tumor cell lines. *Cancer Research*, 60(21):6171–6177.

[Wu et al., 2009] Wu, J. I., Lessard, J., and Crabtree, G. R. (2009). Understanding the words of chromatin regulation. *Cell*, 136(2):200–206.

[Wu et al., 2007] Wu, J. I., Lessard, J., Olave, I. A., Qiu, Z., Ghosh, A., Graef, I. A., and Crabtree, G. R. (2007). Regulation of dendritic development by neuron-specific chromatin remodeling complexes. *Neuron*, 56(1):94–108.

[Yoo et al., 2009] Yoo, A. S., Staahl, B. T., Chen, L., and Crabtree, G. R. (2009). Microrna-mediated switching of chromatin-remodelling complexes in neural development. *Nature*, 460(7255):642–646.

[Yun et al., 2011] Yun, M., Wu, J., Workman, J. L., and Li, B. (2011). Readers of histone modifications. *Cell Research*, 21(4):564–578.

[Zeisig et al., 2012] Zeisig, B. B., Kulasekararaj, A. G., Mufti, G. J., and So, C. W. E. (2012). Snapshot: Acute myeloid leukemia. *Cancer Cell*, 22(5):698–698.e1.

[Zengerle et al., 2015] Zengerle, M., Chan, K.-H., and Ciulli, A. (2015). Selective small molecule induced degradation of the bet bromodomain protein brd4. *ACS Chemical Biology*, 10(8):1770–1777.

[Zhang et al., 2010] Zhang, B., Strauss, A. C., Chu, S., Li, M., Ho, Y., Shiang, K.-D., Snyder, D. S., Huettner, C. S., Shultz, L., Holyoake, T., et al. (2010). Effective targeting of quiescent chronic myelogenous leukemia stem cells by histone deacetylase inhibitors in combination with imatinib mesylate. *Cancer Cell*, 17(5):427–442.

[Zuber et al., 2011a] Zuber, J., McJunkin, K., Fellmann, C., Dow, L. E., Taylor, M. J., Hannon, G. J., and Lowe, S. W. (2011a). Toolkit for evaluating genes required for proliferation and survival using tetracycline-regulated rnai. *Nature Biotechnology*, 29(1):79–83.

[Zuber et al., 2011b] Zuber, J., Shi, J., Wang, E., Rappaport, A. R., Herrmann, H., Sison, E. A., Magoon, D., Qi, J., Blatt, K., Wunderlich, M., et al. (2011b). Rnai screen identifies brd4 as a therapeutic target in acute myeloid leukaemia. *Nature*, 478(7370):524–528.

Appendices

Appendix 1. BRD9 bromodomain inhibitor screening

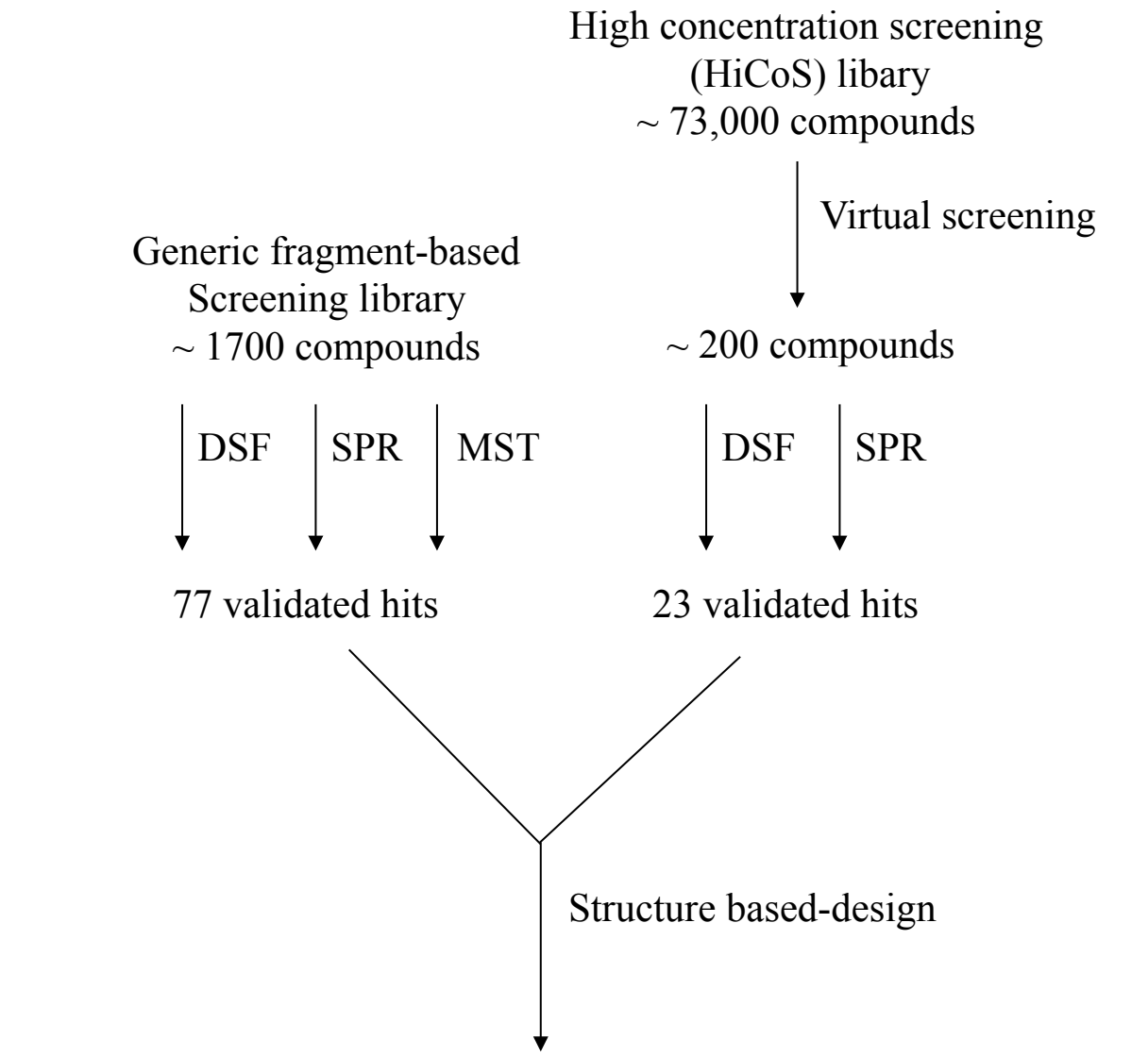

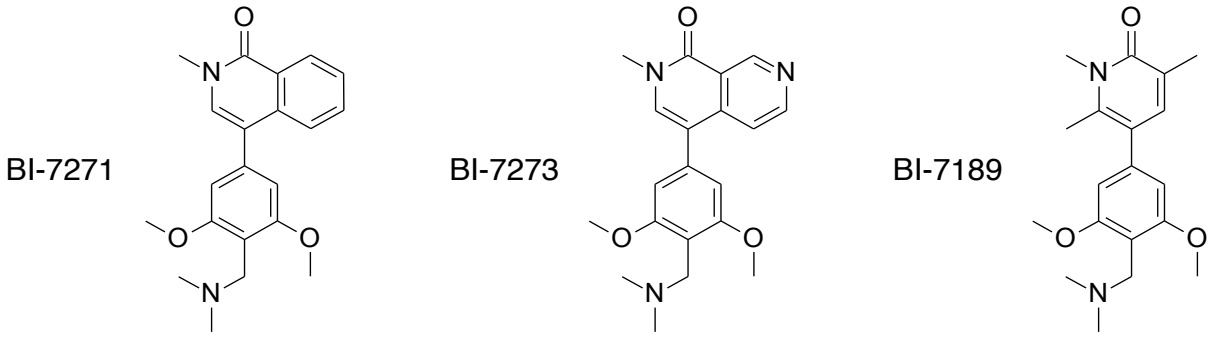

DSF – Differential scranning fluorimetry
SPR – Surface plasmon resonance
MST – Microscale thermophoresis

Appendix 2. Crystal structure data collection and refinement statistics

	BI-7273
Data collection*	
Space group	P 2_1 2_1 2
Cell dimensions	
a, *b*, *c* (Å)	70.80, 125.34, 29.92
a, b, g (°)	90.00, 90.00, 90.00
Resolution (Å)	1.60 (1.79 – 1.60) **
R_{merge} (%)	3.0 (67.0)
CC1/2[ref. 2]	1.0 (0.924)
I / s*I*	26.2 (3.1)
Completeness (%)	99.9 (99.7)
Redundancy	6.3 (6.3)
Refinement	
Resolution (Å)	1.60
No. reflections	35816
R_{work} / R_{free} (%)	17.8/19.2
No. atoms	
Protein	1847
Ligand/ion	52
Water	352
B-factors (Å^2)	
Protein	35.75
Ligand/ion	32.13
Water	47.24
R.m.s. deviations	
Bond lengths (Å)	0.009
Bond angles (°)	0.81

* Values in parentheses are for highest-resolution shell.
** Resolution cutoffs have been determined using the standard parameters of autoPROC[ref. 1]

1. Vonrhein, C., Flensburg, C., Keller, P., Sharff, A., Smart, O., Paciorek, W., Womack, T., Bricogne, G. (2011) Data processing and analysis with the autoPROC toolbox. *Acta Crystallogr D Biol Crystallogr* 67(Pt 4): 293-302

2. Karplus, P.A., Diederichs, K. (2012) Linking crystallographic model and data quality. *Science* 336: 1030-33

Appendix 3. Crystal structure stereo image

Stereo image of BI-7273 bound to BRD9 (wall-eye stereo). The refined $2F_o$-F_c electron density is contoured at 1 σ.

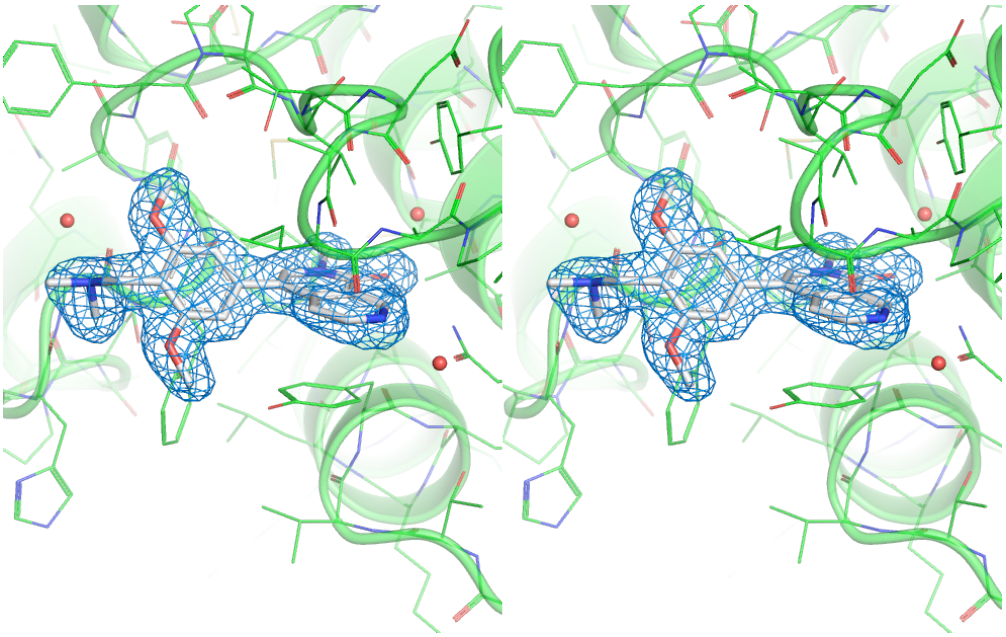

Appendix 4: Synthesis of BRD9 bromodomain inhibitors

Synthesis of compound BI-7273

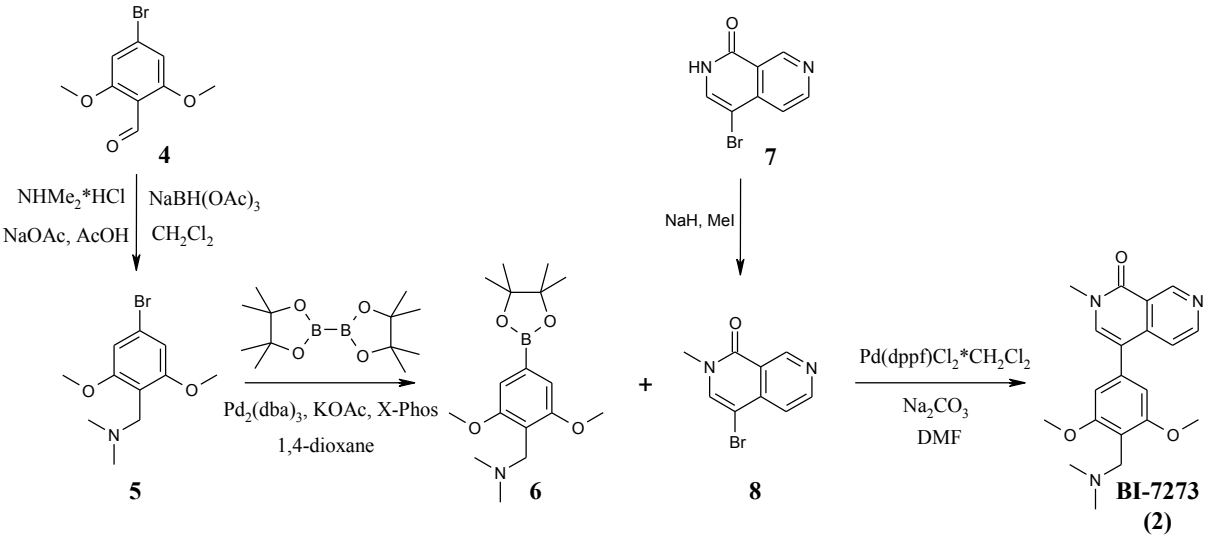

Supplementary Scheme 1: Synthesis of compound **BI-7273**

[(4-Bromo-2,6-dimethoxyphenyl)methyl]dimethylamine (5)

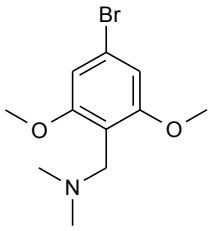

A mixture of NaOAc (17.7 g; 216 mmol), AcOH (8.65 g; 144 mmol) and dimethylamine hydrochloride (17.6 g; 216 mmol) in CH_2Cl_2 (600 mL) is stirred for 10 min at RT. 4-Bromo-2,6-dimethoxybenzaldehyde **(4)** (35.3 g; 144 mmol) is added and stirring is continued. After 30 min sodium triacetoxyborohydride (63.1 g; 298 mmol) is added in one portion and the reaction mixture is stirred at RT for 16 h. Saturated $NaHCO_3$ solution is added and the layers are separated. The aqueous layer is extracted three times with CH_2Cl_2. The combined organic layer is dried over $MgSO_4$, filtered and evaporated to give pure [(4-bromo-2,6-dimethoxyphenyl)methyl]dimethylamine **(5)** (27.3 g; 99.6 mmol; 69 %). ^{1}H-NMR (400 MHz,

$CDCl_3$): δ 6.70 (s, 2H), 3.81 (s, 6H), 3.48 (s, 2H), 2.26 (s, 6H); LC/MS (BAS1): $[M+H]^+$ = 274/276; t_R = 1.11 min.

{[2,6-Dimethoxy-4-(tetramethyl-1,3,2-dioxaborolan-2-yl)phenyl]methyl}dimethylamine (6)

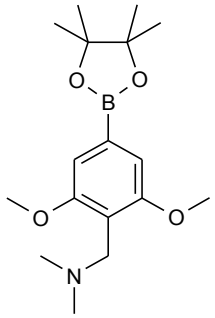

[(4-bromo-2,6-dimethoxyphenyl)methyl]dimethylamine **(5)** (15.7 g; 57.3 mmol) and bis(pinacolato)diboron (43.6 g; 1.86 mol) are dissolved/suspended in 1,4-dioxane (300 mL) under an inert atmosphere (nitrogen). Potassium acetate (17.0 g; 58.8 mmol), tris(dibenzylideneacetone) dipalladium(0) (1.00 g; 1.09 mmol) and 2-dicyclohexyl-phosphino-2′,4′,6′-triisopropylbiphenyl (1.00 g; 2.10 mmol) is added and the mixture is stirred at 90° C for 8 h. After cooling to RT the mixture is concentrated and the residue is taken-up in CH_2Cl_2. Water is added, the layers are separated and the aqueous phase is extracted 2 times with CH_2Cl_2. The combined organic layer is dried over Na_2SO_4, filtered and evaporated. The crude product was purified by preparative HPLC using a MeCN/water (0.2 % TFA added to the water) gradient as eluent to give the TFA salt of {[2,6-dimethoxy-4-(tetramethyl-1,3,2-dioxaborolan-2-yl)phenyl]methyl}-dimethylamine **(6)** which is transferred into the corresponding hydrochloride by dissolving and stirring in HCl/MeOH for 30 min (5.45 g; 17.0 mmol; 30 %). ^{1}H-NMR (500 MHz, DMSO-d6) δ 9.44 (s, 1H), 6.95 (s, 2H), 4.21 (d, *J* = 5.3 Hz, 2H), 3.87 (s, 6H), 2.70 (d, *J* = 5.0 Hz, 6H), 1.32 (s, 12H); LC/MS (BAS1): $[M+H]^+$ = 240 (ester cleaved under basic conditions); t_R = 0.20 min.

4-bromo-2-methyl-1,2-dihydro-2,7-naphthyridin-1-one (8)

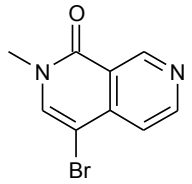

Sodium hydride (3.41 g; 142 mmol) is added slowly to a cooled solution (0 °C) of 4-bromo-1,2-dihydro-2,7-naphthyridin-1-one **(7)** (16.0 g; 71.1 mmol) in DMF (300 mL) and the resulting mixture is stirred for 0.5 h. Methyl iodide (40.4 g; 285 mmol) is added slowly and stirring is continued for 2 h. The reaction mixture is quenched with ice water whereupon the product precipitates. The solid is collected by filtration, washed and dried *in vacuo* to give pure 4-bromo-2-methyl-1,2-dihydro-2,7-naphthyridin-1-one **(8)** (12.0 g; 50.2 mmol; 71 %). ^{1}H-NMR (400 MHz, DMSO-d_6): δ 9.36 (s, 1H), 8.87 (d, J = 5.6 Hz, 1H), 8.26 (s, 1H), 7.62 (d, J = 5.6 Hz, 1H), 3.53 (s, 3H).; LC/MS (BAS1): $[M+H]^+$ = 239/241; t_R = 0.92.

4-{4-[(dimethylamino)methyl]-2,6-dimethoxyphenyl}-2-methyl-1,2-dihydro-2,7-naphthyridin-1-one (BI-7273 (2))

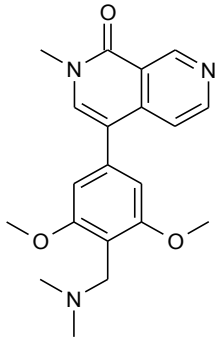

4-Bromo-2-methyl-1,2-dihydro-2,7-naphthyridin-1-one **(8)** (200 mg; 837 µmol) and {[2,6-dimethoxy-4-(tetramethyl-1,3,2-dioxaborolan-2-yl)phenyl]methyl}-dimethylamine **(6)** (375 mg; 1.26 mmol) and 1,1'-bis(diphenylphosphino)ferrocene palladium(II) dichloride·CH_2Cl_2 (70.4 mg; 86.2 µmol) are suspended in DMF (2.0 mL) under argon. A degassed Na_2CO_3-solution (2N; 1.05 mL; 2.10 mmol) is subsequently added and the resulting mixture is heated to 80 °C for 1 h. After cooling to RT DMF is evaporated and a the residue is purified by flash chromatography on SiO_2 using CH_2Cl_2/MeOH (with 1% 2N NH_3) 0-10% as eluent to give pre-purified material.

Subsequent preparative RP-HPLC chromatography yields highly pure 4-{4-[(dimethylamino)methyl]-2,6-dimethoxy-phenyl}-2-methyl-1,2-dihydro-2,7-naphthyridin-1-one **(BI-7273 (2))** (210 mg; 594 µmol; 71 %). ^{1}H NMR (500 MHz, DMSO-d6) δ 9.44 (s, 1H), 8.72 (d, J = 5.7 Hz, 1H), 7.86 (s, 1H), 7.56 (d, J = 5.7 Hz, 1H), 6.72 (s, 2H), 3.80 (s, 6H), 3.60 (s, 3H), 3.46 (s, 2H), 2.13 (s, 6H); ^{13}C NMR (126 MHz, DMSO) δ 160.9, 159.4 (2C), 151.4, 150.9, 141.5, 138.3, 135.5, 120.2, 117.8, 116.5, 113.9, 105.8 (2C), 56.3 (2C), 50.0, 45.5 (2C), 36.9. HRMS (CI+): calculated for $C_{20}H_{24}N_3O_3$ (MH+) 354.1812, found 354.1808, Δ - 1.1 ppm; LC/MS (BAS1): $[M+H]^+$ = 354; t_R = 0.91 min.

Synthesis of compound BI-7271

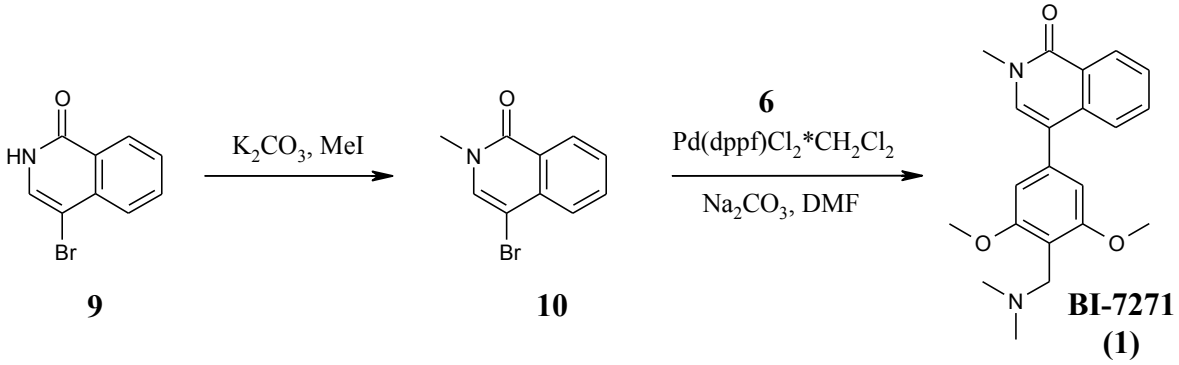

Supplementary Scheme 2: Synthesis of compound **BI-7271**

4-bromo-2-methyl-1,2-dihydroisoquinolin-1-one (10)

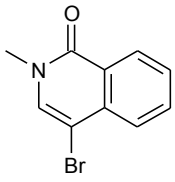

To a suspension of 4-bromo-1,2-dihydroisoquinolin-1-one **(9)** (1.00 g; 4.46 mmol) and potassium carbonate (1.17 g; 8.48 mmol) in THF (10 mL), iodomethane (323 µL; 5.09 mmol) is carefully added and the resulting mixture is stirred at RT for 16 h. Since HPLC-MS of the reaction mixture indicates incomplete conversion additional iodomethane (100 µl; 1.57 mmol) is added and stirring is continued for 5h. Ammonia (10% aqueous solution; 30 mL) is added followed by water

(50 mL). THF is removed under reduced pressure whereupon a precipitation occurs. The solid is collected by filtration, washed with cold water and dried *in vacuo* to give 4-bromo-2-methyl-1,2-dihydroisoquinolin-1-one **(10)** (1.00 g; 4.20 mmol; 94 %) as a yellow solid which is used without further purification. ^{1}H NMR (400 MHz, DMSO-d6) δ 8.28 (d, J = 8.0 Hz, 1H), 7.98 (s, 1H), 7.86 (t, J = 7.6 Hz, 1H), 7.76 (d, J = 8.1 Hz, 1H), 7.62 (t, J = 7.5 Hz, 1H), 3.52 (s, 3H); LC/MS (BAS1): $[M+H]^+$ = 238/240; t_R = 1.02.

4-{4-[(dimethylamino)methyl]-3,5-dimethoxyphenyl}-2-methyl-1,2-dihydroisoquinolin-1-one (BI-7271 (1))

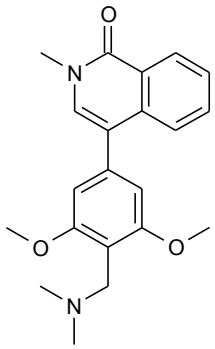

4-bromo-2-methyl-1,2-dihydroisoquinolin-1-one **(10)** (130 mg; 546 µmol) and {[2,6-dimethoxy-4-(tetramethyl-1,3,2-dioxaborolan-2-yl)phenyl]methyl}-dimethylamine **(6)** (284 mg; 884 µmol) and 1,1'-bis(diphenylphosphino)ferrocene palladium(II) dichloride·CH_2Cl_2 (44.6 mg; 54.6 µmol) are suspended in DMF (2.0 mL) under argon. A degassed Na_2CO_3-solution (2N; 683 µL; 1.37 mmol) is subsequently added and the resulting mixture is heated to 100 °C for 1 h. After cooling to RT water is added (several drops) and the mixture is filtered and purified by preparative RP-HPLC (column: X-Bridge C-18 30x50 mm) using a MeCN/water gradient under basic conditions. The product containing fractions are freeze dried. Further purification is achieved by automated silica gel chromatography (Combiflash; column: Redisep RF, 12g) using a CH_2Cl_2/MeOH gradient as eluent (100:0 --> 80:20; MeOH made basic with 0.1% NH_3). The product containing fractions are evaporated, dissolved in MeCN/water and freeze dried to give 4-{4-[(dimethylamino)methyl]-3,5-dimethoxyphenyl}-2-methyl-1,2-dihydroisoquinolin-1-one **(BI-7271 (1))** (84.8 mg; 240 µmol; 44 %). ^{1}H NMR (500 MHz, DMSO-d6) δ 8.34 (d, J = 7.1 Hz, 1H), 7.72 (dd, J = 8.3, 7.1, 1H), 7.65 (d, J = 7.9 Hz, 1H), 7.58 – 7.54 (m, 2H), 6.71 (s, 2H), 3.80 (s, 6H), 3.58 (s, 3H), 3.49 (s, 2H), 2.16 (s, 6H); ^{13}C NMR (125 MHz, DMSO) δ 161.3, 159.3

(2C), 137.0, 136.3, 133.3, 132.8, 127.8, 127.1, 125.5, 124.8, 118.2, 113.4, 106.1 (2C), 56.3 (2C), 50.0, 45.4 (2C), 36.8; HRMS (CI+): calculated for $C_{21}H_{25}N_2O_3$ (MH+) 353.18597, found 353.18568, Δ -0.82 ppm; LC/MS (BAS1): $[M+H]^+ = 353$; $t_R = 1.05$.

Synthesis of compound BI-7189

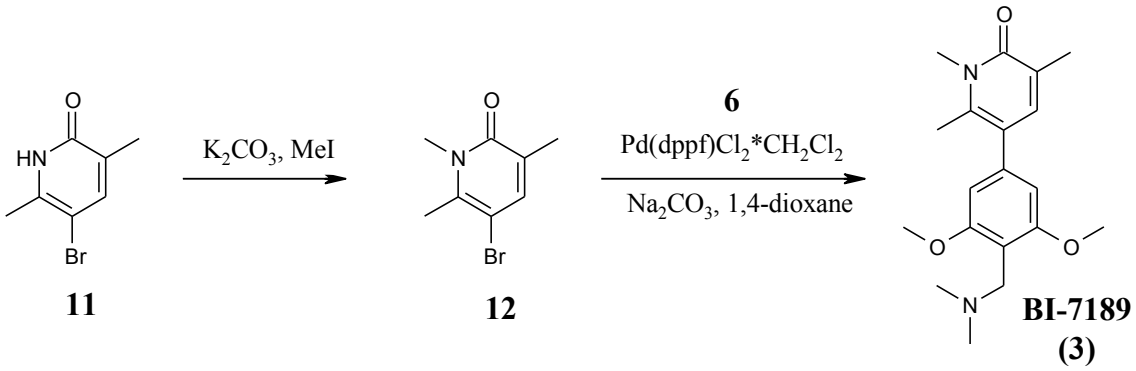

11 **12** **BI-7189 (3)**

Supplementary Scheme 3: Synthesis of compound **BI-7189**

5-bromo-1,3,6-trimethyl-1,2-dihydropyridin-2-one (12)

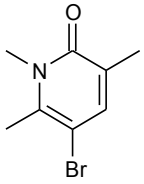

To a suspension of 5-bromo-3,6-dimethyl-1,2-dihydropyridin-2-one **(11)** (2.54 g; 12.6 mmol) and potassium carbonate (4.13 g; 29.9 mmol) in THF (25 mL), iodomethane (811 µL; 13.1 mmol) is carefully added and the resulting mixture is stirred at 80 °C for 16 h. Ammonia (10% aqueous solution; 30 mL) is added followed by water (50 mL). THF is removed under reduced pressure and the aqueous residue is extracted three times with CH_2Cl_2. The combined organic layer is dried over Na_2SO_4 and concentrated *in vacuo* to give crude 5-bromo-1,3,6-trimethyl-1,2-dihydropyridin-2-one **(12)** (2.58 g; 11.9 mmol; 95 %) which is used without further purification.

For analytical purposes a small amount was purified by silica gel chromatography. ^{1}H NMR (400 MHz, DMSO-d6) δ 7.47 (s, 1H), 3.51 (s, 3H), 2.47 (s, 3H), 1.98 (s, 3H); LC/MS (BAS1): $[M+H]^+$ = 216/218; t_R = 0.84.

5-{4-[(dimethylamino)methyl]-3,5-dimethoxyphenyl}-1,3,6-trimethyl-1,2-dihydro-pyridin-2-one (BI-7189 (3))

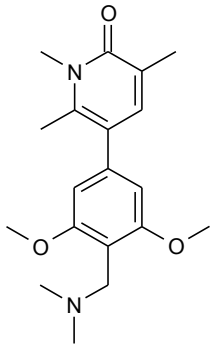

5-bromo-1,3,6-trimethyl-1,2-dihydropyridin-2-one **(12)** (100 mg; 462 µmol) and {[2,6-dimethoxy-4-(tetramethyl-1,3,2-dioxaborolan-2-yl)phenyl]methyl}-dimethylamine (**6**) (216 mg; 672 µmol) and 1,1'-bis(diphenylphosphino)ferrocene palladium(II) dichloride·CH_2Cl_2 (38.8 mg; 47.5 µmol) are suspended in DMF (2.0 mL) under argon. A degassed Na_2CO_3-solution (2N; 576 µL; 1.15 mmol) is subsequently added and the resulting mixture is heated to 100 °C for 1 h. After cooling to RT water is added (several drops) and the mixture is filtered and purified by preparative RP-HPLC (column: X-Bridge C-18 30x50 mm) using a MeCN/water gradient under basic conditions. The product containing fractions are freeze dried. Further purification is achieved by automated silica gel chromatography (Combiflash; column: Redisep RF, 12g) using a CH_2Cl_2/MeOH gradient as eluent (100:0 --> 90:10; MeOH made basic with 0.1% NH_3). The product containing fractions are evaporated, dissolved in MeCN/water and freeze dried to give 5-{4-[(dimethylamino)methyl]-3,5-dimethoxyphenyl}-1,3,6-trimethyl-1,2-dihydropyridin-2-one **(BI-7189 (3))** (46.0 mg; 139 µmol; 30 %). ^{1}H NMR (500 MHz, DMSO-d6) δ 7.29 (s, 1H), 6.53 (s, 2H), 3.77 (s, 6H), 3.53 (s, 3H), 3.47 (s, 2H), 2.32 (s, 3H), 2.16 (s, 6H), 2.04 (s, 3H). ^{13}C NMR (125 MHz, DMSO) δ 162.7, 159.0 (2C), 141.9, 140.5, 138.7, 124.2, 118.9, 105.9 (2C), 56.2 (2C), 50.0, 45.3 (2C), 31.9, 18.5, 17.4, 1 C missing; HRMS (CI+): calculated for $C_{19}H_{27}N_2O_3$ (MH+) 331.20162, found 331.20123, Δ -1.17 ppm; LC/MS (BAS1): $[M+H]^+$ = 331; t_R = 0.92.